# We are IntechOpen, the world's leading publisher of Open Access books
# Built by scientists, for scientists

6,300
Open access books available

171,000
International authors and editors

190M
Downloads

154
Countries delivered to

Our authors are among the
TOP 1%
most cited scientists

12.2%
Contributors from top 500 universities

WEB OF SCIENCE™
Selection of our books indexed in the Book Citation Index in Web of Science™ Core Collection (BKCI)

Interested in publishing with us?
Contact book.department@intechopen.com

Numbers displayed above are based on latest data collected.
For more information visit www.intechopen.com

Chapter

# Multi-core Fiber Technology

*Muhammad Irfan Anis and Hamdan Ali*


## Abstract

Traditional single-mode fiber capacity issues will be mitigated by using space-division multiplexing in future 5G, IoT, and M2M networks. Multi-core fibers are expected as a good candidate for overcoming the capacity limit of a current optical communication system. This chapter describes the recent progress on the Multi-core fibers technology for the application of high capacity space-division multiplexing to be utilized for long-distance transmission systems. Further various optical approaches that enable key functions are discussed, including SDM MUX/DeMUX, switches, transceivers to enable next generation optical network. Moreover, issues like crosstalk, non-linearity is a potential limitation on the achievable data-rates in optical fiber transmission systems using multi-core fibers will be discussed.


**Keywords:** All-optical signal processing, Crosstalk, Fiber capacity, Optical Network, Space division multiplexing

## 1. Introduction

Internet traffic infrastructure is underpinned by optical transmission systems and networks [1]. However, continuous supply of new services like video on demand, Virtual Reality and Augmented Reality have rising data volumes needed to satisfy the requirements of industry, academics, governments, and people presents new challenges to optical communication infrastructure [2]. Fiber-optic communication systems based on conventional single mode single core fibers (SMF) are almost saturated due to amplifier bandwidth, nonlinear noise, and fiber fuse phenomena due to this it's capacity consumption will be beyond capacity limitations by the year 2022 [3]. As a result, researcher has led to a steady push for new, higher bandwidth optical fibers that can replace the SMF.

Space division multiplexing (SDM) methods is one of the potential capacity expansion strategies for an optical transport network. It is transmission fibers that enable concurrent parallel data transmissions on multiple cores in a single cladding or several cores inside a single core to improve speed and data rate [4]. The first demonstration of an SDM link consisting of standard cladding diameter surpassing the typical size of 125 μm 7-core MCFs, highly efficient MC-EDFAs, and MCF connectors transmission above 100 Tbit/s across a 316 km has occurred and considerably greater capacity tests such as over 1 Pbit/s and 1 Ebit/s·km were performed using single mode multi-core fiber [5]. SDM fibers are defined as multi-core fibers (MCFs) and few-mode fibers (FMFs) or multi-mode fiber (MMF) [6]. MCF and multi-mode fiber technologies provide for additional fiber capacity proportional to the number of cores and modes per fiber [7]. Single-mode cores, contained in a shared cladding, are employed independently in the former. An FMF



IntechOpen

has one core, which enables several optical modes, each of which may transmit data independently. MCF is a promising technology for providing enormous bandwidth and capacity with regard to information [8]. The MCF help facilitate the data transmission and the transmission of power in high power devices. Multi-core fibers have many positive attributes over conventional fibers: they have significantly decreased core separation and are very regular when compared to free-standing fibers, and they also provide a monolithic package with several fiber features [9]. Moreover, multi-core fibers that allow a few-mode core to combine the fibers results in an extra 100 optical channels in each transmission, as well as throughputs of over 1 Pb/s [10]. Recently MCF-based fiber-optic transmission, a capacity of 1 Pb/s per 32-core fiber has been achieved [11].

Multi-Mode-Multi-Core Fiber (MM-MCF) significantly increases the number of spatial channels to 114 or more, and transmission of 10 Pbit/s was achieved utilizing this multi-mode MCF. Despite these benefits, the MCF may have limitations such as crosstalk (XT), non-linearities, dispersion, and so forth. Over long distances, the accumulation of MCF crosstalk may be the most limiting issue influencing the performance of an optical communications system. As a consequence, in recent years, research in this field has been driven by the development of ultralow crosstalk MCFs [12]. The impact of XT on MCF system capacity and range has recently been studied [13]. However, the results vary with modulation format and transmission reach, leading to the general notion that different network applications, from short-range to ultra-long haul, need different MCF designs. Standardization and mass production are essential for widespread commercial usage of emerging technologies like MCF. An XT standard per unit length of 55 dB/km has been proposed [14]. In an MCF system, the performance penalty must be evaluated against a non-XT system, regardless of unit size (i.e., a fiber bundle instead of an MCF). Capacity and reach penalties are required. Calculation on an optimal MCF core density for long-distances-independent crosstalk specifications have been done. The crosstalk process was originally described in [15], although the majority of crosstalk on a fiber is continuous, it is at discrete places where crosstalk amplifies the most, when core matching circumstances occur. Since the locations and phases of these sites may change randomly, crosstalk in MCFs follows a random chi-square distribution with 4 degrees in time and wavelength [16].

Using MCF's nonlinear distortions for power-over-fiber operations poses a number of challenges. The structure of MCF, which enables for high-power signal transmission via the fibers, has lately received attention. It is recommended that image processing be used; therefore, the present limitation of single mode fiber must be overcome [17].

A 7-core MCF with reduced inter-core crosstalk was used for trans-oceanic transmission. Using MCF and a spectrum efficient modulation scheme, 201 x 100 Gbit/s transmission across 7326 km produced a capacity-distance product surpassing 1 Exabit/skm [18]. These systems propose the MCF as one of many optical transmission techniques.

To transmit 52.2 Tbit/s across 10230 km, the CDP for SM-SCF transmission is 534 Pbit/s/km. The transmission rate was 1.03 Ebit/s km/h [19]. A preliminary test using seven spatial channels and PDM-QPSK yielded 53.3 Tb/s [20]. Using 8 spatial channels with PDM-8PSK, the capacity was 83.33 Tb/s. MMF allows transmission distances up to 1200 km (3 spatial modes x 40 Gbit/s DP-QPSK) and 13.9 Pbit/skm (CDP with MMF)[21]. Uncoupled MCF allows for considerably longer transmission. The 1500 km transmission used a propagation-direction interleaved design to minimize interference between neighboring cores [19].

This chapter investigates MCF-based novel technologies for creating next-generation optical networks. We first examine the roadmaps towards optical fiber and examine why there is a need for MCF. We also highlight the newest reports' in MCF paradigm covering design and application. Looking into the main technology as a key functional building blocks for next generation optical communication. Next, we demonstrate the experimental setup of MCF. In last section describe the MCF limitation before conclusion.

## 2. The roadmaps towards fiber optics

The global proliferation of hyper photonics, intelligent photonics and frontier wireless communication need an increasing data capacity of tens of percentage each year. Services including IoT, M2M, sensor networks, and linked vehicles will need even greater bandwidth to expand capacity and find more efficient connections via high-speed optical fiber networks, as **Figure 1** shows the innovation technologies. As a result, the forthcoming growth in data transmission will exceed the SMF's maximal transmission capacity due of its low loss and optical amplification of the transmission window. Traditional SMF cannot be ignored in DWDM transmission systems with Raman amplification [23]. An increase in optical infrastructure is required to meet capacity constraints. Introducing extra optical fibers and cables is considerably simpler when contemplating an alternate technology. The future capacity constraint may be averted simply by creating more SMFs. Thus, construction/renewal of the physical infrastructure would be required, which would add to the total expenses. SDM, a fifth physical dimension, may supplement time, wavelength, frequency, and polarization multiplexing, thereby easing future capacity problems [24].

**Figure 2** shows the progress of cable density. 400-pair copper, 400-fiber ribbon, and 400 rollable fiber ribbon cables are indicated by black, blue, and red dots. A solid green line indicates the numerical limit for a hexagonally packed 250 mm fiber bundle with a 2 mm cable sheath [24].

The two spatial dimensions of mode and core are used in the design of optical fiber. MCF stands for multi-core fiber division multiplexing, while MMF stands for multi-mode fiber division multiplexing. For understanding description of a 2D representation of modes and cores inside optical fiber shown in **Figure 3**. With proper use of modes or cores, it is possible to surpass the present geometric limit of conventional optical fiber cable. Using the modes and cores in tandem will almost triple the spatial multiplicity. This recent study concludes that 6-mode and 19-core fiber can provide over 100 spatial channels [25]. It's required that a complicated transmission strategy be used because of the mode coupling and/or mode-dependent transmission properties in optical fiber. Also, MCF has been constantly studied and was pioneering in [24]. MCF is especially capable of using the newest

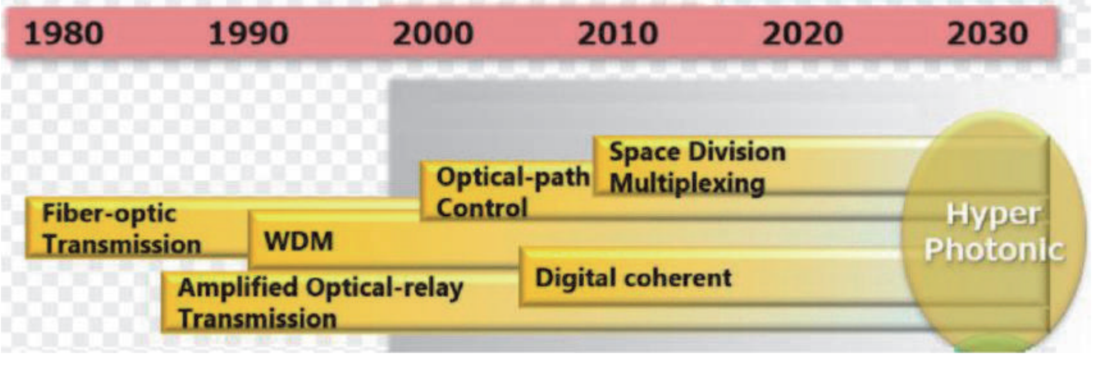


**Figure 1.**
*History of optical network innovation technologies [22].*

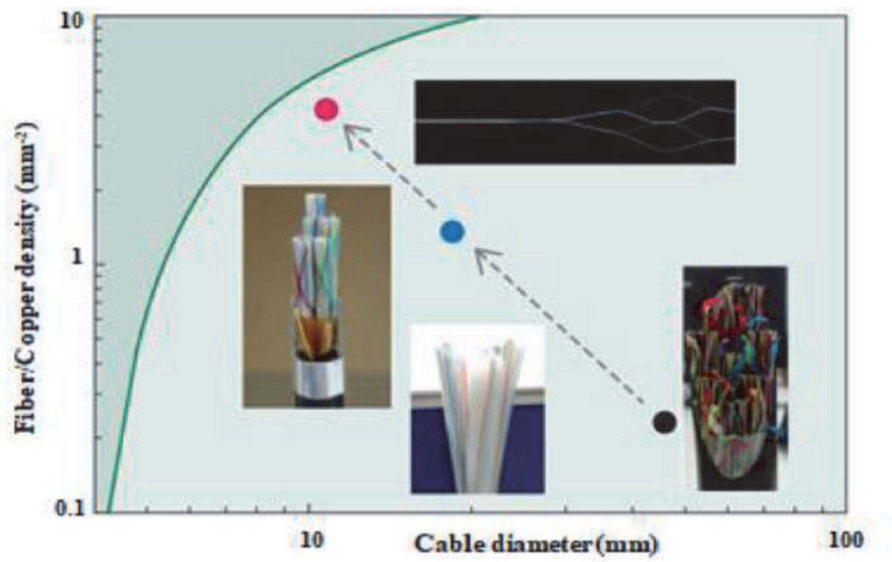


**Figure 2.**
*Evolution of communication cable density over time [7].*

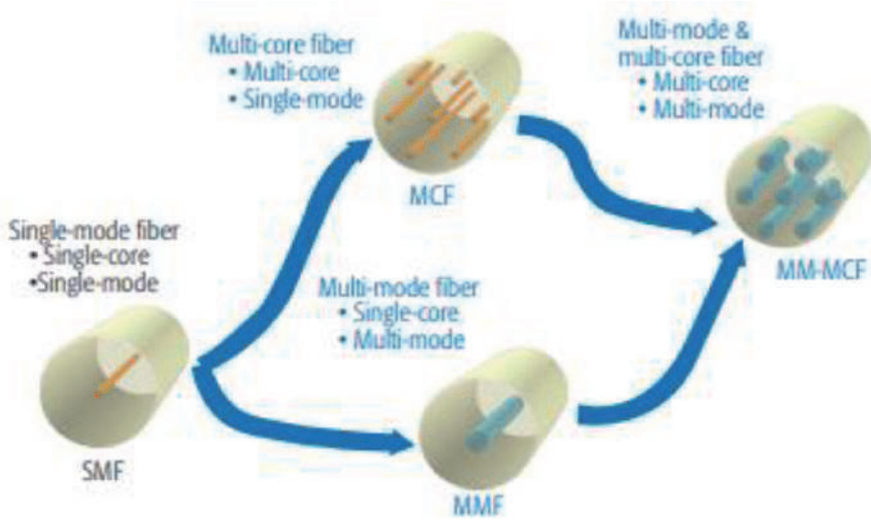


**Figure 3.**
*Schematic image of the two spatial dimensions of mode and core in optical fiber [24].*

single-mode technologies. Here, we'll talk about MCF and the capacity of MCF as an SDM transmission medium.

Signal mixing and propagation time skew are two important characteristics of SDM fibers that have a direct effect on transmission performance. SDM fiber groups are provided by two mixing levels. First, there are uncoupled MCFs (UC-MCFs), few-mode fibers, or few-mode MCFs, which mix signals from several spatial channels during transmission and have minimal inter-core coupling to minimize inter-core crosstalk (XT). Both the first group randomly coupled MCF (RC-MCF) and the second group randomly coupled MCF (RC-MCF) have significant random mode mixing between modes (RC-MCF). UC-MCFs have greater spatial channel density than SMFs with traditional transceivers. To compensate for random coupling, RC-MCFs need MIMO digital signal processing (DSP). However, random coupling may decrease spatial mode dispersion and therefore the MIMO DSP's computational complexity. Other core/mode-dependent restrictions are also prevented by random coupling [26, 27].

MCF with a 125 mm cladding diameter is needed to start MCF tech. A 125 mm cladding diameter MCF design that is optically compatible with current SMF.

| | No of cores | Core layout | Cladding diameter [μm] | Cut off wave length [μm] | Mode field diameter [μm] @nm | Affective area [μm$^2$]@nm | Crosstalk [/km] @nm | Wavelength band | Applications | Parameter/feature | Ref. |
|---|---|---|---|---|---|---|---|---|---|---|---|
| Multi-core Uncoupled-type | 7 | ⬡ | 150 | ≤1.51 | 9.8@1550 | 80@1550 | 6.0x10$^{-9}$ @1625 | C ~ L | LH | Ultra-low Crosstalk | [29] |
| | 7 | ⬡ | 188 | ≤1.47 | 12.2@1550 | 124@1550 | 8.0x10$^{-7}$ @1625 | C ~ L | LH | High Optical SNR | [30] |
| | 31 | ⬡ | 225 | ~1.47 | n/a | 57@1550 | 9.3x10 | C ~ L | LH | High SSE | [31] [32] |
| | 4 | □ | 125 | ≤1.19 | 8.6@1310 | — | 5.0x10$^{-5}$ @1625 | O ~ L | LH | Standard diam. Cladding+ Full wavelength band | [32] [5] |
| | 8 | ○ | 125 | ≤1.24 | 8.4@1310 | — | 3.2x10$^{-7}$ @1310 | O | SR | Standard diam. Cladding +8 cores | [33] |
| | 8 | 2x4 | 180 | ≤1.20 | 8.4@1310 | — | ≤6.3x10$^{-5}$@1550 | O ~ C | SR | Si photonics TRx mounted | [34] |
| | 4 | 1x4 | 98x200 | ≤1.34 | 9.7@1550 | n/a | 3.0x10$^{-4}$@01550 | C ~ L | SR | Non-circular clad. | [35] |

| | No of cores | Core layout | Cladding diam. [μm] | Cut off wave length [μm] | Mode field diameter [μm] @nm | Affective area [μm$^2$] @nm | Spatial mode dispersion [ps/√km] | Wavelength band | Applications | Parameter/feature | Ref. |
|---|---|---|---|---|---|---|---|---|---|---|---|
| Multi-core coupled-type | 3 | △ | 125 | ~1.35 | — | 129@1550 | 30 | S ~ L | LH | 4,200-km MIMO transmission achieved. | [35] |
| | 4 | □ | 125 | ≤1.47 | — | 112@1550 | 3.1 | C ~ L | LH | Has set low SMD and low-loss records for SDM fibers. 10,000 km transmission achieved. | [36] |

**Table 1.**
*Representative examples of reported MCFs [28].*

**Table 1** depicts conventional MCFs provided by Sumitomo Electric, as well as prototype MCFs created by the company via joint research.

### 2.1 Need for multi-core technology

The restricted bandwidth of low-loss transmission and optical amplification, as well as transmission power limitations due to fiber non-linearity, make expanding a single optical fiber's transmission capacity challenging. A growing need for higher-capacity optical fiber communications **Figure 4** shows high-capacity optical fiber transmission test results. Due to the limitations of single-mode single-core fiber, the maximum capacity is 100 Tbit/s. This high-capacity fiber capacity was achieved using MCF. SDM plus MCF or MMF may be able to outperform single-core fiber transmission systems [12, 26, 29].

## 3. MCF paradigm

This section investigates the design and the achievements in MCF technology, which seem promising in the short term yet have certain unknown risks.

### 3.1 Design of MCF

Due to fiber bandwidth depletion and the development of SDMF as a possible alternative to address extra capacity, the spectrum capacity of SSMF is nearing its end. The long-term goal of SDM is to increase the number of fiber cores, guided modes, or both. MCF has many cores in a single optical cable. The core of a conventional single-core fiber is positioned in the center of a 125-m diameter cladding, limiting design freedom. The MCF's success is dependent on more than simply the number of cores. MCFs enable the designer to optimize core design, the number of cores, core arrangement, outer cladding thickness, and cladding diameter in terms of optical and mechanical properties. Fiber design is required based on the application because desirable features differ. SMFs currently have a single fiber core surrounded by 125 mm cladding and coated. Greater cores with the same cladding or larger core diameters allow for more fiber capacity [12]. Adding cores to the

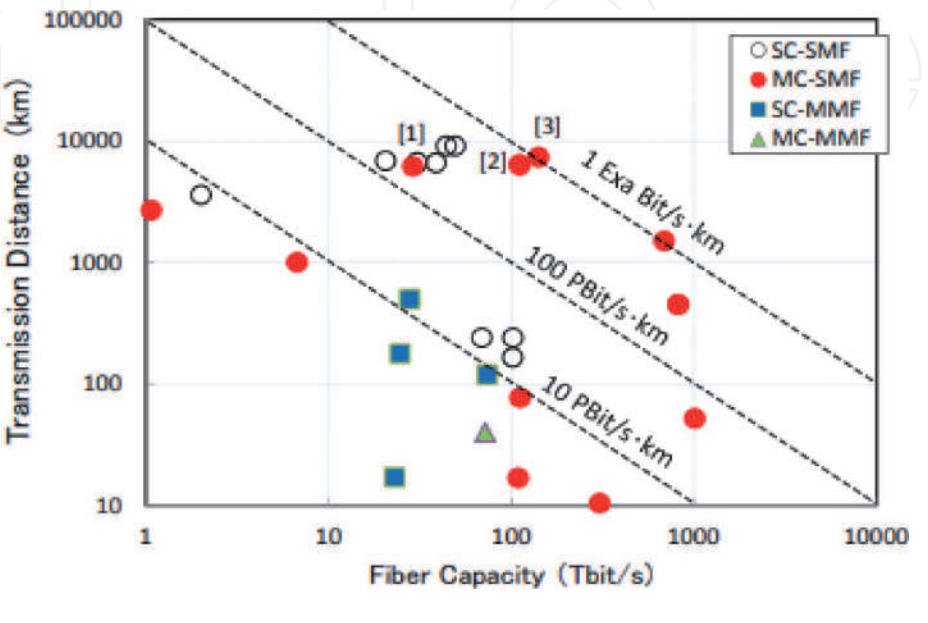


**Figure 4.**
*Recent reports on high capacity transmission [19].*

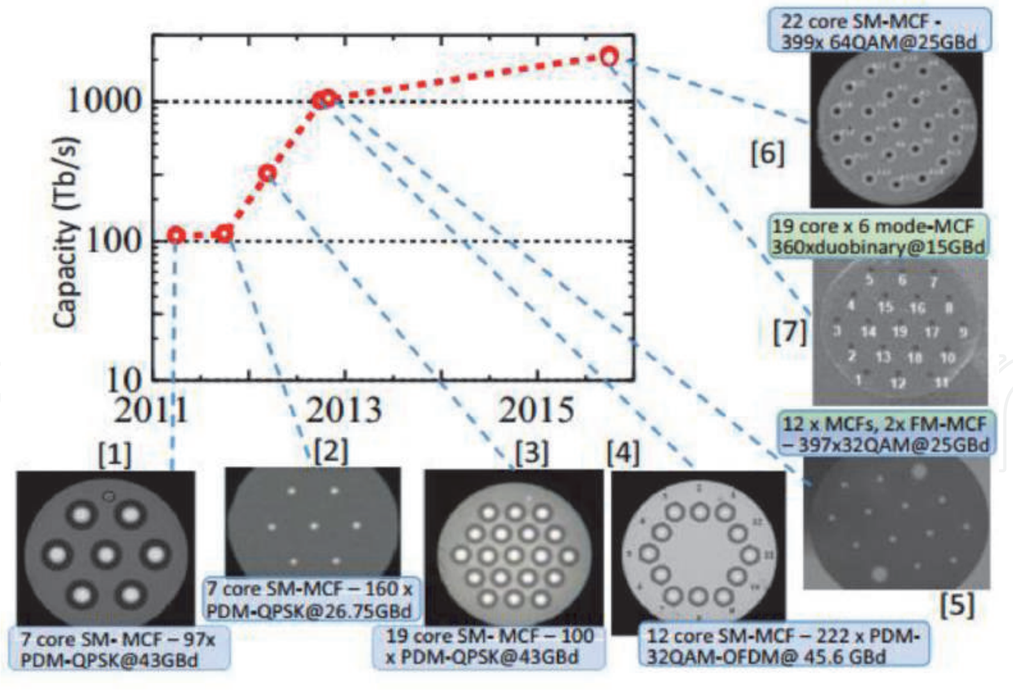


**Figure 5.**
*High-capacity transmission experiments using SM and FM-MCF [12].*

cladding may improve capacity, but it may need changes to the transmission system architecture.

SM–MCF transmission experiments on FMFs have shown fibers with as many as 32 and as little as 45 modes. Adding multi-core fibers that enable a few-mode core to join the fibers results in an additional 100 optical channels in each transmission and throughputs of more than 10 Pb/s [30]. The high-capacity experimental transmission utilizing SM and FM-MCF is shown in **Figure 5**.

A random coupled MCF is one that is MCF if XT is compensated by MIMO DSP. Even though the core is simple, the paired MCF is denser. Furthermore, random coupling in the connected MCF prevents the emergence of nonlinearity impairment, SMD, and mode-dependent loss/gain. In long-distance point-to-point communication, coupled MCF is utilized. Nokia Bell Labs, Sumitomo Electric, and Sumitomo Corporation collaborated to develop and launch new fibers [31].

Few-mode (FM) MCF fiber is a kind of uncoupled MCF (MCF with fiber coupled together) designed for mode-multiplexed transmission. KDDI Research, Inc. received a prototype 36-core fiber created in cooperation with NICT and Yokohama National University. The most recent accomplishments include a 19-core fiber that can be used in the whole C + L bands (1530–1625 nm) for long-distance communications [37]. This fiber achieved 10 Pbit/s per optical fiber in an experiment performed by KDDI Research [30].

The MCF has the potential to enhance data and power transmission for high-power devices. PoF, on the other hand, need MCF due to its nonlinear aberrations. Inside MCF, an eye-catching power transmission capacity was recently discovered. The placement of the cores has an impact on the MCF's performance.

Multi-core fiber architectures such as triangle, ring, square, rectangle, and hexagon were developed after analyzing the number of cores, pitch, and power spectrum. Many people are interested in the MCF fiber-optic structure and the question is how it allows the transmission of powerful signals. One-mode fiber has a lower limit imposed by the MCF and is currently limited by MCF analysis and picture processing. The placement of the cores influences the performance of the MCF.

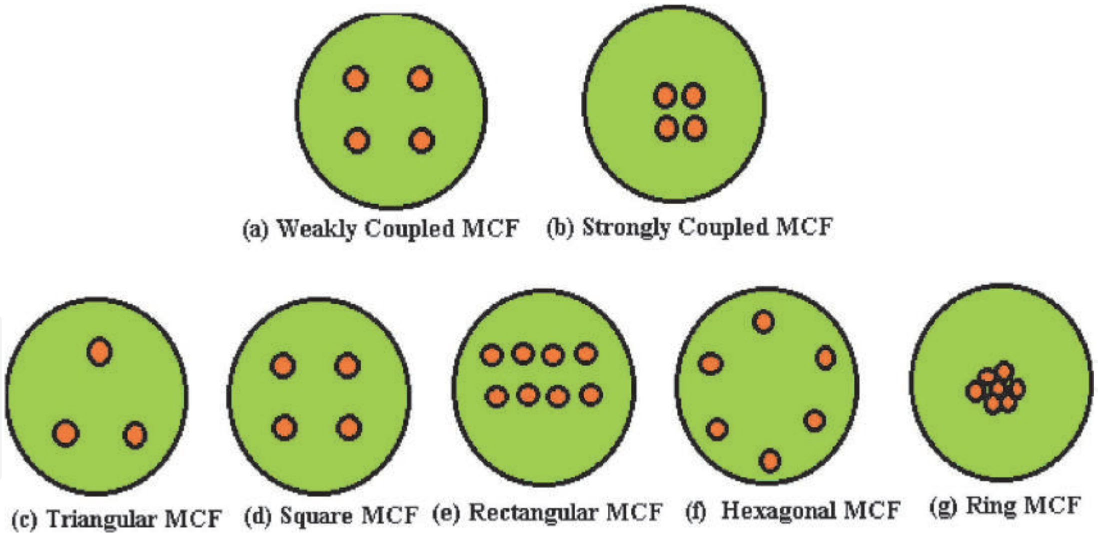


**Figure 6.**
*Structure of multicore fiber with coupling region and with different pattern [17].*

For MCF, strong and weak coupling are illustrated in **Figure 6**. Strongly linked MCF has the smallest core-to-core distance, whereas weakly coupled MCF has the most core-to-core distance. The size of the core may vary with the pitch of the core. The effective area ($A_{eff}$) relies on the number of cores (as shown in **Figure 6**), and their configuration influence the output receiving power. MCF contains several cores with enlarged effective areas, resulting in minimal dispersion and bending losses. The suggested solution to fiber bending losses included four air core MCF. **Figure 6** shows the five distinct MCF structures.

To provide long-distance reliable signal transmission, the XT must be less than -30 dB/100 Km [32]. To get ultra-low XT levels, make changes to MCF structures, such as trenching around the cores. Essentially, trenches are refractive index profiles with lower refractive index than the core and cladding. Trench-assisted method is one of the noteworthy techniques that lowers the coupling between the adjacent cores, therefore helping to minimize existing crosstalk.

With an MCF, if the number of cores in a restricted cladding area grows, crosstalk suppression becomes a problem. XT in MCFs is decreased by decreasing the coupling coefficient between cores. The underlying design, with strong containment of modes is critical to suppressing the mode coupling coefficient. For a higher $A_{eff}$ and lower nonlinear noise, you may choose for a higher-index core with a smaller diameter.

It has three important geometrical features, as shown in **Figure 7**. The outer cladding thickness (OCT) is the distance between the outer core's center and the cladding's perimeter. Optical fiber mechanical reliability is strongly linked to cladding diameter D. A higher D value increases MCF deformations before collapse. Inter-core XT may be reduced by adjusting core and rod radius, cladding and rod relative refractive index differences, and core-to-core distance.

### 3.2 Application

The MCF technologies have been gradually increasing, and now we can see feasible commercial uses for the technologies. Practical use of MCFs will likely occur in near future due to continuous MCF development [28]. **Figure 8** illustrates the whole growth stages of MCF technology. Larger applications in the network such as metro and core may provide challenges to MCF implementation, because they need a complete suite of network components other than the MCF and cable

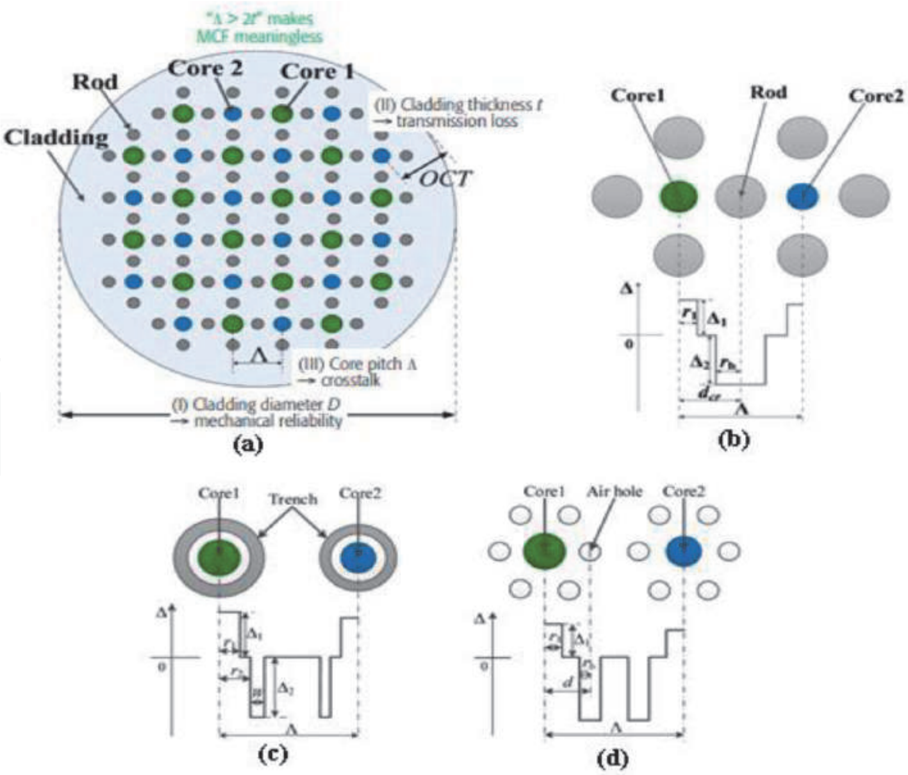


**Figure 7.**
*(a) A 32 core schematic structure shows three key geometrical parameters in MCF. Schematic diagrams of (b) core index profile of heterogeneous rod rod-assisted 32-core fiber (c) trench-assisted (TA) profile, (d) hole-assisted (HA) profile [33].*

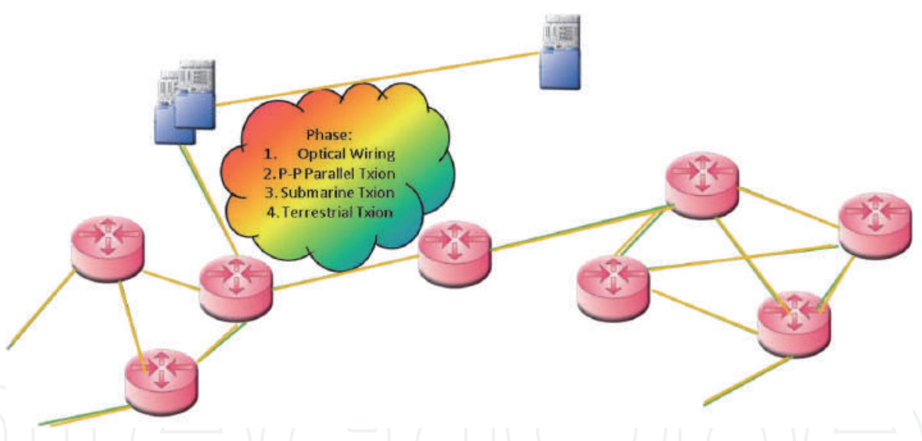


**Figure 8.**
*Schematic image of expansion phases of MCF technology [24].*

(e.g., optical amplifier, and node management technologies). To a large extent, central offices and/or data centres are the primary target for MCF technology since they are maintained and/or optimized separately by experienced operators, making it simpler to upgrade current network components. Here, compatibility with traditional SMF is very essential, especially for connection. Then, in the second deployment phase, we use MCF P2P and/or parallel transmission technology. MCF requires a flexible connection to the optical subsystems. Submarine transmission systems may offer more promise because of their use of the newest technology, and SDM might possibly achieve a power-efficient transmission system [34]. We have finally achieved flexible and dependable SDM nodes [24].

A FORECAST predicts that data center network traffic would increase at a 25% CAGR, with most traffic (about 70%) staying within the data center [35]. Modern data centers utilize dense non-blocking topologies with point-to-point optical transponder connections. Either on end servers or in slots of electronic switching devices, data is electrically switched. This resource-intensive paradigm may cause future data center scaling problems. Modern data center networks are increasingly relying on optical technologies like hybrid electrical-optical switching (HEOS). Recent demonstrations of a time-slotted pSSC and core-joint SDM optical switching system for edge applications [36].

SDM may improve network capacity by multiplexing SMF strands, multicore fiber cores, or even each mode of a few-mode fiber using MIMO digital signal processing [38]. Spatial Division Multiplexing-Elastic Optical Networks will then be the future of optical transport and data center networks (SDM-EON) [39]. MCF front haul multiplexes MIMO signals onto a single cable, enabling multiple optical data streams to be transmitted simultaneously. The MCF may also provide a single optical data signal to each antenna element, with varying delays and phases. Multi-antenna systems need MIMO and beamforming. The MCF front haul uses MIMO signals to transmit multiple optical data streams at the same wavelength. The MCF also uses optical data transmissions with variable phase or time delays to each antenna element. 5G systems need MIMO and beamforming capabilities. **Figure 9** shows a multi-antenna MCF-based RRH-to-remote-site connection with optical beamforming and/or digital MIMO capabilities. These methods enhance system performance.

The system capacity and accessible user bitrate may be enhanced by multiplexing MIMO data streams. A 22 MIMO LTE-A transmission using MCF technology was evaluated early. This research adds 44 MIMO transmission supported by a 4-core fiber capable of feeding four AEs concurrently. The M(22) arrays allow 5G systems to control multiple groups of four AEs. MCF may be used to reduce the size and complexity of beamforming systems. A same data signal is supplied by four separate AEs with varying delays, as shown in **Figure 9**. MCF aligns all optical lines in the beamforming system, simplifying the network [40].

In [36], Making fiber bundles revealed a 19-core MCF. A 7-core MCF Micro-lens array (MLA) claims 47.8 dB return loss and 0.87 dB insertion loss. Tapers were made, then cut apart to make fused fiber. Non-mode-selective, in which the modes spin on the device itself, and mode-selective, with minimal unitary rotation between modes. The most common components were lamps, phase plates, PLCs, and then mode selective PLCs. Ultrafast laser inscription can produce low loss 3D waveguides in conventional optical glass for MCFs. 3 mode FM-MCF fiber with average IL 0.92 and homogeneity 0.1.

SDM enthusiast offered considerable flexibility in fiber light mixing, integrated sensors and controllers. MCF technology has also been used to construct optical fiber sensors, which make them excellent for industrial applications. High

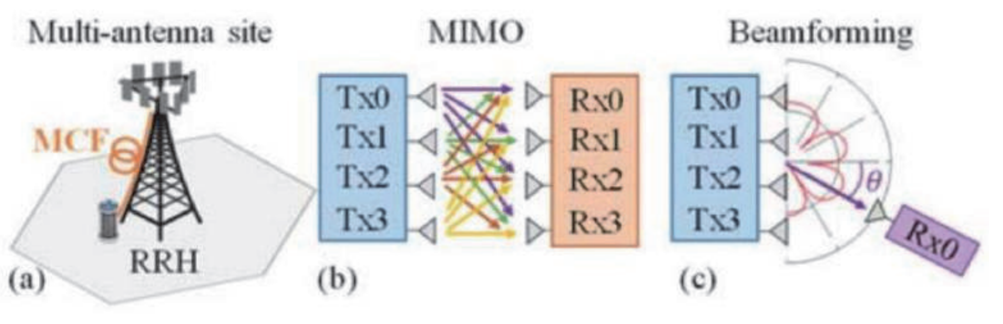


**Figure 9.**
*(a) A multi-antenna site application scenario in which the RRH is linked to the antenna components through MCF. Examples of four-antenna systems with (b) spatial multiplexing using 44 MIMO (4 distinct data streams coded in 4 layers) and (c) 41 beam forming (4 antennas transmitting the same data with different delays) [40].*

temperature sensing to 1000°C using MCF optical sensors with a typical temperature sensitivity of 170 pm/°C Mach–Zehnder (MZ) interferometers may be fabricated by employing MCFs since the slopes of the resultant interference peaks are steeper. Until quite recently, many MCF optical sensors used inefficient methods to throw light into the multi-arm MZ, causing substantial losses for QI processing [41] use novel tapering methods to construct the multi-arm MZ directly into a specially built MCF.

## 4. Key functional building blocks for next generation optical communication

Aspects of future network and technology MCF also requires FI/FO devices, connections, amplifiers, and integration technologies. This section covers the optical network equipment relevant to this research.

### 4.1 Space division multiplexer/demultiplexer

MCF technology uses SDM MUX/DEMUX. There are now numerous options, each with its own footprint, cost, capabilities, multi-mode affinity, etc. An SDM multiplexer or demultiplexer effectively links light between SMF fibers and SDM fiber modes or cores. Spatial MUXs are needed for SDM studies and may be used to link SMF and SDM networks in the future. This connection has been suggested in many creative ways. Direct and indirect coupling methods are widely classified. The optical signal is fully confined inside a waveguide during connection. **Figure 10** shows two typical layouts. As illustrated in **Figure 10**, the SMF cladding diameter is tapered to splice a bundle of SMFs to the SDM fiber. A photonic lantern is made by compressing MCF or SMF cores into an FMF. Alternatively, an unneeded

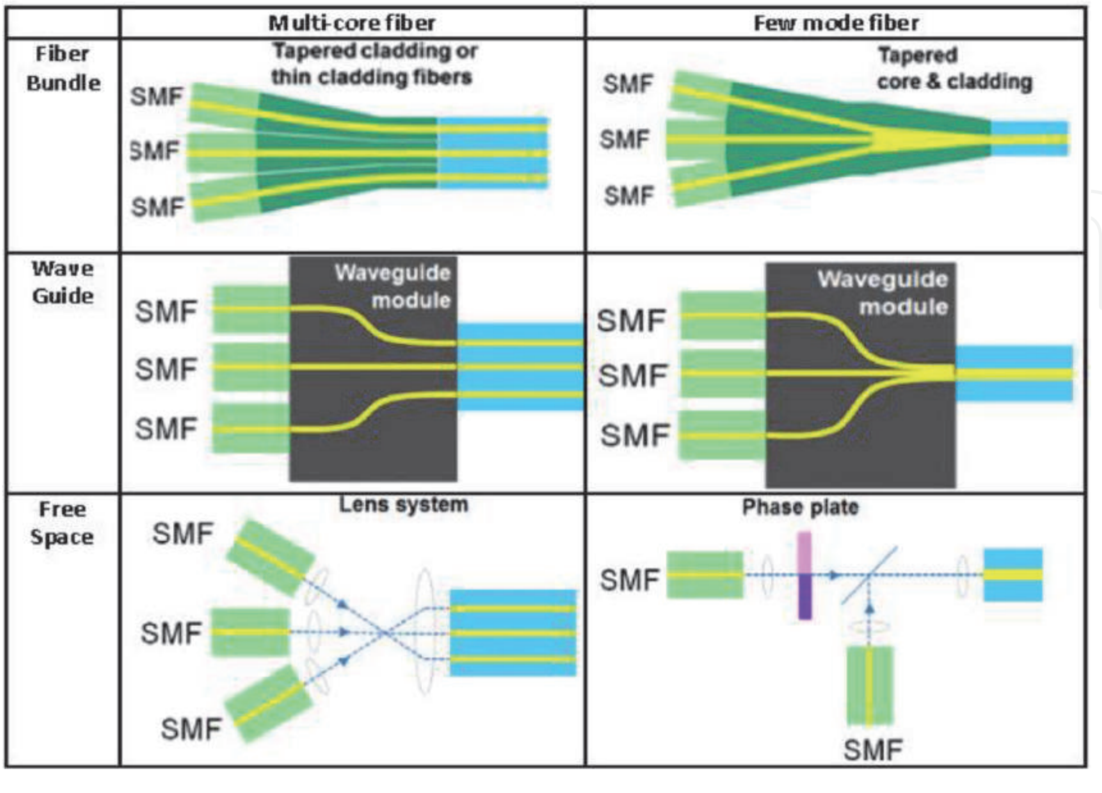


**Figure 10.**
*Fiber bundle, waveguide and free space MUX for MCF and FMF respectively [12].*

waveguide may be used. Inscribed light-guiding cores on a tiny glass block form the waveguide [12].

**Figure 10** shows the inscribed cores in the waveguide output plane separated by the MCF core separation. Input and output SMF arrays are connected using UV-cured glue. In addition to fiber producers, Chiral Photonics uses the fiber bundle technique often. Optoscribe's commercialized 3D waveguide technology is easy to incorporate with photonic integrated circuits (PICs). Indirect coupling uses bulk optics like lenses and prisms [12].

### 4.2 Transceiver

Transceivers are devices that combine the operations of a transmitter and a receiver into a single unit. They connect the network to a computer module in both directions. Their duty is to generate optical signals and then convert them to electronic data. Aside from the form factor and connectors, the optical and electrical properties are significant factors to consider throughout the selection process. The transmitter determines the wave properties of the transmission. The wavelength, spectral breadth, and transmission power are all critical parameters. Other transmitter characteristics include wave modes, reflections, and so on. To receive an optical signal, the receiver must be set to the proper wavelength. Furthermore, the signal's polarization and power must be compatible. Photo-diodes and other light-sensitive semiconductors transform optical impulses into electrical signals that may be monitored for data extraction. The received power must be within the detector's permitted range. If the power is too low, it is impossible to differentiate between signal and thermal noise, resulting in a poor signal-to-noise ratio. The detector gets overwhelmed if the received power is too high. Modulations of the luminous flux are not detectable. Overloading may permanently harm the detector and should therefore be avoided [42].

### 4.3 Connectors

Connectors are devices that connect optical wires. Connectors are required for SDM systems such as fusion splicing in terrestrial and submarine trunk networks. For a variety of cable types and transmission methods, many connection types have been created. Due to the fiber break, the link transmission is lossy. Lenses, end polishing, and forms are utilized to decrease attenuation. M-type connections were used for 7-core MCFs with an IL of 0.13 dB and a 500-fold improvement in MTBF. A multi-fiber MPO connection with over 40 dB return loss and 0.85 dB IL. A 7-core MCF connection with a return loss of 45 dB and an MPO connector for four 7-core fibers with a return loss of 0.3 dB are also shown in the study.

### 4.4 Amplifiers

Erbium-doped MCF amplifiers may be constructed utilizing separate pump lasers. Sharing pumps across multiple cores enhances power efficiency. Another approach is to pump the MCF's cladding, which is outfitted with multi-mode lasers. To achieve greater efficiency than an array of SSMF EDFAs, more power must be injected [43].

### 4.5 Switches

A network's heart is comprised of switches. Switches manage signal paths between nodes. In traditional copper networks, this routing is based on data packet IDs. Routing in optical networks, on the other hand, may be based on physical

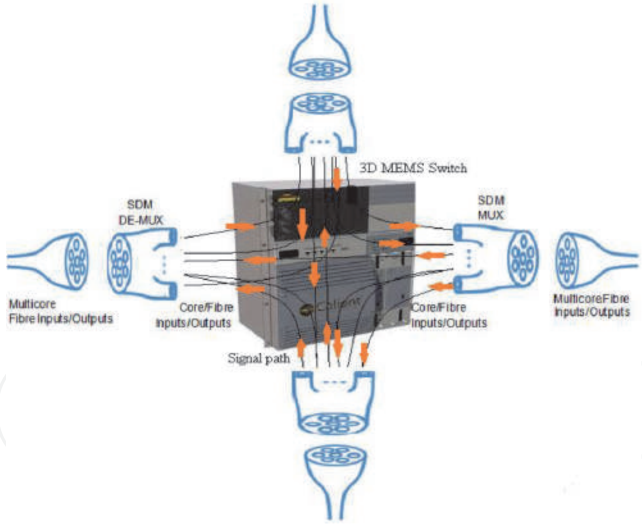


**Figure 11.**
*Core switching with spectrum contiguity within an optical network that uses multi-core fiber transmission.*

signal properties. This may be the wavelength in WDM or the core in multi-core fiber transmission, for example.

**Figure 11** is an example of a signal route in a switch. All the linked wires has seven cores. Every signal has its own core. When routing a signal, it may be done dynamically or statically. The physical routing technique is switch-dependent, which means that different switch types will have different methodologies. Due to physical coupling effects between the various cores, the range of multi-core fiber technology is limited to km. The limited flexibility of single-core fibers is distinct from that of multi-core fibers [44].

Low-speed SDM optical switches are already promising technologies, and preliminary work on SDM optical switches based on MEMS or LCoS technologies has been done. This will benefit WAN networks that need high-layer packets to be routed directly into the optical domain. Optical fast-switching networks have never achieved broad adoption owing to building difficulties, quicker signal degradation, and lower-cost electronics.

These switching granularities arise from the spatial component of SDM networks: Space granularity (joint switching) is needed when all modes intermix. Fibers like FMFs have full wavelength granularity in fractional space. Recently, several papers on SDM optical switches have appeared. In [36], a heterogeneous WSS switches spatial channels in an FMF, SSMF array, and SC-MCF. [36] claims a three-port four-core MCF WSS for SDM with 34 dB crosstalk and IL under 2.2 dB. Reference depicts a silicon PIC with a 7 7 switching matrix (MZIs) with an insertion loss of [4.5, 7.0] dB. Acoustic-optical crystals may also be used to create SDM optical switches. **Figure 12** depicts a CJ-AOM switch for 7 spatial channels. A 10 second switching time with an insertion loss of 10 dB.

There are spectrum resources in each core in SDM-EONs. All Spectrum slots are created equal. Following the spectrum contiguity requirement implies the whole service must utilize the same spectrum slots along the lightpath. To keep spectrum continuity constraint in a fiber, service spectrum slots must be continuous in the spectral dimension. The OFDM method should be used for each core to enhance spectrum efficiency. Spatially and spectrally resolved optical switching fibers are made as shown in **Figure 13**. In the optical switching fabric, core, fiber, and spectrum switching may be accomplished, which enables flexible channel addition, removal, and wavelength-level granularity channel switching. A transceiver pool supplies the necessary sub-transceivers for the different communication

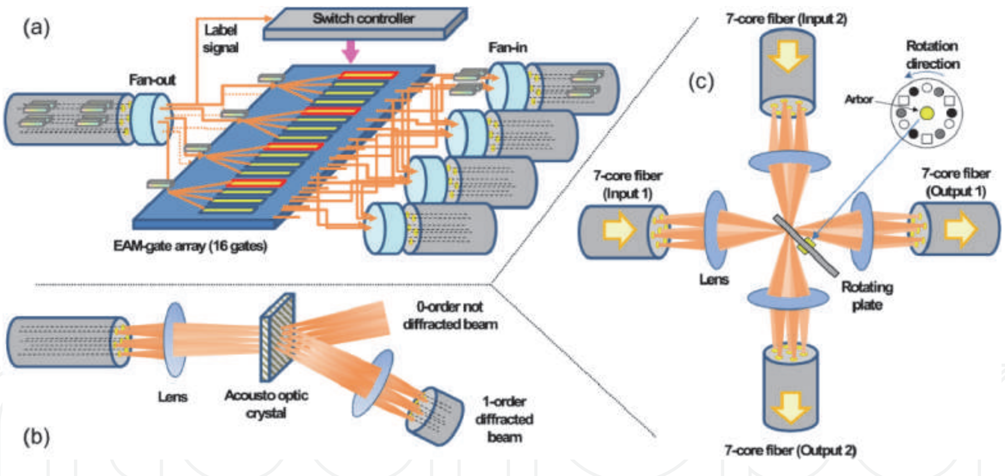


**Figure 12.**
*(a) Core-joint electro-absorption switch diagram, (b) core-joint acousto-optical modulator switch diagram, and (c) core-joint mirror switch diagram [36].*

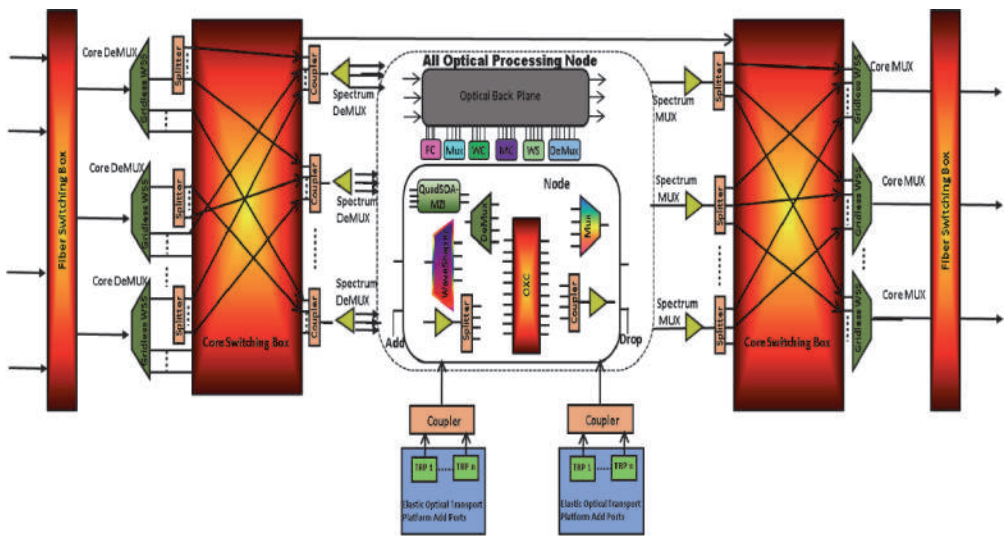


**Figure 13.**
*Spatially and spectrally resolved optical switching fabric.*

requirements. To overcome the spectrum contiguity restriction, spectrum slots in the switch fabric may be swapped between various cores. To summarize, it is possible to flexibly move signal cores without losing spectrum.

## 5. Limitation

Researchers all around the globe are working to reduce problems in order to attain ultra-low signal distortions in fiber optic technology [45]. However, high-capacity transmission systems place extra importance on network reliability [46]. It has gotten a lot of attention as a promising technique for dealing with the capacity limitations that are associated with single-core SMFs and cable size limitations like in datacenter networks and Passive Optical Networks (PONs) (which require high fiber count and high-density). Also, MCFs provide redundant signal lines and primary signal lines, which enable them to construct extremely dependable networks [47].

### 5.1 Cross talk

MCF is currently actively researched for SDM. SDM-based long-haul transmission requires low-crosstalk (XT) architecture. MCF transmission presents an

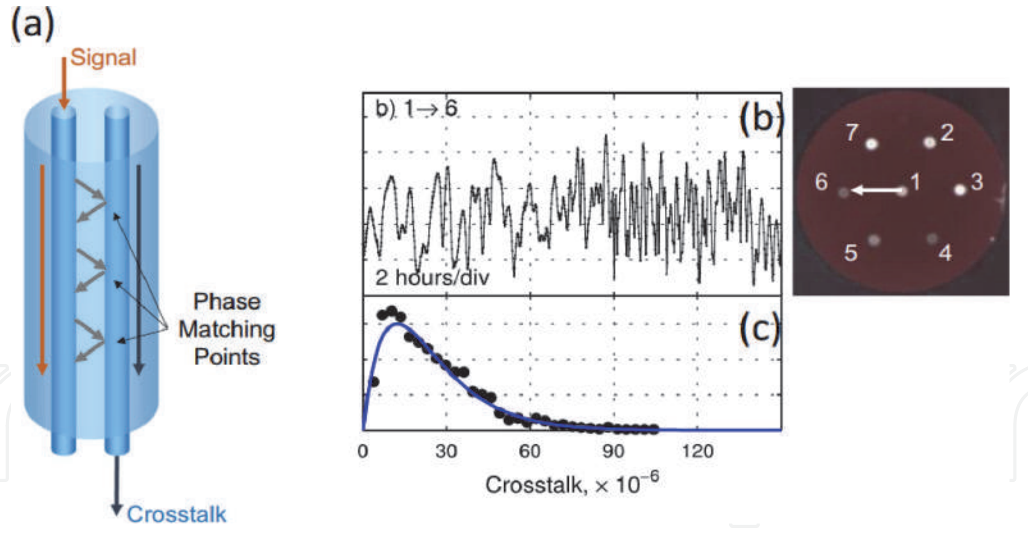


**Figure 14.**
*(a) Mechanism of inter-core crosstalk, (b) time evolution of XT, (c) histogram of XT [12].*

immense difficulty because to crosstalk, which may decrease the quality of optical data, caused by unintentional coupling between cores running in the same direction and wavelength, as shown in **Figure 14**.

Transmission is hampered by crosstalk in an MCF-based optical network, which may be reduced via power and mode coupling. So cladding widths vary. The cladding's strength decreases with increasing diameter. Each of these parameters must be changed. The MCF inter-core crosstalk is now calculated using coupled-mode and coupled power theories. First, MCF systems must agree on allowable crosstalk per length. Modern coherent optical communication systems have MCF crosstalk requirements regardless of transmission distance. Tolerable crosstalk has penalties for capacity, reach, universality transponder installation, and system link implementation [48, 49].

Ratio-reach trade-off of optical transponders capable of fine-tuning their modulation format to the channel circumstances through methods like probabilistic constellation shaping (PCS) for Nyquist pulses,

$$SE = 2.\log_2\left[1 + \frac{1}{\eta_{TRX}}\frac{P_S}{\left(\eta_L P_{ASE} + \chi P_S^3 + kP_s\right)}\right] \quad (1)$$

where $\text{SNR} = \frac{P_S}{\left(\eta_L P_{ASE} + \chi P_S^3 + kP_s\right)}$.

Ps is the per-channel (dual-polarization) signal launch power, and PASE is the per-channel (dual-polarization) amplified spontaneous emission power. For example, non-perfect amplification causes noise enhancement, beginning with PASE as the ASE from ideal distributed amplification. The parameter represents nonlinear interference noise (NLIN) and is calculated utilizing [50] formalisms. It indicates the average XT power due to other signals co-propagating at the same wavelength in different MCF cores. In the low coupling regime studied here, XT may be represented as AWGN, k increases linearly with distance, and interactions between XT and fiber nonlinearities can be disregarded.

MCF optical network crosstalk research for spectrum and fiber core allocations are many. As a consequence, to reduce crosstalk, all of the methods suggested reduced network capacity. A nearby core is already transmitting data on the same wavelength, therefore they do not send data on it. Recent work in [51] shows that optical signal counter-propagation across MCF cores may decrease crosstalk.

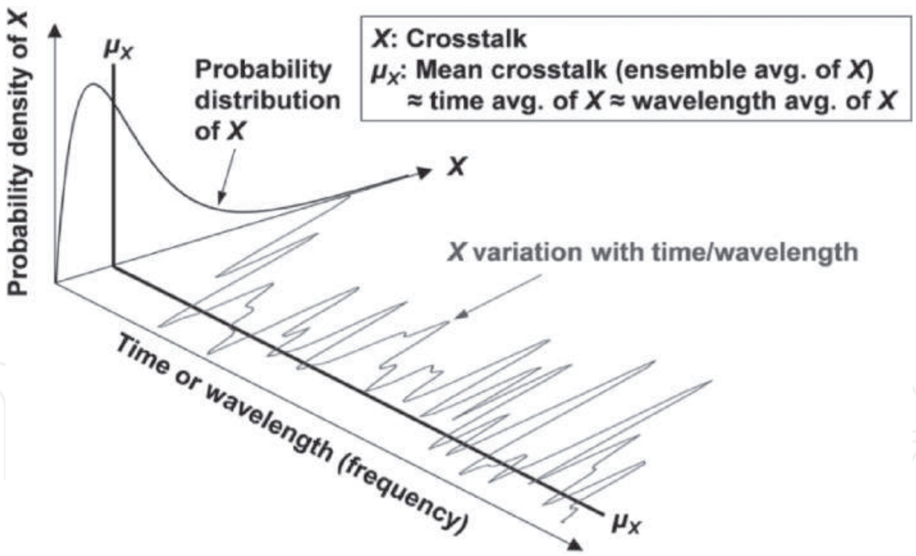


**Figure 15.**
*Schematic diagram explaining stochastic behaviors and statistical parameters of XT in MCF [28].*

**Figure 15** shows XT's stochastic nature. The ensemble average X is characterized by the unpredictability of its behavior. The values of X are present in the MCF literature, but not explicitly stated. The instantaneous frequency of light is constant while the spectrum of the signal light is flat. Components of XT components that are sufficiently broad act as Gaussian noise, also called ASE noise, or nonlinear interference noise.

## 5.2 Non linearity

As a result of the numerous nonlinear distortions, the traditional single mode fiber properties are harmed. Many kinds of SDM fibers have been proposed. In all optical transmission and network scenarios, no single SDM fiber seems to be better than parallel SMF or ribbon fiber. To mention a few, connected core MCFs (CC-MCFs) have shown to be more resistant to non-linearity, resulting in a longer transmission distance as well as processing and amplification benefits. However, FMFs or FM-MCFs have more spatial channels per cladding diameter, making them more suited for short-distance, high-capacity connections [12, 17].

### *5.2.1 Self phase modulation (SPM)*

The intensity dependence of the refractive index is the main source of SPM (i.e. optical Kerr effect). The change in refractive index as the signal passes through the fiber. Positive and negative refractive index gradients have leading and trailing edges. The total load at the user end of a PoF connection is dictated by the PV cell's conversion efficiency (detector). Eq. (2) states the mathematical connection, Eq. (3).

$$P_{load} = P_{in} * \eta_{pv} \tag{2}$$

$$P_{in} = \frac{P_{load}}{\eta_{pv}} \tag{3}$$

The nonlinear phase change due the SPM is given by the Eq. (**4**).

$$\varphi_{nl} = k_{nl} * P_{in} * L_{eff} \tag{4}$$

Where $k_{nl}$ denotes the nonlinear component of the propagation constant and $L_{eff}$ denotes the effective length. The following phase equation may be recast in terms of $P_{load}$, demonstrating that the nonlinear phase distortion in Eq is caused by load power (5).

$$\varphi_{nl} = k_{nl} * \frac{P_{load}}{\eta_{pv}} * L_{eff} \tag{5}$$

*5.2.2 Cross phase modulation (XPM)*

It is a nonlinear optical phenomenon produced by intensity changes in refractive index. XPM is guided by SPM since both rely on the refractive index and intensity of separate transmission pulses. Asymmetric spectrum broadening and signal distortion are caused by power and refractive index changes. The effective refractive index is given by Eq. (6).

$$\eta eff = \eta\,\mathrm{l} + \eta\mathrm{nl}\left(\frac{P_{in}}{A_{eff}}\right) \tag{6}$$

This is the linear component of the refractive index profile. Similarly, as seen in Eq., the propagating constant is defined as linear and nonlinear (7)

$$k_{eff} = k_l + k_{nl} * A_{eff} \tag{7}$$

The effective refractive index and propagation constant are proportional to the effective area. It is possible that the number of cores required for high power applications has a substantial effect on the link's nonlinear distortion. Also in Eq., the core multiplicity factor [21] and N-number of core and D-cladding diameters define the $A_{eff}$ (8)

$$A_{eff} = \left[CMF * \left(\frac{D}{2}\right)^2 * \pi\right]/N \tag{8}$$

Thus the Eq. (7) can be re written

$$\eta_{eff} = \eta_l + \eta_{nl}\frac{N}{CMF * (D/2)^2 * \pi} \tag{9}$$

According to Eq. (9), the effective refractive index (cause of XPM) is likewise affected by the number of cores in MCF.

*5.2.3 Stimulated Raman scattering (SRS)*

MCF has a large doped area where several optical beams may propagate. SRS is created when nonlinear acoustic vibrations interact with optical photons. The overlapping of the signal and pump electric fields at different excitation settings determines SRS efficacy. The effect of SRS for MCF for PoF connection has not been investigated. Because $A_{eff}$ and $L_{eff}$ influence threshold power, the number of cores, cladding diameter, and input pump power impact output power. Long-distance transmission weakens power signals, and optical beams' frequency changes downstream, producing signal loss [52].

#### *5.2.4 Stimulated Brillouin scattering (SBS)*

The performance of every optical link is affected by scattering. The number of cores improves the fiber's high power transmission capacity while decreasing the back scattered photon power, which influences the medium's nonlinearity and the acoustic photon. Within the core region, both weakly and strongly connected cores may be linear, triangular, rectangular matrix, tightly spaced hexagonal, or any other symmetric or asymmetric structure. The small core pitch type fiber has the greatest crosstalk and possible photo interaction. A PoF connection's maximal optical power transmission is limited by this interaction. Since the large numerical aperture (NA) is responsible for beam diffraction, the number of cores determines the SBS threshold. SBS changes depending on the medium's characteristics (homogeneous or birefringent) and the optical source. The thermally generated photon field affects the spectral breadth. The temperature of the fiber and its surroundings induce heat dispersion. The strain produced by internal heat may damage the fiber, reducing the output optical power. SBS has a lower effect on MCF than single mode fiber [53].

#### *5.2.5 Optical pulse compression*

MCF uses pulse compression and combination extensively. All MCF cores combine the injected optical signal. Structure and density determine signal compression. The MCF's nonlinearity produces self-focusing, anomalous dispersion, and wave collapse at high power levels. Due to the constant distance between MCF cores, the spatial non-uniformity of coupling is very important. The coupling coefficient, which determines Gaussian statistics, fluctuates with distance. Inhomogeneity in coupling causes phase mismatches and pulse delays that require special care [54].

#### *5.2.6 Capacity wastage*

If network capacity is bidirectional, overusing data centers wastes considerable capacity. To minimize MCF network effects, we asymmetrically distribute the fiber cores. It minimizes inter-core interference and allows for varying the amount of fiber cores on each side of a fiber connection. This minimizes network capacity wastage owing to mismatched bidirectional traffic demand. The suggested approach is tested on the MCF optical network's routing, spectrum, and core assignment (RSCA) problems. Two ILP models and a graph-based heuristic method are suggested to improve network spectrum usage [51].

## 6. Conclusion and future direction

Over the last decade, it has become apparent that MCF technologies are the only viable solution to the optical network's "capacity crunch" and other issues. Due to fiber nonlinearity, which limits growing transmission power and amplifier bandwidth. MCF should be operating by 2025. SDM's endurance and demand for telecommunications services must be shown. MCF just exceeded SSMF's maximum capacity. Increased capacity, dependability, and cost-effectiveness are required to allow broad use. New possibilities in multi-mode, spatial coding, and efficient DSP are anticipated to improve the performance of next-generation optical communication systems. This chapter examines the realities of multi-core fiber-based SDM optical wiring. The most common SDM fiber is the UC-MCF. SDM fibers use MIMO DSP to cope with modal XT.

Bidirectional traffic demand asymmetry is growing, leading to substantial capacity waste while building and running an optical transport network. Asymmetric and counter-propagating MCF fiber core allocation is advised for MCF optical networks. Assigning a flexible number of fiber cores in opposing directions to reduce network capacity waste owing to asymmetric traffic demand.

Inter-core crosstalk and traffic demand imbalance are significant factors in MCF optical network design. This network's design reduces inter-core crosstalk and capacity waste owing to bidirectional traffic demand imbalance.

Assemblies and PIC fabrication procedures are all part of SDM. When light couples the fibers, the cores converge and link the PICs. It includes extending the cores and attaching them to the PIC entrances through photonic wire bonding. Complicated handling and fusing are needed, but time-control introduces propagation delays.

Power over fiber technique uses multicore fiber structures. This chapter examined various MCF variations. The hexagonal MCF form is recommended for high power applications. Our MCF losses were also addressed. Nonlinear distortions in MCF act differently than in SMF. Some nonlinearity compensating methods, such pre-distortion, may also help reduce the impact of such distortions. The fiber cores, modes, or a mix of both provide new difficulties and possibilities for future research.

## Acknowledgements

We thank Dr. Muneer Azam for assistance with particular for comments that greatly improved the manuscript.

IntechOpen

## Author details

Muhammad Irfan Anis* and Hamdan Ali
High Performance Research Group, FEST, Iqra University, Karachi, Pakistan

*Address all correspondence to: mirfananis@iqra.edu.pk

IntechOpen

© 2021 The Author(s). Licensee IntechOpen. This chapter is distributed under the terms of the Creative Commons Attribution License (http://creativecommons.org/licenses/by/3.0), which permits unrestricted use, distribution, and reproduction in any medium, provided the original work is properly cited. (cc) BY

## References


[1] H. Furukawa and R. S. Luis, “Petabit-class Optical Networks Based on Spatial-Division Multiplexing Technologies,” *2020 24th Int. Conf. Opt. Netw. Des. Model. ONDM 2020*, pp. 21–23, 2020, doi: 10.23919/ONDM48393.2020.9132998.

[2] Mansour A, Mesleh R, Abaza M. New challenges in wireless and free space optical communications. Opt. Lasers Eng. 2016;**89**:95-108. DOI: 10.1016/j.optlaseng.2016.03.027

[3] Al-zubaidi FMA. *Towards High Bandwidth Communication Systems : From Multi-Gbit / s over SI-POF in Home Scenarios to 5G Cellular Networks over SMF by*, no. May. 2021

[4] Y. Sagae, T. Matsui, T. Sakamoto, and K. Nakajima, “Ultra-Low Crosstalk Multi-Core Fiber with Standard 125-$µ$m Cladding Diameter for 10,000 km-Class Long-Haul Transmission,” *IEICE Trans. Commun.*, p. 2019OBI0001, 2020.

[5] T. Matsui *et al.*, “Multi-Core Fiber with Standard Cladding Diameter,” pp. 4–5.

[6] Matsui T, Sagae Y, Sakamoto T, Nakajima K. Design and applicability of multi-core fibers with standard cladding diameter. J. Light. Technol. 2020;**38**(21): 6065-6070. DOI: 10.1109/JLT.2020.3004824

[7] Zhao Y, Hu L, Zhu R, Yu X, Wang X, Zhang J. Crosstalk-Aware Spectrum Defragmentation Based on Spectrum Compactness in Space Division Multiplexing Enabled Elastic Optical Networks with Multicore Fiber. IEEE Access. 2018;**6**(4):15346-15355. DOI: 10.1109/ACCESS.2018.2795102

[8] Kitayama KI, Diamantopoulos NP. Few-Mode Optical Fibers: Original Motivation and Recent Progress. IEEE Commun. Mag. 2017;**55**(8):163-169. DOI: 10.1109/MCOM.2017.1600876

[9] Kareem FQ et al. A Survey of Optical Fiber Communications: Challenges and Processing Time Influences. Asian J. Res. Comput. Sci. 2021;**7**(4):48-58. DOI: 10.9734/ajrcos/2021/v7i430188

[10] Van Weerdenburg J et al. 138-Tb/s Mode- and Wavelength-Multiplexed Transmission over Six-Mode Graded-Index Fiber. J. Light. Technol. 2018; **36**(6):1369-1374. DOI: 10.1109/JLT.2018.2791100

[11] Y. Awaji, “Review of space-division multiplexing technologies in optical communications,” *IEICE Trans. Commun.*, no. 1, 2019, doi: 10.1587/transcom.2017EBI0002.

[12] Awaji Y et al. High-capacity transmission over multi-core fibers. Opt. Fiber Technol. 2017;**35**:100-107. DOI: 10.1016/j.yofte.2016.09.008

[13] Y. Xie, L. Pei, J. Sun, J. Zheng, T. Ning, and J. Li, “Optimal design of a bend-insensitive heterogeneous MCF with differential inner-cladding structure and identical cores,” *Opt. Fiber Technol.*, vol. 53, no. March, p. 102001, 2019, doi: 10.1016/j.yofte.2019.102001.

[14] Y. Xie, L. Pei, J. Zheng, Q. Zhao, T. Ning, and J. Li, “Low-DMD and low-crosstalk few-mode multi-core fiber with air-trench/holes assisted graded-index profile,” *Opt. Commun.*, vol. 474, no. June, p. 126155, 2020, doi: 10.1016/j.optcom.2020.126155.

[15] C. Antonelli, G. Riccardi, T. Hayashi, and A. Mecozzi, “Role of polarization-mode coupling in the crosstalk between cores of weakly-coupled multi-core fibers,” *Opt. Express*, vol. 28, no. 9, p. 12847, 2020, doi: 10.1364/oe.391092.

[16] H. Yuan *et al.*, "Experimental Analysis on Variations and Accuracy of Crosstalk in Trench-Assisted Multi-core Fibers," pp. 1–14, 2020, [Online]. Available: http://arxiv.org/abs/2008.08034.

[17] A. K. Vyas, "Analysis of different structure and nonlinear distortion of multicore fiber for power over fiber applications," *Optik (Stuttg).*, vol. 168, pp. 184–191, 2018, doi: 10.1016/j.ijleo.2018.04.106.

[18] Shibahara K, Mizuno T, Lee D, Miyamoto Y. Advanced MIMO Signal Processing Techniques Enabling Long-Haul Dense SDM Transmissions. J. Light. Technol. 2018;**36**(2):336-348. DOI: 10.1109/JLT.2017.2764928

[19] I. Morita, K. Igarashi, H. Takahashi, T. Tsuritani, and M. Suzuki, "Trans-oceanic class ultra-long-haul transmission using multi-core fiber," *Opt. Express*, vol. 22, no. 26, p. 31761, 2014, doi: 10.1364/oe.22.031761.

[20] Mendinueta JMD, Shinada S, Hirota Y, Luis RS, Furukawa H, Wada N. Converged inter/intradata center optical network with packet super-channels and 83.33 Tb/s/port. J. Light. Technol. 2019;**37**(2):571-578. DOI: 10.1109/JLT.2018.2877815

[21] M. Jiang, C. Chen, B. Zhu, and F. Hu, "MIMO-free WDM–MDM bidirectional transmission over OM3 MMF," *Opt. Commun.*, vol. 473, no. April, p. 125988, 2020, doi: 10.1016/j.optcom.2020.125988.

[22] K. Nakajima, T. Matsui, K. Saito, T. Sakamoto, and N. Araki, "Space division multiplexing technology: Next generation optical communication strategy," in *2016 ITU Kaleidoscope: ICTs for a Sustainable World (ITU WT)*, 2016, pp. 1–7.

[23] Kaur G, Kaur G, Sharma S. Performance optimization of broadband communication system using hybrid parametric amplifier. Int. J. Appl. Eng. Res. 2017;**12**(14):4484-4490

[24] Nakajima K, Matsui T, Saito K, Sakamoto T, Araki N. Multi-core fiber technology: next generation optical communication strategy. IEEE Commun. Stand. Mag. 2017;**1**(3):38-45

[25] Sakamoto T et al. Spatial Density and Splicing Characteristic Optimized Few-Mode Multi-Core Fiber. J. Light. Technol. 2020;**38**(16):4490-4496. DOI: 10.1109/JLT.2020.2987351

[26] T. Hayashi *et al.*, "Field-Deployed Multi-Core Fiber Testbed," *OECC/PSC 2019 - 24th Optoelectron. Commun. Conf. Conf. Photonics Switch. Comput. 2019*, pp. 1–3, 2019, doi: 10.23919/PS.2019.8818058.

[27] B. J. Puttnam *et al.*, "Characteristics of homogeneous multi-core fibers for SDM transmission," *APL Photonics*, vol. 4, no. 2, 2019, doi: 10.1063/1.5048537.

[28] T. Hayashi and T. Nakanishi, "Multi-core optical fibers for the next-generation communications," *SEI Tech. Rev.*, no. 86, pp. 23–28, 2018.

[29] T. Hayashi, T. Taru, O. Shimakawa, T. Sasaki, and E. Sasaoka, "Uncoupled multi-core fiber enhancing signal-to-noise ratio," *Opt. Express*, vol. 20, no. 26, p. B94, 2012, doi: 10.1364/oe.20.000b94.

[30] Puttnam BJ et al. 0.61 Pb/s S, C, and L-Band Transmission in a 125μm Diameter 4-Core Fiber Using a Single Wideband Comb Source. J. Light. Technol. 2021;**39**(4):1027-1032. DOI: 10.1109/JLT.2020.2990987

[31] Cho J et al. Trans-Atlantic Field Trial Using High Spectral Efficiency Probabilistically Shaped 64-QAM and Single-Carrier Real-Time 250-Gb/s 16-QAM. J. Light. Technol. 2018;**36**(1):103-113. DOI: 10.1109/JLT.2017.2776840

[32] Peng G-D. *Handbook of Optical Fibers*. Springer; 2019

[33] Xie X, Tu J, Zhou X, Long K, Saitoh K. Design and optimization of 32-core rod/trench assisted square-lattice structured single-mode multi-core fiber. Opt. Express. 2017;**25**(5):5119-5132

[34] A. Turukhin *et al.*, "105.1 Tb/s power-efficient transmission over 14,350 km using a 12-core fiber," *2016 Opt. Fiber Commun. Conf. Exhib. OFC 2016*, pp. 105–107, 2016, doi: 10.1364/ofc.2016.th4c.1.

[35] Z. Luo, S. Yin, L. Jiang, L. Zhao, and S. Huang, "Routing, Spectrum and Core Assignment based on Auxiliary Matrix in the Intra Data Center Networks using Multi-Core Fibers with Super Channel," in *Asia Communications and Photonics Conference/International Conference on Information Photonics and Optical Communications 2020 (ACP/IPOC)*, 2020, p. M4A.279, doi: 10.1364/ACPC.2020.M4A.279.

[36] J. M. D. Mendinueta, S. Shinada, Y. Hirota, H. Furukawa, and N. Wada, "High-Capacity Super-Channel-Enabled Multi-Core Fiber Optical Switching System for Converged Inter/Intra Data Center and Edge Optical Networks," *IEEE J. Sel. Top. Quantum Electron.*, vol. 26, no. 4, 2020, doi: 10.1109/JSTQE.2020.2969558.

[37] V. N. Korshunov, I. A. Ovchinnikova, S. S. Shavrin, N. A. Shishova, and A. Y. Tsym, "Spectral Efficiency and Information Transfer Rate over Optical Fibers in Spatial Parallelism," 2020 Syst. Signals Gener. Process. F. Board Commun., vol. 4, no. 1, pp. 0–3, 2020, doi: 10.1109/IEEECONF48371.2020.9078609.

[38] García Cortijo S. Distributed radiofrequency signal processing based on space-division multiplexing fibers. Valencia (Spain): Universitat Politècnica de València; 2020

[39] Tang F, Li Y, Shen G, Rouskas GN. Minimizing inter-core crosstalk jointly in spatial, frequency, and time domains for scheduled lightpath demands in multi-core fiber-based elastic optical network. J. Light. Technol. 2020;**38**(20): 5595-5607

[40] M. Morant, A. M. Trinidad, E. Tangdiongga, and R. Llorente, "Multi-core Fiber Technology supporting MIMO and Photonic Beamforming in 5G Multi-Antenna Systems : (Invited paper)," *2019 IEEE Int. Top. Meet. Microw. Photonics, MWP 2019*, pp. 1–4, 2019, doi: 10.1109/MWP.2019.8892041.

[41] J. Cariñe *et al.*, "Multi-core fiber integrated multi-port beam splitters for quantum information processing," *Optica*, vol. 7, no. 5, p. 542, 2020, doi: 10.1364/optica.388912.

[42] B. Annighoefer, A. Zeyher, and J. Reinhart, "Multi-core Fiber and Power-limited Optical Network Topology Optimization with MILP," 2021, [Online]. Available: http://arxiv.org/abs/2103.16981.

[43] Lee SH. Experimental study. Sch. Res. Music. 2017:81-88. DOI: 10.4324/9781315458090

[44] A. Samir, J. Ratkoceri, and B. Batagelj, "Multi-core optical fiber in a passive optical local area network," in *2018 International Conference on Innovative Trends in Computer Engineering (ITCE)*, 2018, pp. 77–82.

[45] D. Kumar and R. Ranjan, "Crosstalk Suppression using Trench-assisted Technique in 9-core Homogeneous Multi Core Fiber," *2017 14th IEEE India Counc.* Int. Conf. INDICON *2017*, pp. 6–9, 2018, doi: 10.1109/INDICON.2017.8487586.

[46] Rademacher G et al. High Capacity Transmission in a Coupled-Core Three-Core Multi-Core Fiber. J. Light. Technol. 2021;**39**(3):757-762. DOI: 10.1109/JLT.2020.3013966

[47] Lee Y, Tanaka K, Hiruma K, Nomoto E, Sugawara T, Arimoto H. Experimental demonstration of a highly reliable multicore-fiber-based optical network. IEEE Photonics Technol. Lett. 2014;**26**(6):538-540. DOI: 10.1109/LPT.2013.2296100

[48] A. Macho Ortiz, "Multi-Core Fiber and Optical Supersymmetry: Theory and Applications," 2019.

[49] Gene JM, Winzer PJ. A universal specification for multicore fiber crosstalk. IEEE Photonics Technol. Lett. 2019;**31**(9):673-676. DOI: 10.1109/LPT.2019.2903717

[50] C. Antonelli, O. Golani, M. Shtaif, and A. Mecozzi, "Nonlinear interference noise in space-division multiplexed transmission through optical fibers," *Opt. Express*, vol. 25, no. 12, p. 13055, 2017, doi: 10.1364/oe.25.013055.

[51] Tang F, Yan Y, Peng L, Bose SK, Shen G. Crosstalk-Aware counter-propagating core assignment to reduce inter-core crosstalk and capacity wastage in multi-core fiber optical networks. J. Light. Technol. 2019;**37**(19):5010-5027. DOI: 10.1109/JLT.2019.2927025

[52] Ceballos-Herrera DE, Gutierrez-Castrejon R, Alvarez-Chavez JA. Stimulated raman scattering and four-wave mixing effects on crosstalk of multicore fibers. IEEE Photonics Technol. Lett. 2018;**30**(1):63-66. DOI: 10.1109/LPT.2017.2774501

[53] Z. Zhao, M. A. Soto, M. Tang, and L. Thévenaz, "Demonstration of distributed shape sensing based on Brillouin scattering in multi-core fibers," *25th Int.* Conf. Opt. Fiber Sensors, vol. 10323, p. 1032393, 2017, doi: 10.1117/12.2267486.

[54] A. M. Rubenchik, I. S. Chekhovskoy, M. P. Fedoruk, O. V. Shtyrina, and S. K. Turitsyn, "Nonlinear pulse combining and pulse compression in multi-core fibers," *Opt. Lett.*, vol. 40, no. 5, p. 721, 2015, doi: 10.1364/ol.40.000721.

# We are IntechOpen, the world's leading publisher of Open Access books
# Built by scientists, for scientists

**6,300**
Open access books available

**171,000**
International authors and editors

**190M**
Downloads

**154**
Countries delivered to

Our authors are among the
**TOP 1%**
most cited scientists

**12.2%**
Contributors from top 500 universities

WEB OF SCIENCE™

Selection of our books indexed in the Book Citation Index
in Web of Science™ Core Collection (BKCI)

Interested in publishing with us?
Contact book.department@intechopen.com

Numbers displayed above are based on latest data collected.
For more information visit www.intechopen.com

Chapter

# Functional Tapered Fiber Devices Using Polymeric Coatings

*Oscar González-Cortez, Rodolfo A. Carrillo-Betancourt, Juan Hernández-Cordero and Amado M. Velázquez-Benítez*

## Abstract

A wide variety of fiber devices can be created by adding special coatings on tapered sections of optical fibers. In this work we present the fundamentals for the fabrication of tapered optical fibers coated with functional polymers. The required aspects of light propagation in tapered sections of optical fibers are introduced and the relevant parameters enabling light interaction with external media are discussed. A special case of interest is the addition of polymeric coatings with prescribed thicknesses in the tapered sections allowing for adjusting the light propagation features. We assess the use of liquid polymer coatings with varying thicknesses along the taper profile that can be tailored for tuning the transmission features of the devices. Hence, we introduce a methodology for obtaining coatings with predefined geometries whose optical properties will depend on the polymer functionality. As demonstrated with numerical simulations, the use of functional polymer coatings in tapered optical fibers allows for obtaining a wide variety of functionalities. Thus, controlled polymer coating deposition may provide a simple means to fabricate fiber devices with adjustable transmission characteristics.

**Keywords:** Tapered fibers, thin coatings, polymers, evanescent wave

## 1. Introduction

Optical fiber-based devices and sensors have been widely used in many fields of science and technology for different applications. In most applications, the transmission of light through in-line fiber devices is modified by an external perturbation and this can be quantified through variations in one or more characteristic features of the guided optical wave. Although extrinsic interaction of the light with the surrounding media is possible, the use of the evanescent portion of the guided wave offers some advantages. Exposure of the optical wave to the surrounding media in specific sections of the optical fibers is usually done by two alternatives [1–5]: removing the cladding material, or upon tapering a section of the optical fiber. The latter is the preferred approach to expose the evanescent wave since it involves a simple and reproducible process yielding low-loss devices. Although the description and basics of tapering optical fibers have been described since early 1990's by Birks *et al.* [1], new applications for these devices have been a subject of research due to their potential use in many fields of science and technology. Some of these applications include physical and biomedical sensing [6–10], interferometry [11],


IntechOpen

excitation of surface plasmons [12, 13], atom detection [14, 15], and light coupling to micro-resonators [8, 16], just to name a few.

Tapering techniques and systems have evolved over the years resulting in optimized devices and standardized processes. As a result, tapering of optical fibers has been employed for modifying the light propagation conditions in fibers, and further allowing for the guided light to interact with other structures or materials. The latter capabilities allow for creating fiber-based devices incorporating coatings with controlled thicknesses and different optical properties. In this chapter we present the main aspects and basic guidelines for achieving a proper guidance of light through tapered devices providing also adequate interaction with the surrounding medium.

### 1.1 Basics of light propagation in optical fibers

Light propagation in optical fibers occurs within the fiber core (radius $a$) following the total internal reflection condition from Snell's law. Propagation conditions are defined by the physical characteristics of the core and cladding sections of the fiber: refractive indices and diameters. Due to the cylindrical geometry of the optical fibers and the small refractive index difference between the core and cladding materials, the propagating modes are obtained in a cylindrical coordinate system ($r$, $\varphi$, $\phi$) and in terms of Bessel equations [17, 18]. Rigorous analysis and proper boundary conditions are used to obtain mathematical expressions describing the components of the electric and magnetic fields for the core ($r \leq a$) and the cladding ($r \geq a$) regions. The combination of these propagating fields allows for an alternative description in terms of linearly polarized modes, denoted as $LP_{lm}$, in which $l$ and $m$ are respectively the axial and radial indices. As an example, the electric field for the set of $LP_{0m}$ modes can be shown to be given by:

$$E_{LP_{0m}} = \begin{cases} E_0 J_0\left(\frac{u\,r}{a}\right), & r \leq a \\ E_0 \frac{J_0(u)}{K_0(w)} K_0\left(\frac{w\,r}{a}\right), & r > a \end{cases}, \tag{1}$$

where $E_0$ is the field amplitude, $J_0$ is the zeroth-order Bessel function of the first kind, and $K_0$ is the zeroth-order modified Bessel function of the second kind. The parameters $u$ and $w$ are respectively the normalized propagation and attenuation constants, defined as:

$$u = a\sqrt{k^2 n_{core}^2 - \beta^2}, \quad w = a\sqrt{\beta^2 - k^2 n_{cladd}^2}, \tag{2}$$

involving the propagation constant of the guided wave ($\beta$), the wave number ($k$) and the refractive indices of the core ($n_{core}$) and the cladding ($n_{cladd}$). The description in terms of the $LP_{lm}$ modes is very useful as these can be experimentally observed as intensity patterns ($I_{lm}$) whose mathematical representations are [17]:

$$I_{lm} = \begin{cases} I_0 J_l^2\left(\frac{u\,r}{a}\right) sin^2(l\phi), & r \leq a \\ I_0 \left(\frac{J_l(u)}{K_l(w)}\right)^2 K_l^2\left(\frac{w\,r}{a}\right) sin^2(l\phi), & r > a \end{cases}. \tag{3}$$

Another important parameter to assess the modal features of an optical fiber is the normalized frequency or $V$ number, defined as:

$$V = \sqrt{u^2 - w^2} = \frac{2\pi a \sqrt{n_{core}^2 - n_{cladd}^2}}{\lambda}. \tag{4}$$

The normalized frequency is typically used as an indicator of how many modes are supported by the fiber. It can be shown that standard single mode fibers (SMFs) supporting only the fundamental ($LP_{01}$) mode have a $V < 2.405$. Hence, this condition is typically used as an indicator of single-mode propagation in an optical fiber.

### 1.2 Light propagation in tapered optical fibers

Tapered optical fibers are fabricated such that the physical dimensions of the core and cladding are reduced, thereby modifying the light propagation conditions [8, 19, 20]. The implication of this reduction in the physical dimensions of the fiber is a decrease in the effective refractive index of the core and thus a change in the light confinement. An effect caused by the core reduction is the compression of the light inside the core, although the evanescent wave increases in magnitude. However, there is a physical limit for the core reduction since the light cannot be effectively guided inside this region under certain conditions. After reaching this "guiding threshold" in the dimensions of the core, light escapes to the cladding material, which acts as the new core of the optical fiber while the surrounding media becomes the new cladding. As a consequence, the evanescent wave is effectively exposed to the external medium, granting the possibility of light interaction with different materials or structures.

Typically, tapered optical fibers are segmented in three sections for their analysis [1]: *the non-tapered segment of the optical fiber*, the *transition* and the *waist sections*, as depicted in **Figure 1a**. The waist section of the fiber is where the fiber is tapered down to its final diameter after which it remains constant across all its length. Usually, the interaction or coupling to other structures or materials takes place at this section. The transition sections of the fiber are those at which the diameter goes from the original diameter to the tapered section, and vice versa. Although the transition regions are commonly not used for sensing or coupling, they are significantly important as disturbances or non-desired alterations to light can occur in these sections. Such effects appear when the transition between diameters is not smooth or non-adiabatic.

Adiabaticity criteria comes from the tapering angle, which must be small enough for the fundamental mode to smoothly propagate across all the sections with minimal power loss [19]. Any sudden change in the dimensions or geometry of the fiber will provoke imminent light leaking from the core. This is avoided by performing the tapering process at a very slow rate. Considering the case of tapering a SMF, an adequate transition should maintain the fundamental mode through all the sections of the tapered fiber with negligible losses. Conversely, a non-adiabatic tapering

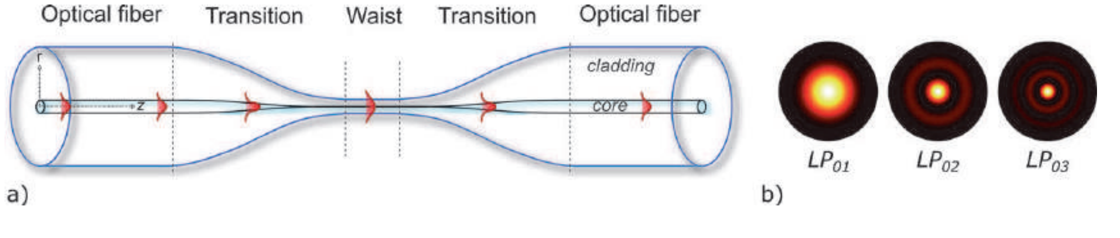


**Figure 1.**
*(a) Tapered optical fiber profile indicating the three zones: non-tapered, transition and waist. (b) Intensity distributions of the* $LP_{om}$ *modes excited in the transition section and propagating in the waist of the taper.*

process will produce a "leakage" of light into the cladding exciting higher order modes.

The parameter used to define the adiabaticity of the tapered fiber is the *local length-scale* of the taper ($z_t$), resulting from the ratio of the core radius ($r$) over the tapering angle ($\Omega$), expressed as $z_t = \frac{r}{\Omega}$. Notice that both variables ($r$ and $\Omega$) vary with length, i.e., $r = r(z)$ and $\Omega = \Omega(z)$ [19]. To achieve adiabaticity, the length of the taper must be larger than the length required to couple the fundamental mode to the predominant cladding mode. This coupling length is given by the beat length ($z_b$), which in turn depends on the propagation constant, $\beta = kn_{eff}$, with $k = \frac{2\pi}{\lambda}$. Thus, this variable is given by the expression [19]:

$$z_b = \frac{2\pi}{\beta_1 - \beta_{CM}}, \tag{5}$$

where $\beta_1$ is the propagation constant of the fundamental $LP_{01}$ mode, and $\beta_{CM}$ corresponds to the propagation constant of the excited cladding mode. In an axially symmetric tapered fiber, the fundamental mode will only couple to azimuthally symmetric higher order modes (i.e., the $LP_{0m}$ modes) supported by the cladding structure (see **Figure 1b**).

To illustrate the phenomena related to tapering optical fibers, we will use as an example a step-index standard single-mode silica fiber with core radius of 4.1 μm, cladding radius of 62.5 μm and refractive index difference $\Delta n = 0.061$. These are typical dimensions for the standard telecommunication fibers that are commonly used for the fabrication of tapered fibers for evanescent coupling of light to other photonic devices. Upon considering an adiabatic tapering process, firstly can be noticed that by reducing the core radius the $V$ number is also modified. This implies that the effective refractive index ($n_{eff}$) of the waveguide will be modified as well and thus the propagation constant. The solutions in terms of the Bessel approximations yield the values of the propagation constants ($\beta$) resulting from these changes in geometry [17, 18]. **Figure 2** shows results from numerical calculations illustrating that a reduction in the propagation constant is obtained as the core radius decreases. Notice also that for $V < 1$, a sudden decrease in $\beta$ occurs indicating that light cannot be longer confined in the core and hence it couples to the cladding material. Such

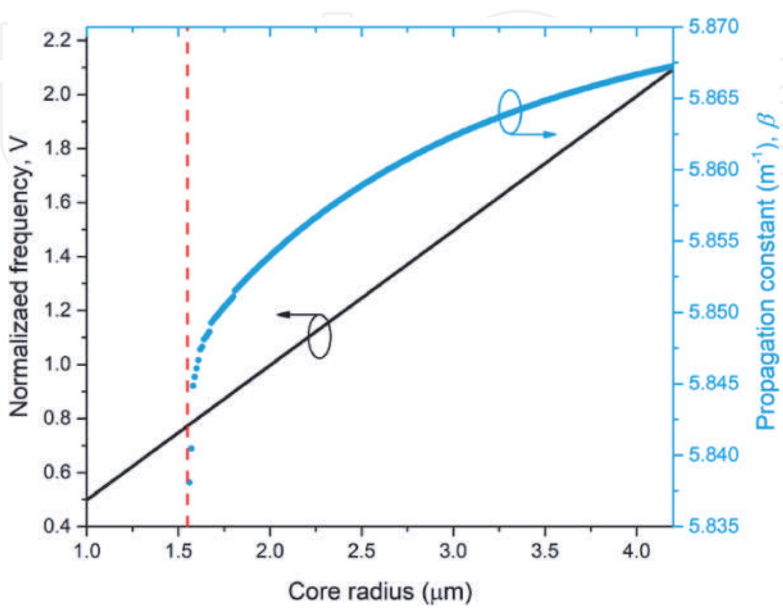


**Figure 2.**
*Variation of the normalized frequency (V) and propagation constant (β) for different core radii corresponding to different tapering ratios. The dashed line shows the "guiding threshold" of the fiber core.*

phenomenon implies that the whole material of the optical fiber, core and cladding, acts together as the new core of the waveguide, while the surrounding medium serves as the new cladding. The first reports on this phenomenon mention values for this guiding threshold $V_{TH}$ near 0.8 [8, 19] to achieve this condition. Our numerical results indicate that light confinement in the fiber core is sustained until $V_{TH} \approx 0.77$, which corresponds to an approximate core radius of 1.55 μm, as illustrated in **Figure 2**.

The intensity distribution of the fundamental mode is modified as the fiber is tapered. For core diameters above the guiding threshold, a tighter confinement of light within the core is achieved. However, the amount of light in the evanescent portion of the wave increases and so its extension inside the cladding. Once the guiding threshold is surpassed, light confinement shifts from the core to the cladding, distributing across the entire waist material. This effect is illustrated in **Figure 3**, showing light confinement at different tapering ratios. Instantly, as the guided light is exposed to the external media, light confinement and propagation are determined by the surrounding materials. At this stage, interaction with the surrounding media occurs via the evanescent wave. Nonetheless, the amount of light exposed to the external media can be tailored by defining the final waist diameter. For a fiber surrounded by air, due to the large refractive index difference with respect to the silica, the $V$ number substantially increases allowing to reduce the fiber core down to very small diameters. Subwavelength waist diameters have been reported for tapered fiber devices in sensing and other applications [8, 15, 21].

The wavelength of light is also relevant in this phenomenon as in every waveguiding structure. Light confinement in the fundamental mode will change depending on the wavelength, showing a larger amount of evanescent wave for

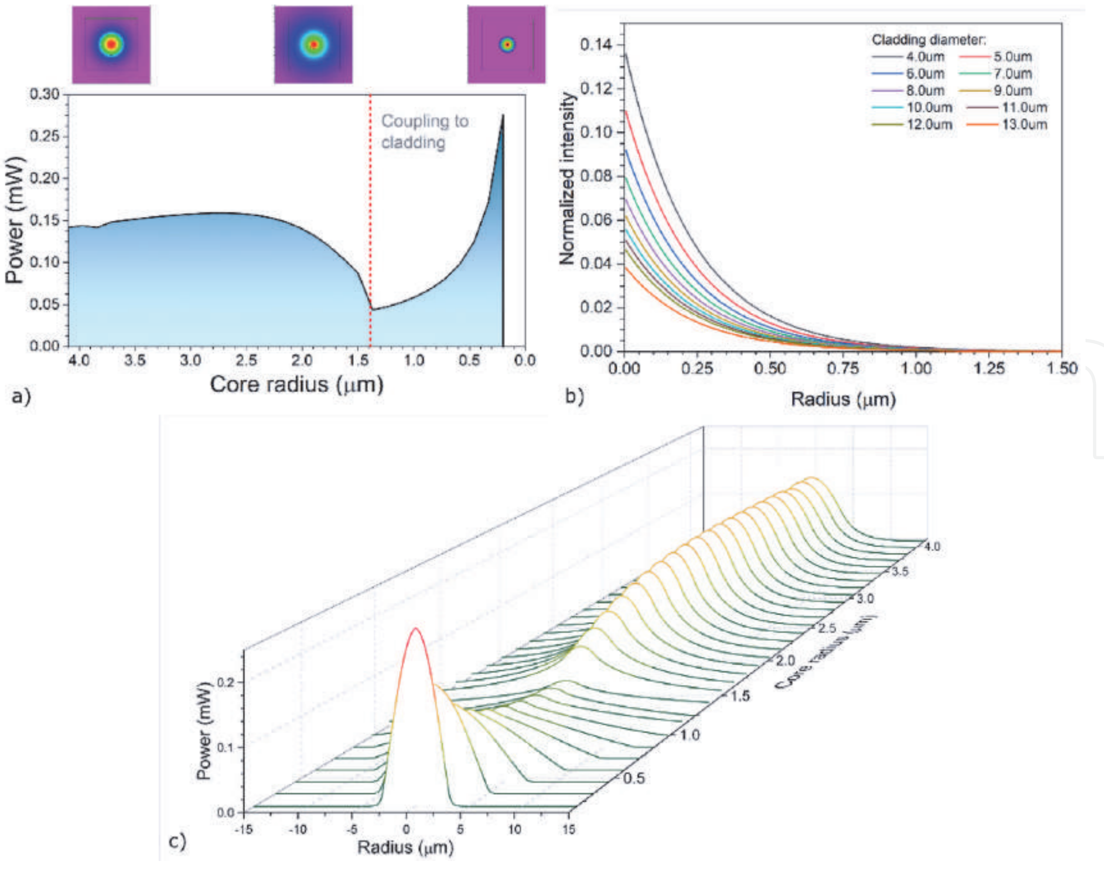


**Figure 3.**
*Light confinement in tapered optical fibers. Fundamental mode power evolution at different core radii corresponding to different tapering ratios: (a) peak power and (b) power distribution. (c) Evanescent wave extension for different tapering ratios.*

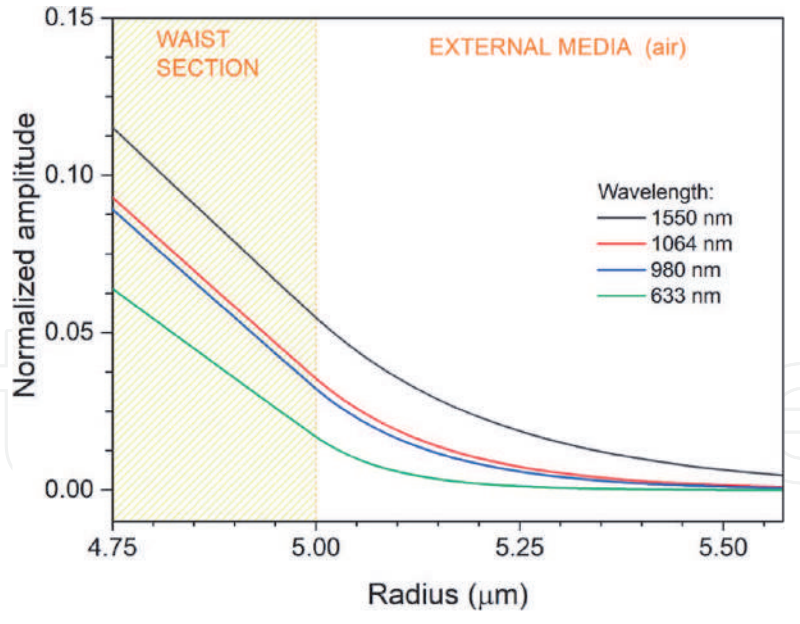


**Figure 4.**
*Wavelength dependence of the penetration of the evanescent wave of the fundamental mode to external media at the waist of a tapered optical fiber.*

longer wavelengths. Assuming an adiabatically tapered SMF with a 5 μm waist radius with air as the surrounding medium, the extension of the evanescent wave will present a significant increase as illustrated in **Figure 4**. Hence, for a given tapered device with specific dimensions, wavelength selection is essential as this will change the exposure and hence the interaction of the evanescent wave with the external medium.

Light exposure through evanescent wave is useful for the creation of functional devices by means of adding different materials as coatings. The amount of evanescent wave exposed to the surrounding media determines the range of coating thicknesses that can be effectively used for efficient interaction depending on the materials as well. The fundamentals of fiber coating and main aspects to consider for the creation of devices using diverse materials as coatings are discussed in the following sections.

## 2. Fiber coating

There are multiple reports using diverse techniques for coating optical fibers with tapered sections. We will focus on a method based on the deposition of liquid materials over specific sections of optical fibers since these are convenient for post-processing fibers. We consider in particular the use of liquid polymers as coating materials, since they offer a wide variety of functionalities. Polymers have been used for recoating fiber devices such as Bragg gratings, amplifiers or splices, just to mention the most important. Various works have demonstrated the effectiveness of using this technique for diverse purposes [22–25], and recoating systems to perform such task have been readily reported [26].

The process for deposition of controlled layer coatings on optical fibers using liquid materials, such as polymers, are suitably described by the wire coating technique [27–29]. This involves the immersion of the fiber into the liquid and retrieve it at a prescribed speed to obtain a desired thickness, as illustrated in **Figure 5**. The main factors involved in this process include the characteristics of the liquid such as viscosity ($\eta$) and surface tension ($\gamma$), and the velocity ($v$) at which the process takes

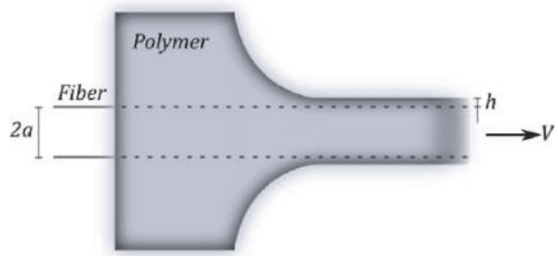


**Figure 5.**
*Wire coating technique scheme. A layer of coating material (thickness h) is left on the surface of the wire (radius a) by pulling the coating material at a constant velocity (v) through a liquid container.*

place. The ratio of the viscosity to the surface tension, multiplied by the velocity of the coating process, is defined as the capillary number, which allows to compare the behavior of different liquids. This ratio is a dimensionless number defined explicitly as $Ca = \eta v/\gamma$. For liquids with $Ca << 1$, the resulting coating thickness $(h)$ deposited on a fiber of radius $(a)$ can be obtained as [29]:

$$h = 1.34aCa^{2/3}. \quad (6)$$

This expression holds only for $Ca < 1$ since the fluid dynamics are different for larger values of the capillary number. Nonetheless, proper adjustments to this theory can be made yielding a correction factor for the thickness [30]. This wire coating theory has been largely investigated and described in the field of fluidics describing in detail multiple scenarios and materials.

Given the nature of the liquids, an additional factor to consider for their use as fiber coatings is the Rayleigh-Plateau instability [31]. This effect leads to the breakdown of the uniform layer into a periodic array of droplets. Such behavior will always occur at characteristic time $(t_0)$ given by:

$$t_0 = 12\frac{\eta(r+a)^4}{\gamma h^3}. \quad (7)$$

This is an important effect that must be considered when applying liquid coatings because it indicates the maximum time in which the liquid layer will remain with a uniform thickness. Therefore, the coating must be solidified before this characteristic time in order to preserve its shape. Hence, different polymeric materials cured by means of chemical, thermal or photo-active processes must account for this breakdown time.

## 3. Coatings on tapered optical fibers

In most cases, the coatings on the tapered sections of the fiber are sought to be with uniform thickness in order to obtain interaction with the evanescent wave. Ideally, only the waist section of the taper should be coated, as indicated in the green region in **Figure 6a**. However, there are two aspects that must be also considered when designing the coating: the actual exposition of the evanescent wave and the coating process itself. In practice, coating only the waist section of the tapered fiber might represent a challenging task since the liquid to be deposited is usually contained within a reservoir with prescribed dimensions that do not match the length of the waist. Extraction of the fiber from the reservoir can also be a potential factor to

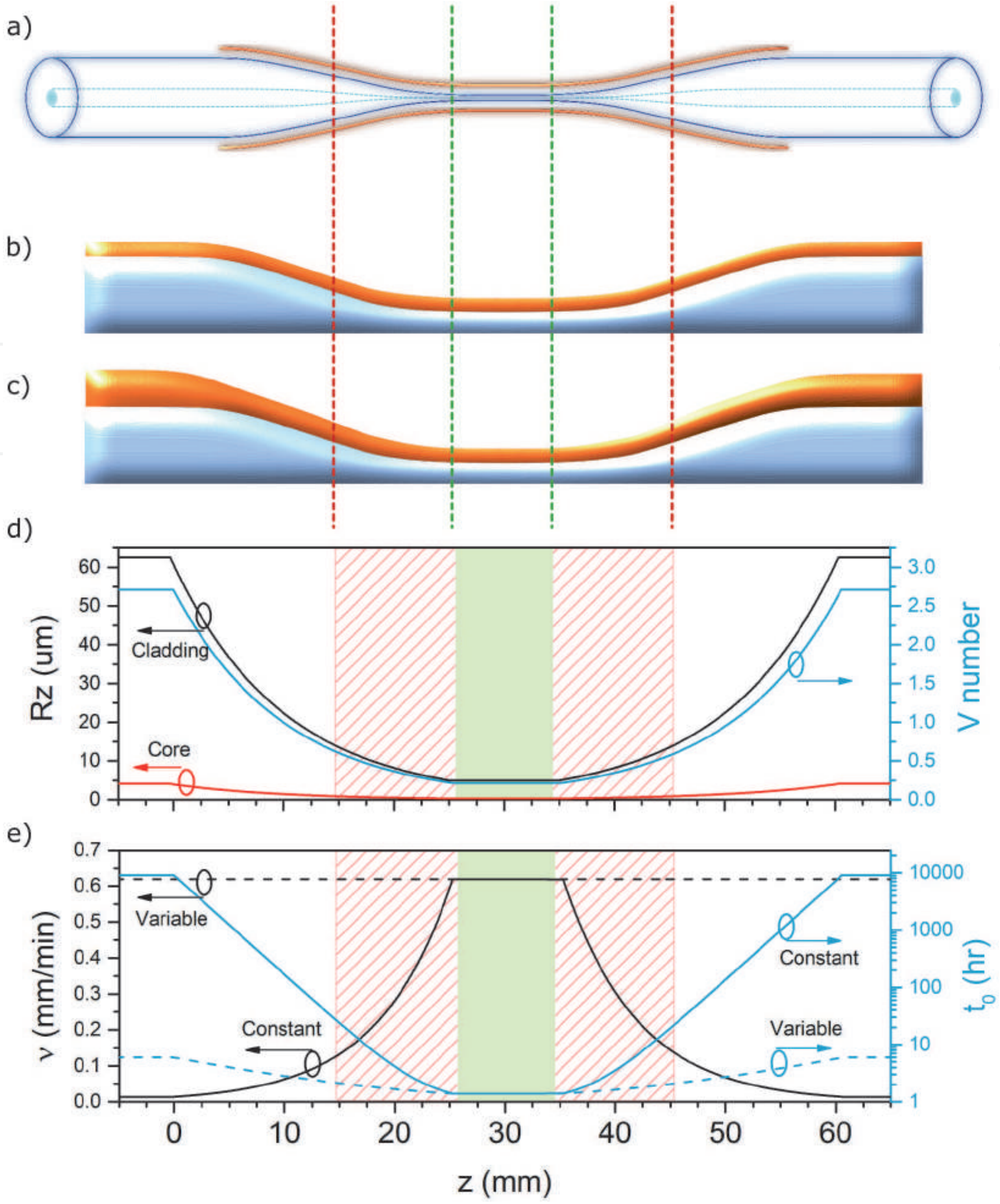


**Figure 6.**
*Coatings on optical fibers. (a) Schematic of a coated tapered optical fiber in different regions showing the regions where coupling from the core to the cladding occurs and the modal distribution in the waist section. (b) Constant and (c) variable thickness coatings along the tapered fiber. (d) Variation of the normalized frequency (V number) of the fiber core along the taper; the red regions indicate the core-cladding coupling zones and light interacts with coating; the green zone indicates the uniform waist section. (e) Coating speeds* (v) *required to obtain constant and variable coating thicknesses along the taper; the plot includes the corresponding characteristic time ($t_o$) for the instabilities.*

generate a non-uniform coating; this task is usually performed upon pulling the fiber from the non-tapered section and hence liquid is also deposited in other regions of the tapered fiber. The transition zones of the tapered fiber are therefore coated as well, and this minimizes any perturbations generated by the reservoir.

Non-uniformities in the coating thickness are a potential source of perturbation that may result in light leaking in the optical fiber. Given the variable radius profile of the tapered fiber and the radius dependency for the resultant thickness given by (6), the profile of the coating can be modified depending on the velocity of the process. Then, two scenarios can result from the coating process: a uniform coating along the entire fiber obtained upon adjusting the speed (**Figure 6b**), or a variable coating layer using a constant speed during the process (**Figure 6c**). In all cases, it is also important to consider the cross-linking mechanism of the coating polymer.

Once the coating is deposited, it might require a longer period of time for achieving solidification.

To exemplify these possibilities, we consider a tapered optical fiber coated with polydimethylsiloxane elastomer (PDMS, Sylgard 184 from Dow), which has a $\eta = 3.5[Pa \bullet s]$ and $\gamma = 0.0198[N \bullet m^{-1}]$ [26, 32]. For the SMF tapered down to a waist radius of 5 μm, the lengths of the waist and transitions are 10 and 25 mm, respectively; the transitions are assumed to have an exponential profile as described in [1]. For this specific fiber light couples into the cladding, and thus evanescent wave exposition into the surrounding media occurs along the transition section (red region in **Figure 6**). The radii of the fiber core and the cladding are compared with the modification of the normalized frequency in **Figure 6d**. The nature of the curing or solidifying process of the polymer is crucial and should be considered due to the possible appearance of instabilities. To avoid this, both the coating and curing processes needs to be shorter than the characteristic time ($t_0$) in the waist section.

PDMS is a polymer cured by heating, requiring from several minutes to hours for complete solidification, depending on the temperature of the curing process. For achieving a 200 nm thick uniform PDMS coating at the waist section, a speed coating process of around $\nu = 0.62\left[mm \bullet min^{-1}\right]$ is required, and the critical time is $t_0 = 1.4[hr]$. The conditions required for generating a coating with constant or variable thickness layers are analyzed in **Figure 6e**. For obtaining a coating with constant thickness (solid line), the required coating speed increases inversely with the fiber diameter. Although the instabilities mostly appear at larger times along the tapered fiber, the total duration of the process will be in general longer. In contrast, the variable coating (dashed line) implicates overall shorter times for instabilities to appear, and the process must be performed much faster.

Depending on the application, fiber coatings can be designed to optimize the interaction of the evanescent wave with the surrounding media. This means that the thickness of the coating can be extended to completely enclose the evanescent wave, or simply to favor some interaction and leave a remaining portion of light still interacting with the external media. Having this in mind, one must also consider the refractive index of the material: while low refractive index materials will require thinner coatings to completely isolate the evanescent wave, high refractive index

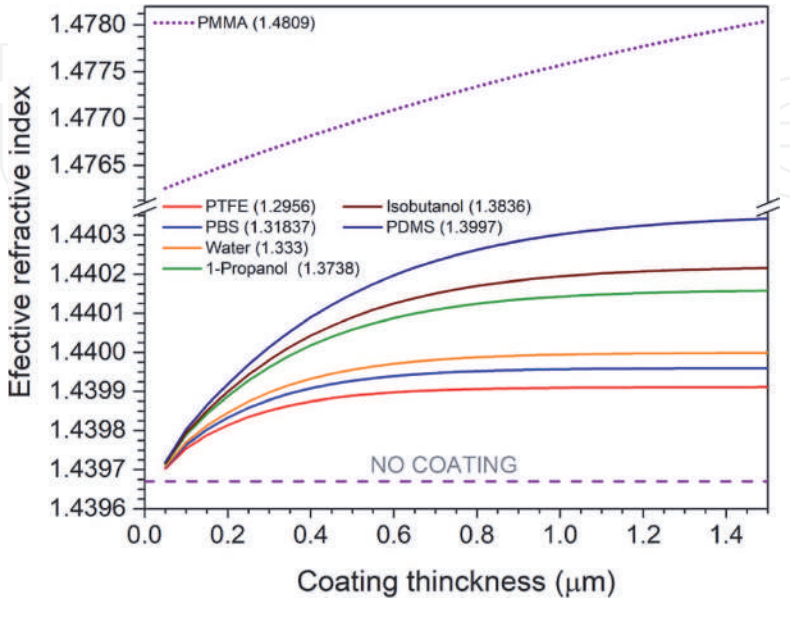


**Figure 7.**
*Effective refractive index at the waist section of the fiber as a function of the coating thickness for materials commonly used for taper coating and for sensing applications: PTFE [33], PBS [34], water [34], 1-propanol [35], isobutanol [35] and PDMS [26, 32].*

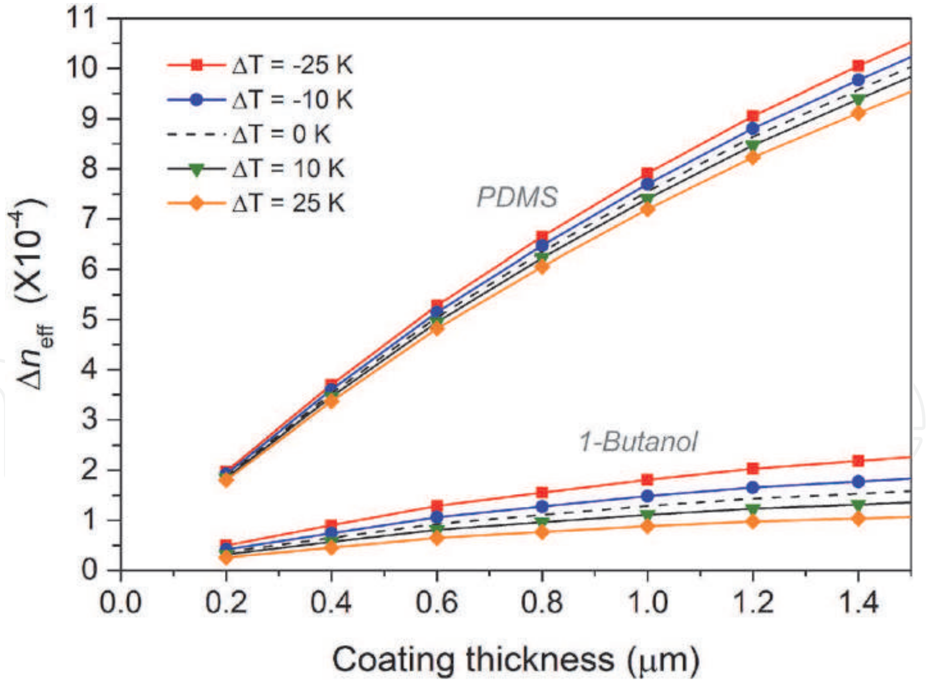


**Figure 8.**
*Temperature dependence of the $LP_{01}$ mode effective refractive index ($n_{eff}$) for different thicknesses of PDMS coatings.*

materials will allow to use thicker coatings before isolating the evanescent wave, as illustrated in **Figure 7**. Of course, to have efficient and low loss light propagation in the tapered fiber, the refractive index of the coating material must be lower than the refractive index of the optical fiber. Otherwise, this will induce losses since the light propagated in the cladding will never been coupled again the core.

## 4. Applications of coatings for devices

Different effects can be generated in the guided wave depending on the optical properties of the coating material. For instance, the sensitivity of the tapered device to physical parameters can be tailored up to some extent. Using again as an example PDMS coatings, the effective refractive index of the fundamental mode can be adjusted with the coating thickness. It is well known that PDMS experiences changes with temperature due to its thermal expansion coefficient and to its thermo-optic coefficient ($^{\Delta n}/_{\Delta T}[K^{-1}] = -1.8 \times 10^{-4}$) [32]. As the thickness of the PDMS coating is increased, the effective refractive index will increase its variation with temperature, as shown in **Figure 8**. Evidently, this "tunability" in sensitivity is limited, and it further depends on the thermo-optical properties of the polymer. To illustrate this, we have also included in **Figure 8** an example using 1-Butanol as the coating material [35]. Notice that in this case, lower effective indices are obtained and their variations with coating thickness are not as pronounced as obtained for PDMS. However, the sensitivity of the effective index to temperature changes for this coating is larger than that of PDMS.

## 5. Conclusions

We have introduced guidelines for coating tapered sections of optical fibers with liquid materials. Specifically, we undertake the subject of polymeric thin layers deposited by the wire coating technique and the interaction of the coating with the evanescent wave. Firstly, the propagation considerations to achieve light interaction with the surrounding media via evanescent wave were described. This aspect depends on the physical dimensions, refractive indices of the materials and propagating wavelength. As shown upon analyzing the wire coating technique, it is possible to define parameter for the coating process that will allow for controlling the coating thickness and avoid coating instabilities. Essentially, once the properties of the liquid polymer and the dimensions of the taper are known, the coating velocity may be calculated in order to obtain a prescribed coating thickness. Finally, light propagation for different coating thickness with different materials was discussed in terms of the influence on the effective refractive index in the waist section of the fiber. These aspects should be of interest for obtaining photonic devices with functional polymers coatings that may be useful for sensing applications.

## Acknowledgements

This work was possible thanks to the funding by DGAPA-PAPIIT project TA101220. The Authors want to thank to Synopsys by the licensing of RSoft.

## Conflict of interest

The authors declare no conflict of interest.

## Author details

Oscar González-Cortez[1], Rodolfo A. Carrillo-Betancourt[1,2], Juan Hernández-Cordero[2] and Amado M. Velázquez-Benítez[1]*

1 Instituto de Ciencias Aplicadas y Tecnología, Universidad Nacional Autónoma de México, Mexico City, Mexico

2 Instituto de Investigaciones en Materiales, Universidad Nacional Autónoma de México, Mexico City, Mexico

*Address all correspondence to: amado.velazquez@icat.unam.mx

IntechOpen

© 2021 The Author(s). Licensee IntechOpen. This chapter is distributed under the terms of the Creative Commons Attribution License (http://creativecommons.org/licenses/by/3.0), which permits unrestricted use, distribution, and reproduction in any medium, provided the original work is properly cited.

## References

[1] Birks TA, Li YW. The shape of fiber tapers. Journal of Lightwave Technology. 1992 Apr;10(4):432-438. DOI: 10.1109/50.134196

[2] Baker, Chams, and Martin Rochette. "A generalized heat-brush approach for precise control of the waist profile in fiber tapers." Optical Materials Express 1.6 (2011): 1065-1076. DOI: 10.1364/OME.1.001065

[3] Haddock HS, Shankar PM, Mutharasan R. Fabrication of biconical tapered optical fibers using hydrofluoric acid. Materials Science and engineering: B. 2003 Jan 15;97(1):87-93. https://doi.org/10.1016/S0921-5107(02)00434-8

[4] Ko S, Lee J, Koo J, Joo BS, Gu M, Lee JH. Chemical wet etching of an optical fiber using a hydrogen fluoride-free solution for a saturable absorber based on the evanescent field interaction. Journal of Lightwave Technology. 2016 Aug 15;34(16): 3776-3784. DOI: 10.1109/JLT.2016.2583061

[5] Nikbakht, Hamed, Hamid Latifi, Mohammadreza Oraie, and Tahere Amini. "Fabrication of tapered tip fibers with a controllable cone angle using dynamical etching." Journal of Lightwave Technology 33, no. 23 (2015): 4707-4711. DOI: 10.1109/JLT.2015.2453365

[6] Villatoro, Joel, David Monzón-Hernández, and Efrain Mejía. "Fabrication and modeling of uniform-waist single-mode tapered optical fiber sensors." Applied optics 42, no. 13 (2003): 2278-2283. DOI: 10.1364/AO.42.002278

[7] Yang, Rui, Yong-Sen Yu, Cong-Cong Zhu, Yang Xue, Chao Chen, Xuan-Yu Zhang, Bao-Lin Zhang, and Hong-Bo Sun. "PDMS-coated S-tapered fiber for highly sensitive measurements of transverse load and temperature." IEEE Sensors Journal 15, no. 6 (2015): 3429-3435. DOI: 10.1109/JSEN.2015.2388490

[8] Brambilla G, Xu F, Horak P, Jung Y, Koizumi F, Sessions NP, Koukharenko E, Feng X, Murugan GS, Wilkinson JS, Richardson DJ. Optical fiber nanowires and microwires: fabrication and applications. Advances in Optics and Photonics. 2009 Jan 30;1 (1):107-161. https://doi.org/10.1364/AOP.1.000107

[9] Leung, Angela, P. Mohana Shankar, and Raj Mutharasan. "A review of fiber-optic biosensors." Sensors and Actuators B: Chemical 125, no. 2 (2007): 688-703. DOI: 10.1016/j.snb.2007.03.010

[10] Tian, Ye, Wenhui Wang, Nan Wu, Xiaotian Zou, and Xingwei Wang. "Tapered optical fiber sensor for label-free detection of biomolecules." Sensors 11, no. 4 (2011): 3780-3790. DOI: 10.3390/s110403780

[11] Yadav, T. K., R. Narayanaswamy, MH Abu Bakar, Y. Mustapha Kamil, and M. A. Mahdi. "Single mode tapered fiber-optic interferometer based refractive index sensor and its application to protein sensing." Optics Express 22, no. 19 (2014): 22802-22807. DOI: 10.1364/OE.22.022802

[12] Verma, Rajneesh K., Anuj K. Sharma, and B. D. Gupta. "Surface plasmon resonance based tapered fiber optic sensor with different taper profiles." Optics Communications 281, no. 6 (2008): 1486-1491. DOI: 10.1016/j.optcom.2007.11.007

[13] Monzón-Hernández, David, Joel Villatoro, Dimas Talavera, and Donato Luna-Moreno. "Optical-fiber surface-plasmon resonance sensor with multiple resonance peaks." Applied optics 43, no. 6 (2004): 1216-1220. DOI: 10.1364/AO.43.001216

[14] O'Shea, Danny, Christian Junge, Jürgen Volz, and Arno Rauschenbeutel. "Fiber-optical switch controlled by a single atom." Physical review letters 111, no. 19 (2013): 193601. DOI: 10.1103/PhysRevLett.111.193601

[15] Wu X, Tong L. Optical microfibers and nanofibers. Nanophotonics. 2013 Dec 16;2(5–6):407-428. https://doi.org/10.1515/nanoph-2013-0033

[16] Monifi, Faraz, Sahin Kaya Özdemir, Jacob Friedlein, and Lan Yang. "Encapsulation of a fiber taper coupled microtoroid resonator in a polymer matrix." IEEE Photonics Technology Letters 25, no. 15 (2013): 1458-1461. DOI: 10.1109/LPT.2013.2266573

[17] Buck JA. Fundamentals of optical fibers. John Wiley & Sons; 2004 Apr 27.

[18] Okamoto K. Fundamentals of optical waveguides. Academic press; 2006.

[19] Love JD, Henry WM, Stewart WJ, Black RJ, Lacroix S, Gonthier F. Tapered single-mode fibres and devices. Part 1: Adiabaticity criteria. IEE Proceedings J (Optoelectronics). 1991 Oct 1;138(5): 343-354. DOI: 10.1049/ip-j.1991.0060

[20] Black, R. J., S. Lacroix, F. Gonthier, and J. D. Love. "Tapered single-mode fibres and devices. II. Experimental and theoretical quantification." IEE Proceedings J-Optoelectronics 138, no. 5 (1991): 355-364. DOI: 10.1049/ip-j.1991.0061

[21] Sumetsky, M. "Nanophotonics of optical fibers." Nanophotonics 2, no. 5-6 (2013): 393-406. DOI: 10.1515/nanoph-2013-0041

[22] Kakarantzas, George, Sergio G. Leon-Saval, T. A. Birks, and P. St J. Russell. "Low-loss deposition of solgel-derived silica films on tapered fibers." Optics letters 29, no. 7 (2004): 694-696. DOI: 10.1364/OL.29.000694

[23] Li, Bao-li, Jin-hui Chen, Fei Xu, and Yan-qing Lu. "Periodic micro-structures in optical microfibers induced by Plateau-Rayleigh instability and its applications." Optics express 25, no. 4 (2017): 4326-4334. DOI: 10.1364/OE.25.004326

[24] Vélez-Cordero, J. Rodrigo, A. M. Velázquez-Benítez, and J. Hernández-Cordero. "Thermocapillary flow in glass tubes coated with photoresponsive layers." Langmuir 30, no. 18 (2014): 5326-5336. DOI: 10.1021/la404221p

[25] Xu, Z. Y., Y. H. Li, and L. J. Wang. "Versatile technique to functionalize optical microfibers via a modified sol-gel dip-coating method." Optics letters 39, no. 1 (2014): 34-36. DOI: 10.1364/OL.39.000034

[26] Velázquez-Benítez, Amado M., Moisés Reyes-Medrano, J. Rodrigo Vélez-Cordero, and Juan Hernández-Cordero. "Controlled deposition of polymer coatings on cylindrical photonic devices." Journal of Lightwave Technology 33, no. 1 (2014): 176-182. DOI: 10.1109/JLT.2014.2377173

[27] Landau, Levich, and B. Levich. "Dragging of a liquid by a moving plate." In Dynamics of curved fronts, pp. 141-153. Academic Press, 1988. DOI: 10.1016/B978-0-08-092523-3.50016-2

[28] De Ryck, Alain, and David Quéré. "Inertial coating of a fibre." Journal of Fluid Mechanics 311 (1996): 219-237. DOI: 10.1017/S0022112096002571

[29] Quéré, David. "Fluid coating on a fiber." Annual Review of Fluid Mechanics 31, no. 1 (1999): 347-384. DOI: 10.1146/annurev.fluid.31.1.347

[30] White, David A., and John A. Tallmadge. "A theory of withdrawal of cylinders from liquid baths." AIChE Journal 12, no. 2 (1966): 333-339. DOI: 10.1002/aic.690120223

[31] Rayleigh, Lord. "On the instability of jets." Proceedings of the London mathematical society 1, no. 1 (1878): 4-13. DOI: 10.1112/plms/s1-10.1.4

[32] Li, Bei-Bei, Qing-Yan Wang, Yun-Feng Xiao, Xue-Feng Jiang, Yan Li, Lixin Xiao, and Qihuang Gong. "On chip, high-sensitivity thermal sensor based on high-Q polydimethylsiloxane-coated microresonator." Applied Physics Letters 96, no. 25 (2010): 251109. DOI: 10.1063/1.3457444

[33] Yang, Min K., Roger H. French, and Edward W. Tokarsky. "Optical properties of Teflon® AF amorphous fluoropolymers." Journal of Micro/Nanolithography, MEMS, and MOEMS 7, no. 3 (2008): 033010. DOI: 10.1117/1.2965541

[34] Hoang, Van Thuy, Grzegorz Stępniewski, Karolina H. Czarnecka, Rafał Kasztelanic, Van Cao Long, Khoa Dinh Xuan, Liyang Shao, Mateusz Śmietana, and Ryszard Buczyński. "Optical properties of buffers and cell culture media for optofluidic and sensing applications." Applied Sciences 9, no. 6 (2019): 1145. DOI: 10.3390/app9061145

[35] Moutzouris, Konstantinos, Myrtia Papamichael, Sokratis C. Betsis, Ilias Stavrakas, George Hloupis, and Dimos Triantis. "Refractive, dispersive and thermo-optic properties of twelve organic solvents in the visible and near-infrared." Applied Physics B 116, no. 3 (2014): 617-622. DOI: 10.1007/s00340-013-5744-3

# We are IntechOpen, the world's leading publisher of Open Access books
# Built by scientists, for scientists

6,300
Open access books available

171,000
International authors and editors

190M
Downloads

154
Countries delivered to

Our authors are among the
TOP 1%
most cited scientists

12.2%
Contributors from top 500 universities

WEB OF SCIENCE™

Selection of our books indexed in the Book Citation Index in Web of Science™ Core Collection (BKCI)

## Interested in publishing with us? Contact book.department@intechopen.com

Numbers displayed above are based on latest data collected.
For more information visit www.intechopen.com

Chapter

# Optical Inhouse Networks

*Ulrich H.P. Fischer, Matthias Haupt and Peter Kußmann*

## Abstract

Optical fiber networks are currently the standard for delivering high bandwidth to customers. Various access technologies to business networks with a very high bandwidth up to access networks for buildings and individual consumers have emerged. In the area of business networks, bandwidths of 10 Gb/s have become established, while in the area of customer bandwidths of 100 Mb/s to 1 Gb/s are used. This chapter will focus on the optical network connections inside buildings. The use of optical glass fibers or/and polymeric optical fibers in different network topologies in connection to high-speed actual WIFI- technologies will be discussed.

**Keywords:** optical fiber, distributed network structure, optical polymeric fibers, local area networks, open building reference model

## 1. Introduction

Depending on how far the glass fiber extends into the access network, one speaks of “Fiber to the Curb” (FTTC), “Fiber to the Building” (FTTB), “Fiber to the Home” (FTTH), “Fiber to the Desk” (FTTD). As an alternative, DSL technology, outdoor DSLAMs and VDSL with vectoring, contribute data transmission rates of up to 200 Mbit/s for broadband distribution to the subscriber, whereby these copper-based connection technologies have reached now their capacity limits [1].

As shown in **Figure 1**, the international optical network is essentially divided into three levels. Based on the international level of the global area network with

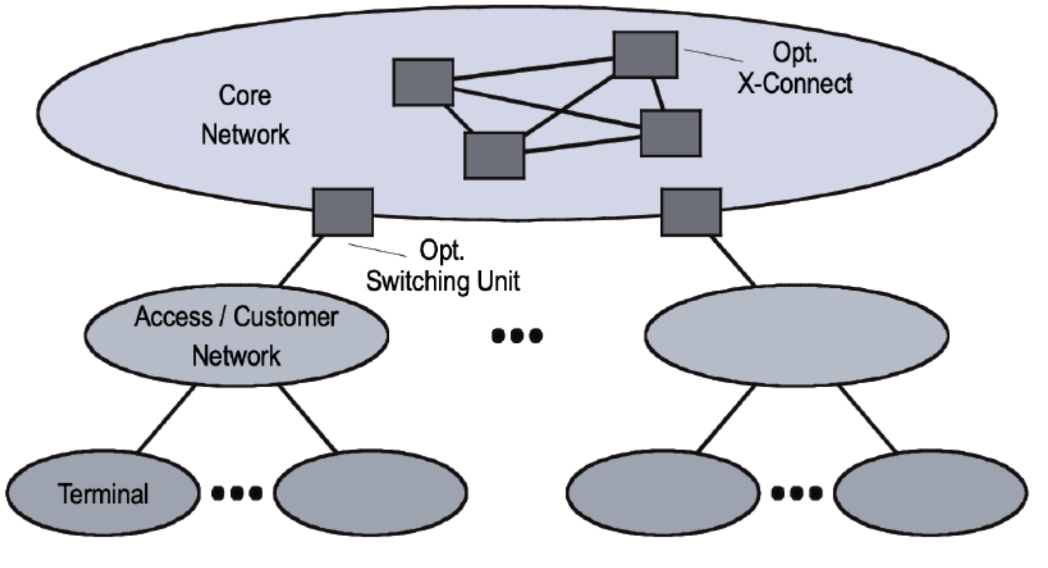


**Figure 1.**
*Worldwide optical network structure.*

very high data rates of 10–100 Gb/s, branches go to the level of regional networks with data rates of 1–10 Gb/s and from there to the third level of the customer network. There we speak of data rates of 100 Mb/s to 10 Gb/s. Based on this core network, the wireless networks (4G, 5G) to supply the mobile devices in the area with up to 1Gb/s are realized [2].

The mobile networks with LTE or 5G and the cable television networks also use this term for the part of their networks that includes the subscriber connections and offers access to higher network levels. However, radio technology can only be seen as an alternative to fiber optic infrastructure in rural areas, as little cabling needs to be installed. Unfortunately, the bandwidth of these radio networks decreases quadratic by the distance to the radio base station, so that the effectively transferable data rate will fall down strictly in rural areas. The cable television networks are currently based on DOCSYS 3.1 and already use fiber optic connections as FTTB variants and are therefore to be seen as fiber optic technology despite different software and hardware configurations. Currently, most of the optical fiber optic connections are made in the FTTB area [3, 4].

At a connection point in the basement of the building, the fiber optic cable coming from the outside is connected to a router or switch. Starting from there, the data is transferred to the different areas and floors of the office building or the apartment block either via fiber optics, polymer fibers or electrical Ethernet cables (e.g. CAT 7). This is referred as network levels 3 and 4, before branching from the different floors to the individual offices or apartments via switches. The other cabling in the apartments and offices is called network level 5. Here, in turn, there are appropriate routers for the apartments or switches for the offices in order to distribute the data in the individual rooms. Levels 3–5 are nowadays mainly connected via optical cables and will be analyzed in this chapter in a differentiated manner and discussed with examples. This also includes the use of additional technologies such as WiFi, Zigbee, Bluetooth or dLAN/powerline [5] in the home and office [6–8].

## 2. Distributed network structures

Computer networks in apartments, small buildings and office environments (Small Office/Home Office - SoHo) are typical fields of application for Ethernet-based communication networks [9]. Local services such as network printers or file shares are implemented on these network structures, or DSL and cable providers offer their customers IP-based services such as Internet access, IP-TV or VoIP (Voice over IP).

For the implementation of Ethernet/POF-based SoHo networks, different areas must be conceptually considered (e.g. laying cables, selection and structuring of electronic components), implemented and connected to the Internet using suitable devices and processes [10–13].

Based on the sub-areas to be implemented for the realization of a network in the desired SoHo target market, the protocols and standards to be considered are so diverse that the existing orientations as well as the derived test methods and devices appear unsuitable.

For the design of a general and expandable structure in the SoHo environment, an abstraction model was developed - which is suitable as a basis for orientation for the implementation of network structures, service models and test methods in the SoHo environment.

In the telecommunication networks a special scheme is applied to distribute the data from the source/headend to the customer. The distribution is divided into five levels (see **Table 1** and **Figure 2**):

| Network level | Task |
|---|---|
| 1 | Content production |
| 2 | Operation of the head-end stations that receive and forward the TV and radio signals |
| 3 | Street/curb distributors |
| 4 | House distributors |
| 5 | Between router in the home and telephone/Internet devices |

**Table 1.**
*Network levels in the telecommunication network.*

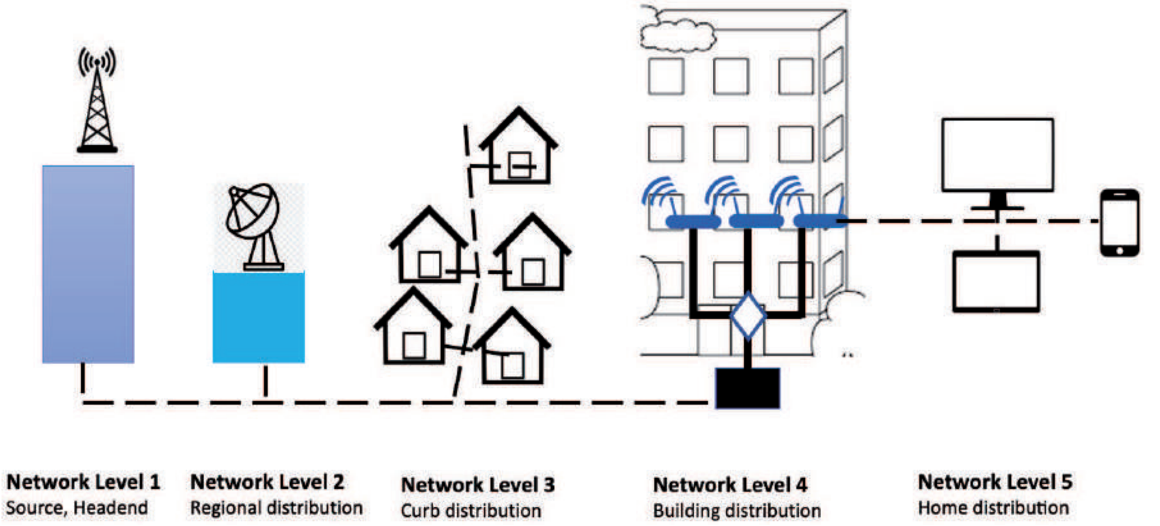


**Figure 2.**
*Distribution of the telecommunications transmission path from the provider via the curb distribution to the building and in the building to the flats.*

Level 1: Content/data production.

These include program providers such as Premiere, the public and private broadcasting stations and also Cloud applications.

Level 2: Operation of head-end stations.

The internet data is received via these stations and then passed on. In the case of the TV cable network, one of these head-end stations is always required, as this is where the signals from the satellite are converted and processed for cable reception, among other things. The reception technology in the cable networks has been completely converted to the digital standard since DOCSYS 3.1 [14] and is therefore at the same level as the telecommunications networks. Typical data rates are between 10 Gb/s up to 100Gb/s.

Level 3: Street distributor/curb.

This refers to the network areas that were relocated from the head-end stations to the residential areas (FTTC-fiber to the curb). Typical data rates are between 1 Gb/s up to 10Gb/s.

Level 4: house distributor.

Customers can only be reached via the fourth network level into the houses (FTTB - fiber to the building). Many small operators are exclusively active here, the number of which is estimated at several thousand. In order to offer new products and services, the operator must be able to feed them into the network. This requires an adaptation of several network levels, which, however, often turns out to be very difficult due to the large number of responsible companies at the various levels. Only in the rarest of cases does an operator have several levels, which makes the actual structure difficult to understand for the end user. Typical data rates are between 100 Mb/s up to 10Gb/s.

Level 5: Flat distribution.

The network connection directly with the customer is now being rolled out worldwide via optical fibers, since only these technologies enable a correspondingly high bandwidth. This level is between router and telephone/Internet devices such as smartphones, tablets or IP TV realized. Typical data rates are between 10 Mb/s up to 1Gb/s (FTTH - fiber to the home).

## 3. Open building interconnection reference model - OBI

Based on the different orientations of the four identified work areas (building blocks) (see **Figure 3**) as well as the multitude of standards and guidelines to be taken into account, which data center operators are familiar with - but not known to house and apartment owners in the targeted SoHo target market - the following situation arises:

A model is required that includes the four identified work areas - defines interfaces and thus offers orientation for further work [15, 16]. All areas relevant for the conception, construction and operation of SoHo networks and in-house communication can be structured, edited and tested in a reproducible manner [17, 18].

Based on the basic services defined within the OBI model, the conception of test scenarios was started. For this it is necessary to classify the network structure that is likely to be encountered. Starting from a transfer point (e.g. DSL [19], FTTH, DOCSIS [20] that connects to the public wide area data network (WAN) [18], SoHo routers are used that provide services for the internal network that are defined using an operating system (firmware) (LAN) (e.g. switch, WLAN, FXS (Foreign eXchange Station), FITH (Fiber In The Home)). The owner of the SoHo network has no influence on the implementation of the WAN area, apart from the choice of provider and product. The situation is different with the implementation of the LAN structure. Which implementation is used primarily defines the intended use of the LAN. The router already mentioned shows the following structure (**Figure 4**) taking into account its functions (**Figure 5**):

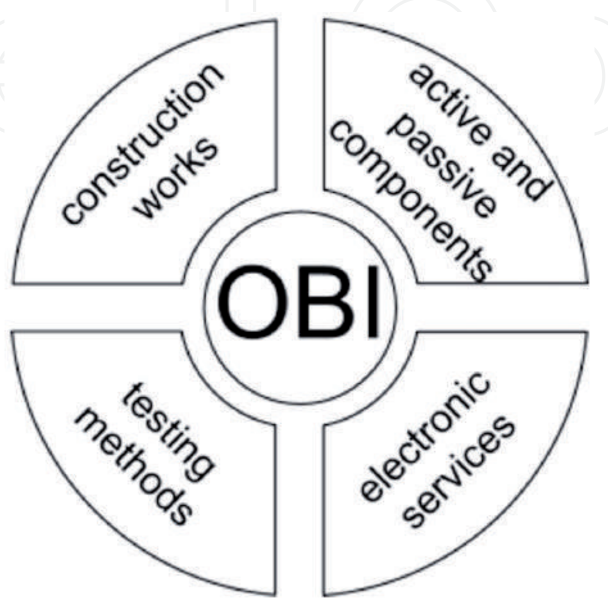


**Figure 3.**
*O B I - open building reference model.*

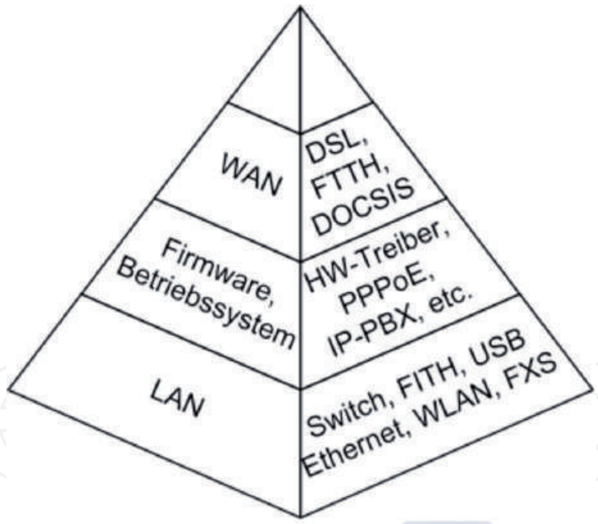


**Figure 4.**
*Functional overview of a SoHo router.*

| | WAN | Router | LAN |
|---|---|---|---|
| Symbol |  |  |  |
| Funktion | DSL, FTTH, DOCSIS | HW-Treiber, PPPoE, IP-PBX, Firewall | Switch, FITH, Ethernet, WLAN, FXS |

**Figure 5.**
*Network structure in the SoHo-environment.*

Due to the owner's preference, all technical options (e.g., WLAN, fiber optic, POF, Cat [5–7], etc.) as well as the associated active and passive components are available for a structure.

If the SoHo network is viewed from the point of view of the services operated on it, the guarantee of the correct functioning and the quality of service by the provider of the WAN connection ends in the SoHo router which is depicted in **Figure 6**. It is assumed here that the provider of the WAN connection terminates the VoIP traffic on a SIP registrar [21] integrated in the SoHo router. All local end devices contact this SIP registrar, which in turn forwards the VoIP traffic to the telephone server of the WAN provider for termination using a SIP trunk.

The configurations, implementations and functions in the LAN area for mapping the functional correctness and quality of service for the defined basic services (network access, VoIP, WLAN) are part of the current work. For the investigation of the bandwidth-prioritized VoIP, a test scenario specially adapted to SoHo environments was designed.

In order to obtain reproducible results, the dependency on external disturbances (on the WAN side) must be excluded, which is why a local VoIP registrar was configured (codecs: g.711u [22], h264 [23]) and used. The SIP video telephones use - for the VoIP within the LAN - different transmission media, e.g., Cat (5/6/7), POF and WLAN and different combinations and configurations of the active and passive components. The ITU standards for PESQ [24] and the E-model [25] are used for objective assessment of the voice quality of VoIP calls.

Both test methods take into account all parameters involved in the transmission (e.g., noise, SNR, latencies, jitter, echoes, packet losses, etc.) as well as their mutual dependency. For the examination, a defined language file is transmitted (see **Figure 7**- red/

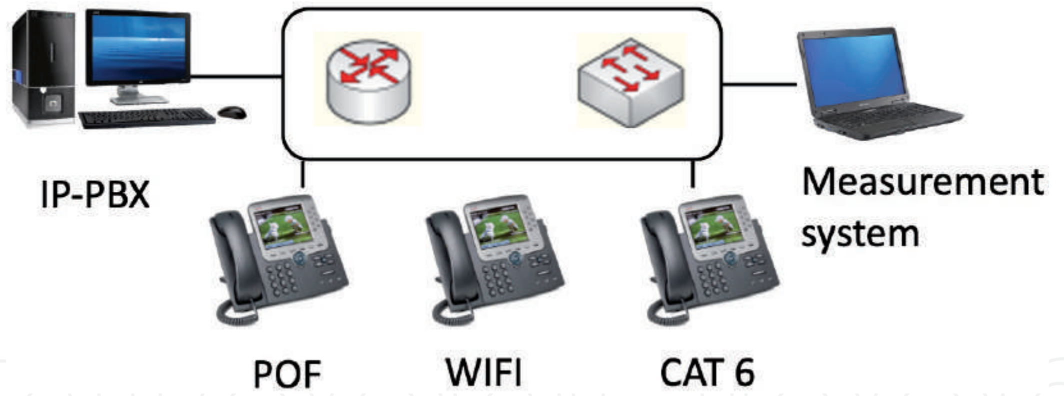


**Figure 6.**
*SoHo - network topology for VoIP test.*

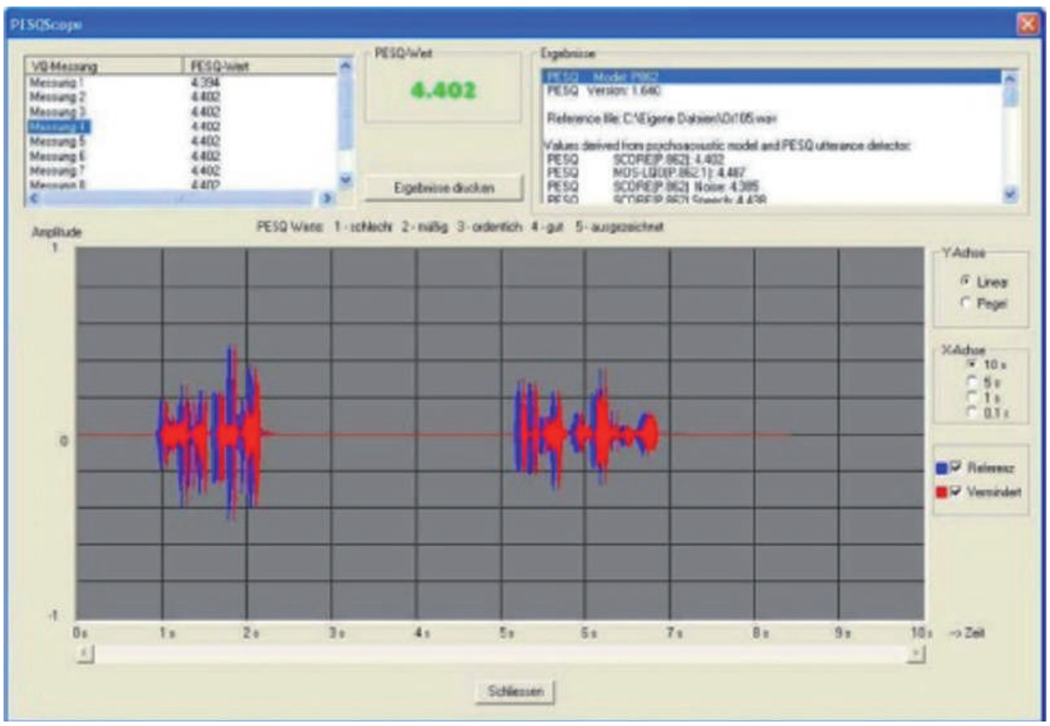


**Figure 7.**
*PESQ-measurement in SoHo network topology.*

reduced) and compared with the original file (see **Figure 7**- blue/reference). The result is a numerical score value (PESQ-MOS factor for PESQ, R factor for E-model) for the comparison tables.

After calibration of the individual transmission links and selection of suitable test parameters and routines, the configurable parameters of the active components (e.g., QoS, VLAN, IPv6) can be examined in the context of "Influence on the quality of VoIP transmissions in SoHo environments". Statements can also be made about the influence of the codecs used (e.g., H264, G711, G722 [26]) or the number of maximum SIP connections in the context of the bandwidth limit of the existing network topology. By using the VoIP registrar function in commercially available SoHo routers that are already available on the market (today already with all major Internet providers), the test routines can be run through - without measurement setups and configurations - and thus provide comparable results. By using the OBI model, communication and network structures in SoHo environments, especially for technology-supported care assistance systems [27] with the personal data that arise there, can be referenced and verified.

## 4. Network types in the building

### 4.1 Glass fibers vs. polymeric fibers vs. CAT

Optical waveguides are made of optical glasses or assembled, partially assembled, provided with plug connections cables and lines for the transmission of light in the visible as well as ultraviolet or infrared range. Fiber optic cables form flexible connections for the transmission of optical signals. Depending on the application, the fiber optic cables consist of Quartz glass, e.g. pure silicon dioxide (SiO2) or organic glass Polymeric fibers consist of acrylic glass [28]. From a physical point of view, both optical waveguides are dielectric waveguides.

Today, fiber optic cables [29] are mainly used as a transmission medium for wired telecommunication processes. In addition, there are diverse applications: fiber optic cables for laser radiation for material processing [30, 31], in medicine for lighting and imaging purposes: microscope lighting [32], endoscopes [33], decoration lighting [34], for contact-free sensors [35], in measurement technology, e.g. in infrared thermometers and spectrometers [36].

Today, fiber optic cables are increasingly used for information transmission, in telecommunications and also in the area of computer networking. The term optical fiber is standardized in DIN 47002 and VDE 0888 and means that it is a conductor in which modulated light is transmitted. The fiber optic cable can be made of fiberglass or plastic. With plastic fiber-optic cables, the so-called POF, high transmission rates can be achieved, which can be up to several million bit/s. Furthermore, POF are insensitive to electromagnetic interference, largely secure against eavesdropping and have very low attenuation values compared to copper conductors.

A comparison of different fiber optical waveguides in glass and in polymeric materials are depicted in **Figure 8**. There are multimode fibers (MMF) available in two sizes, 62.5 or 50 microns, and four classifications: OM1 (62.5/125 μm), OM2, OM3, OM4 (50/125 μm) [37]. The GOF fiber type for SoHo applications is the multimode GOF with a diameter 50 μm core and 125 μm cladding. The bandwidth of this device is typically 1–10 GBit/s over 100–500 m. The POF has a very limited bandwidth of 1 Gbit/s over 100 m link length in Ethernet networks.

As depicted in **Figure 9** the single mode GOF (SMF) offers the highest bandwidths of over 10 Gbit/s, which go well beyond the bandwidths required in the

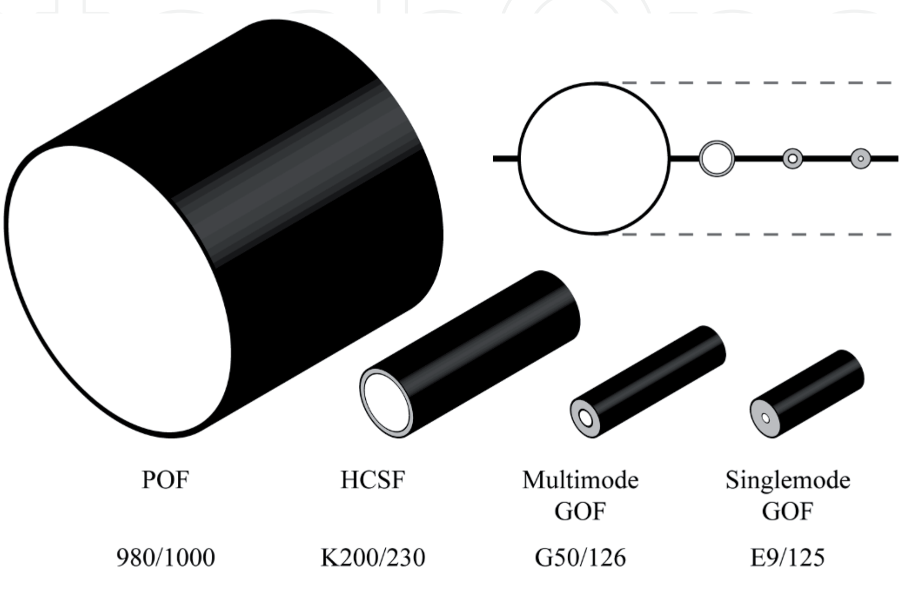


**Figure 8.**
*Dimensions of GOF and POF fiber types.*

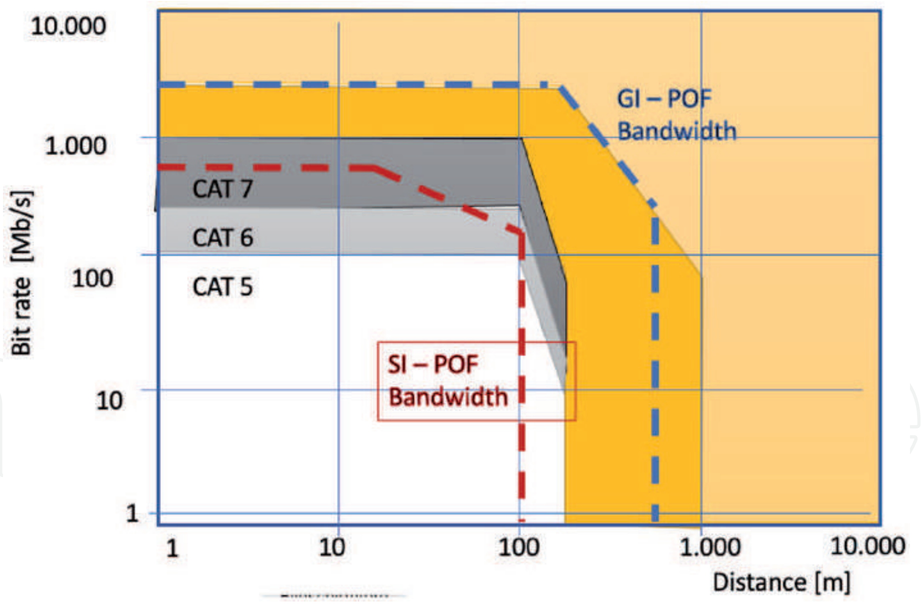


**Figure 9.**
*Transmission speeds of single mode and multimode GOF, POF and CAT for inhouse applications.*

SoHo area. This is why the SMF still plays a subordinate role in the short-term computing area in buildings. On the other hand, the multimode GOF (MMF) with bandwidths of 1 Gbit/s has significantly higher application potential, since the connectors and other active components such as transmitters and receivers are significantly cheaper than those of SMF components. The POF has significantly expanded its bandwidth potential in recent years and with gradient index POF (GI-POF) can also allow up to 10 Gbit/s over 50 m transmission distance, but has only been investigated in research studies to date. The step index POF (SI-PF), which can be used commercially with a maximum of 1 Gbit/s, is significantly worse in terms of transmission bandwidth. On the other hand, experimental studies show, that Wavelength Division Multiplex (WDM) techniques [38] applied in the POF spectrum of 400 nm to 780 nm can overcome the bandwidth restrictions and can realize more than 15 Gb/s via 4 chromatic transmission channels [39]. Additional WDM sources can extend the overall bandwidth to more than 40 Gb/s [40].

The copper technology of the CAT cables currently also achieves gigabit transmission speeds, but is very susceptible to installation errors such as bending radii that are too small. However, the CAT cable connection has the advantage of passive networking without further active transmitter/receiver elements.

### 4.2 POF fibers for inhouse applications

For signal transmission over short to medium distances of up to approx. 100 m, optical waveguides made of acrylic glass (polymethyl methacrylate or PMMA), so-called POF, are used.

Polymer fiber technology for optical data transmission has developed very dynamically over the past 10 years [41]. Starting with simple transmission options for the consumer sector such as digital links between DVD players and preamplifiers in the home multimedia sector (TOSLINK [42] system) with data rates of a few Mb/s, the technology has now established itself in the automotive sector with the use of MOST bus [43]. Here, POF is used in the visible wavelength range, since the components at this level of application must be manufactured as cost-effectively as possible for the end user. Mobile multimedia applications are of particular importance in the automotive sector, where over 50 vehicle types (approx. 15 million vehicles) have been equipped with POF bus systems since its introduction in 2001.

In addition to the higher data rate and the resulting improved integration of multimedia applications in busses or automobiles, considerable weight reductions in the cable of 30% are also achieved [44, 45].

For these reasons, optical data transmission is increasingly being used in close proximity, e.g. in office and house communication, in production facilities, in medical technology or in bus systems for cars, trains and planes.

In the following, the optical basics of fibers, called POF (polymer optical fibers) for short, their active and passive components for network technology and their fields of application in the in-house area are presented.

### 4.3 Optical properties and advantages of POF

Optical fibers consist of a highly transparent core, a cladding and a protective coating and/or buffer. The light-guiding core is used to transmit the signal. The cladding has a lower optical refractive index (density) than the core. As a result, the cladding causes total reflection at the boundary layer and thus guiding the radiation in the core of the optical waveguide. However, light can also get into the cladding through bending or coupling at the beginning of the route. This is usually undesirable and the jacket and protective coating are therefore designed in such a way that this light is strongly attenuated.

The outer protective coating helps against mechanical damage and protects the fiber from environmental influences. The POF consists of PMMA (acrylic glass), has a core diameter of approx. 1 mm (**Figures 10** and **11**) and has a bandwidth of

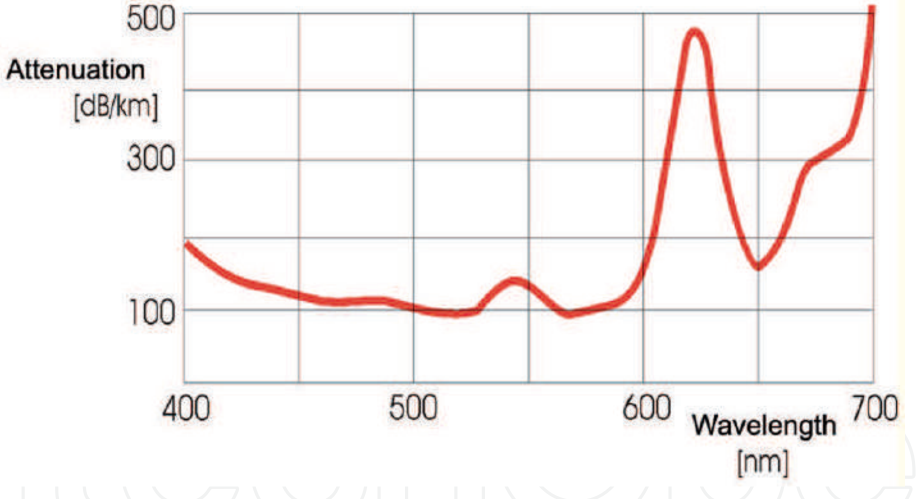


**Figure 10.**
*Attenuation diagram of POF in the visible regime.*

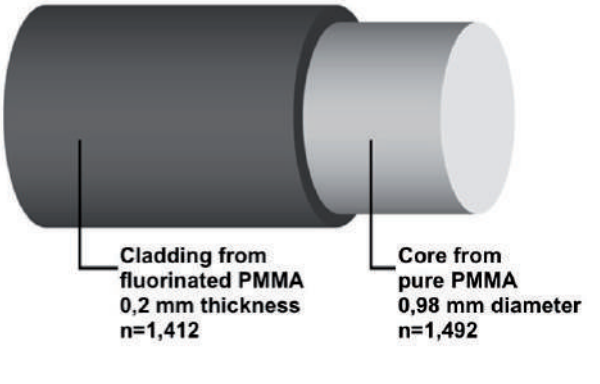


**Figure 11.**
*Schematic draw of a polymeric fib.*

| | POF | GOF | CAT |
|---|---|---|---|
| EMV | ++ | ++ | — |
| Galvanic isolation | ++ | ++ | — |
| Bug security | + | + | — |
| Risk in explosive environments | ++ | ++ | + |
| **Low weight** | ++ | + | — |
| **Small bending radius** | + | — | — |
| **Flexibility** | + | — | + |
| **Low cost** | ++ | — | + |
| **Bandwidth** | + | ++ | + |
| **Attenuation/m** | — | ++ | — |
| **Cable and connector assembly costs** | ++ | — | + |

*++ very good, + good, – unsatisfactory.*

**Table 2.**
*Comparison of GF, CAT and POF transmission connections in SoHo environment [46].*

100 Mb/s over 100 m, which can be expanded to 1000 Mb/s with special modulation techniques and laser transmitters. The advantages of POF in laying technology are obvious in several areas compared to WiFi, powerline/dLAN or CAT solutions (see **Table 2**, [46]):

1. Practical aspects
    - Very inexpensive, easy to work with
    - Low weight, very small diameter: 1/10 of copper cables
    - More flexible and cheaper than glass fiber optic cables
    - Easy handling
    - EMC insensitivity
2. Security aspects
    - Better insurability
    - Security against eavesdropping
    - Short-circuit protection, free of hum loops
3. Technical aspects
    - Data rates can be expanded in a future-proof manner (investment security)
    - Several signals can be transmitted on one fiber
    - Significantly cheaper and easier to lay than glass fibers

The 1 mm fiber type is the cheapest to manufacture and is therefore used in 95% of all commercial applications. The refractive index is constant over the entire core cross-section (SI-POF). With other fiber types, for example gradient index fibers (GI) or multi-level index fibers (MSI), significantly higher bandwidths (currently 2.3GHz/100m) can be achieved in the laboratory, but these do not play a role in the consumer market segment. The advantages of the standard SI-POF lie in the wide availability, the very low price, the favorable attenuation behavior (**Figure 10**) a very high numerical aperture, which enables a simple and effective coupling and extraction of light.

## 5. Usable connectors for glass fibers and polymeric fibers in the home

The optical polymer fiber POF has particularly good and simple properties for the connection technology between fibers and optical transmitters and receivers [47]. Due to its simple structure, which with a core of 0.98 mm and a cladding of 0.2 mm corresponds exactly to 1 mm outer diameter, the cable can be cut straight with a cutter knife (see illustration) very easily. In contrast to fiber optic connections, the separation and cutting of a plastic fiber is much easier because the fiber optics require very complex mechanics and the dismantling of the fiber optic cables (see YouTube video [48]). A connection of two fibers has particularly low losses, since the large diameter reduces the mechanical boundary conditions for the accuracy of the alignment to + −0.1 mm. This corresponds to a 100 times lower necessary accuracy compared to a fiber optic connector. Because the alignment accuracy between the fiber and the optical element can be measured very generously without generating large losses, the plug-in connections are correspondingly easy to assemble. The **Figure 12** shows an overview of the typical plug connections for POF cables.

A distinction is made between metallic and plastic plugs. The metallic plugs are used in the area of rough environments like car entertainment busses or factory environments for stable connections. The plastic plugs were used in the area of in-house networks without large load peaks.

No plugs are typically used for use in the home, while the fibers can be simply cut off (see **Figure 14**) and butt-inserted into the receptacle of a media converter. This saves a lot of costs and unnecessary time for the connector assembly, as well

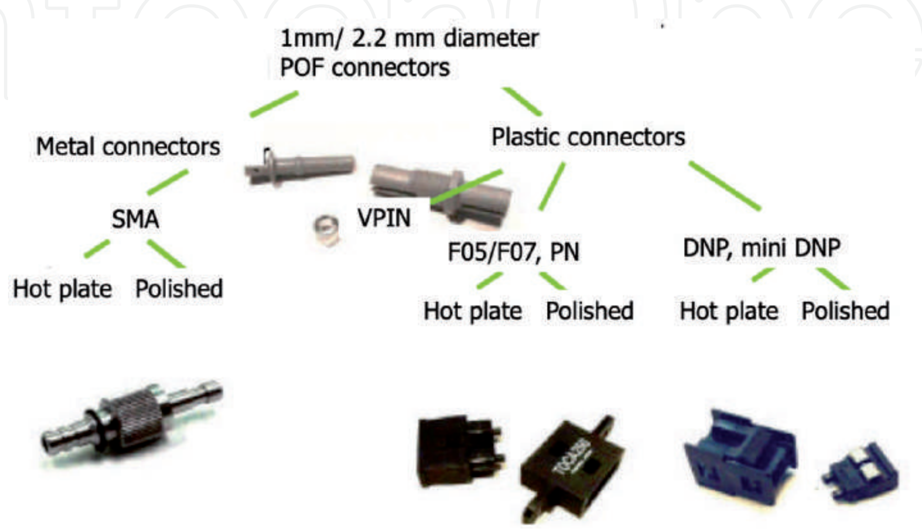


**Figure 12.**
*Typical plugs for POF connections.*

as a simple possibility for the non-specialist to lay network cables himself without special knowledge. Typical connectors for butt-inserted connections are shown in **Figure 15**.

Another area for the introduction of POF network technology is the construction and connection technology, e.g. of splicing for POF. This would make it possible to directly couple POF without additional components. This technology is established in fiber optic technology, but in a technology that cannot be used for POF. That is why it would be of crucial importance for the cable laying technology of POF to have such a connection technology with innovative approaches. A splice kit (**Figure 13**) has been implemented at the HarzOptics GmbH Company with industrial partners using injection molding technology, which provides very good conditions for an easy-to-use splice [49]. Very low attenuation of 0.2 dB is typical for this spice method. The basic idea is that the fibers are fit very exact into the splice core of 0.98 mm and the core hoe was filled before with glue. The refractive index of the glue is 1,5 and the hardening of the glue is realized by the use of a UV light lamp, which took only 3 minutes to be hardened (**Figure 15**).

**Figure 13.**
*Optical splice with low attenuation.*

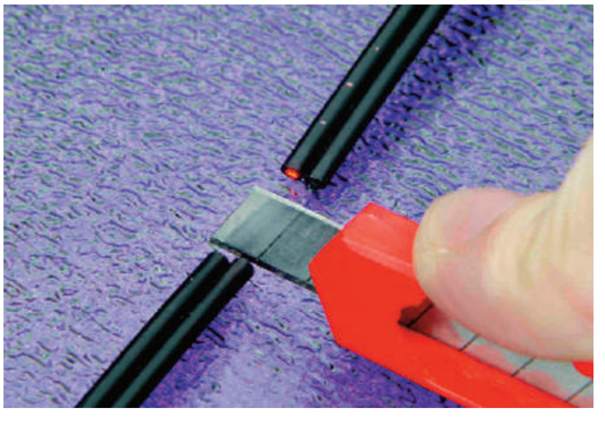

**Figure 14.**
*POF fiber cutting easy with cutter knife.*


**Figure 15.**
*POF media convertors, Ethernet switches and 4-port optical POF switch RJ-45 wall outlets with WiFi-Accesspoint (Rutenbeck GmbH).*

For the home sector, also known as domotics, an increasing demand for bandwidth is to be expected over the next few years. One reason for this development is the triple play promoted by the leading telecommunications companies, which means a bundled range of services such as IP telephony, IP TV and the Internet (**Figure 16**). Another term used in this context is the "active house". The development of this concept represents the integration of communication and entertainment, as well as the active control of all functional processes in the house (control of the heating, blinds, monitoring systems, etc.), also known as building automation.

For these areas, active components on the one hand, e.g., media converters for setting up dynamic network structures, and on the other hand, passive optical components such as splitters for the inexpensive construction of such networks are available in sufficient numbers for Ethernet applications up to 1000 Mb/s. There are a variety of applications and simple installation techniques for POF media converters or POF adapters (**Figure 15**) and POF Ethernet switches for installation in flush-mounted switch boxes are available for setting up home networks with polymer fibers [50]. On the user side, one or more ports with RJ-45 interfaces (10/100/1000Base-Tx) are available for connecting the end devices. The polymer fiber is connected on the installation side. The POF is connected to the optical interfaces (1000Base-Fx) using plug-in terminals.

The switch shown also allows the construction of star, bus, tree and ring structures with polymer fiber cables. Some of the ports of POF Ethernet switches even offer Power over Ethernet (PoE) functionality, so that IP telephones, IP cameras or WLAN access points with IEEE 802.11n data rates (up to 240 Mb/s net data rate [51]) can be operated on the POF network without plug-in power supplies.

## 6. Example of an in-house network with optical POF fibers

A typical example of an application in a single-family home is shown in **Figure 16**. The data which is supplied from outside from the so-called network level 3 via fiber optics or DSL to the house is sent to a router at the house transfer point.

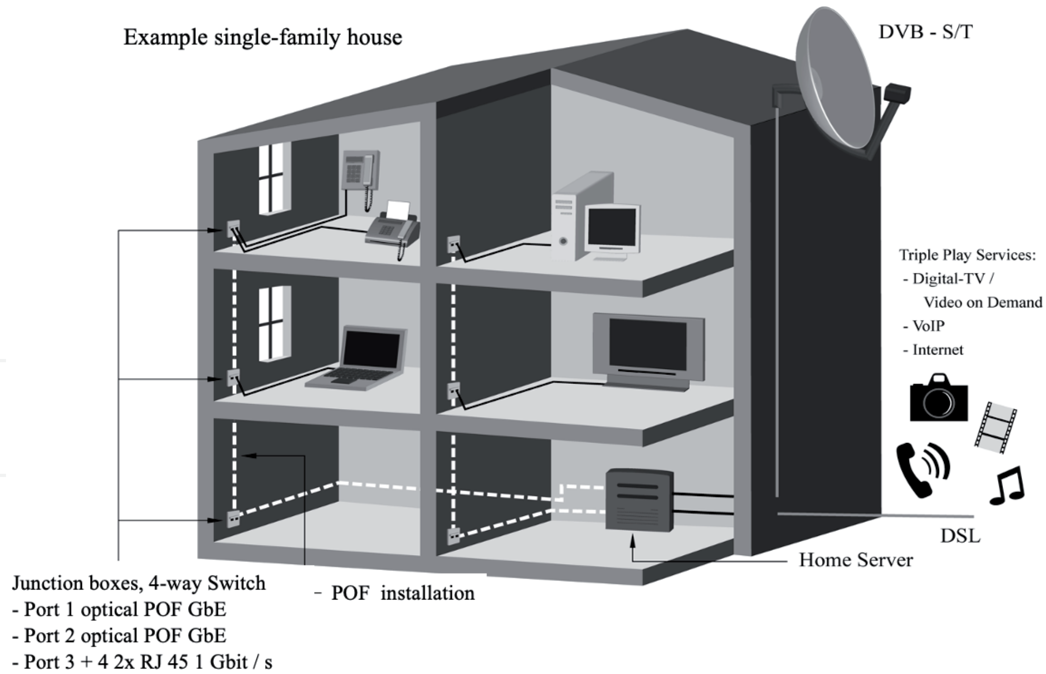


**Figure 16.**
*Optical POF bus in the home network.*

From this router, optical POF fiber cables are installed in all rooms in the house with active switches with four ports and connected there. Forwarding via additional switches the data can easily be routed to each room and connected. Furthermore, a corresponding WiFi module can be integrated in these switches, which can illuminate each room individually with small radio energy and is available for mobile devices in this room. By reducing the radio energy, each room can be connected to its own WiFi radio network and thus does not interfere with the transmission quality of the adjoining rooms. The radio energy must be set so low that the radio waves from the individual WiFi areas in the room do not get into the neighboring room and are attenuated enough by the walls.

It is also possible to lay the polymer fiber slightly behind baseboards in existing structures and thus not have to finance complex and expensive construction measures.

## 7. Conclusions

Optical fiber networks are currently the standard for delivering high bandwidth to customers. It was discussed, that there are various access technologies to local networks with a very high bandwidth up to access individual customers in their homes or flats. The use of optical glass fibers or/and polymeric optical fibers in different network topologies in connection to high speed actual WiFi- technologies have been discussed.

Both, the copper networks with CAT connections, as well as the networking with optical glass fiber and optical were compared and their strengths and weaknesses were shown. The Polymer Optical Fiber exhibits many advantages in comparison to glass fiber and copper as the medium for communication. The mentioned applications show different special sectors to the application of one of the three transmission technologies.

The focus in this work lies on the possibility of conveying high data rates, as well as the simplest possible relocation of network components in the SoHo area. In the area of permanently installed network components, the use of POF fibers proved to be particularly suitable for network bandwidths of up to 1 Gb/s. In addition to the almost relocated optical components, the installation of a wireless network via WiFi is a particularly good addition to make mobile devices easily networkable for the customer. Thus, a recommendation can be issued for both, optical polymer fibers with Ethernet network technology in combination with current WiFi technology. Both system components will experience further expansion stages in the range in the next few years and thus always remain applicable and expandable.

## Author details

Ulrich H.P. Fischer[1]*, Matthias Haupt[2] and Peter Kußmann[1]

1 Harz University of Applied Sciences, Wernigerode, Germany

2 Jade University of Applied Sciences, Wilhelmshaven, Germany

*Address all correspondence to: ufischer@hs-harz.de

IntechOpen

© 2021 The Author(s). Licensee IntechOpen. This chapter is distributed under the terms of the Creative Commons Attribution License (http://creativecommons.org/licenses/by/3.0), which permits unrestricted use, distribution, and reproduction in any medium, provided the original work is properly cited.

## References


[1] European Commission. Broadband: Technology overview [Internet]. Broadband: Technology overview. 2020. p. 2. Available from: https://digital-strategy.ec.europa.eu/en/policies/broadband-technology-overview

[2] Shafi M, Molisch AF, Smith PJ, Haustein T, Zhu P, De Silva P, et al. 5G: A Tutorial Overview of Standards, Trials, Challenges, Deployment, and Practice. IEEE J Sel Areas Commun. 2017;35(6):1201-21.

[3] German Telecom. Fiber to the X - The architecture of fiber-optic lines [Internet]. 14.06.2021. 2021. p. 3. Available from: https://www.telekom.com/en/company/details/ftth-fttb-fttc-fiber-optic-lines-in-fiber-optic-networks-608068

[4] Grötschel M, Raack C, Werner A. Towards optimizing the deployment of optical access networks. EURO J Comput Optim [Internet]. 2014;2(1):17-53. Available from: https://doi.org/10.1007/s13675-013-0016-x

[5] Sagar N. Powerline communications systems. 2011. 147 p.

[6] Suryo Prayogo S, Al Rafi F, Mukhlis Y. Design and Built IoT Home Panic Button for Smart City. In: Journal of Physics: Conference Series. 2019.

[7] Mendes TDP, Godina R, Rodrigues E, Matias J, Catalão J. Smart Home Communication Technologies and Applications: Wireless Protocol Assessment for Home Area Network Resources. Energies. 2015;8:7279-311.

[8] Danbatta SJ, Varol A. Comparison of Zigbee, Z-Wave, Wi-Fi, and Bluetooth Wireless Technologies Used in Home Automation. In: 2019 7th International Symposium on Digital Forensics and Security (ISDFS). 2019. p. 1-5.

[9] DIN EN 50173: Information technology - Generic cabling systems,. 2010 p. 20.

[10] Dave Hood ET. Introduction. In: Gigabit-Capable Passive Optical Networks [Internet]. John Wiley & Sons, Ltd; 2012. p. 1-8. Available from: https://onlinelibrary.wiley.com/doi/abs/10.1002/9781118156070.ch1

[11] Dave Hood ET. System Requirements. In: Gigabit-Capable Passive Optical Networks [Internet]. John Wiley & Sons, Ltd; 2012. p. 9-47. Available from: https://onlinelibrary.wiley.com/doi/abs/10.1002/9781118156070.ch2

[12] Dave Hood ET. Optical Layer. In: Gigabit-Capable Passive Optical Networks [Internet]. John Wiley & Sons, Ltd; 2012. p. 49-125. Available from: https://onlinelibrary.wiley.com/doi/abs/10.1002/9781118156070.ch3

[13] Dave Hood ET. Transmission Convergence Layer. In: Gigabit-Capable Passive Optical Networks [Internet]. John Wiley & Sons, Ltd; 2012. p. 127-218. Available from: https://onlinelibrary.wiley.com/doi/abs/10.1002/9781118156070.ch4

[14] Fischer UHP, Schulze H-M, Reinboth C. NGA im ländlichen Raum: Erfahrungsbericht aus der Harzregion NGA in rural areas: Experiences from the Harz region. In: ITG-Fb 262: Breitbandversorgung in Deutschland Beiträge der 10 ITG-Fachkonferenz, 18-19 April 2016 in Berlin [Internet]. Berlin: VDE Verlag , Berlin; 2016. p. 5. Available from: https://www.vde-verlag.de/buecher/454193/itg-fb-262-breitbandversorgung-in-deutschland.html

[15] Zygiaris S. Smart City Reference Model: Assisting Planners to

Conceptualize the Building of Smart City Innovation Ecosystems. J Knowl Econ [Internet]. 2013;4(2):217-31. Available from: https://doi.org/10.1007/s13132-012-0089-4

[16] Borgia E. The Internet of Things vision: Key features, applications and open issues. Comput Commun [Internet]. 2014;54:1-31. Available from: https://www.sciencedirect.com/science/article/pii/S0140366414003168

[17] Tucker WD, Blake EH, Marsden G. Open User Interconnect and Quality of Communication. In: D. Browne (ed.), editor. Southern African Telecommunication Networks and Applications Conference (SATNAC). Stellenbosch, South Africa; 2004. p. 261-262.

[18] Gazis V, Görtz M, Huber M, Leonardi A, Mathioudakis K, Wiesmaier A, et al. A survey of technologies for the internet of things. In: 2015 International Wireless Communications and Mobile Computing Conference (IWCMC). 2015. p. 1090-5.

[19] ITU G.992.1: Asymmetric digital subscriber line (ADSL) transceivers.

[20] ITU J.122: Second-generation transmission systems for interactive cable television services - IP cable modems Recommendation.

[21] Jabel AN, Manickam S, Ramdas S. A study of SIP trunk security and challenges. In: 2012 IEEE International Conference on Electronics Design, Systems and Applications (ICEDSA). 2012. p. 239-43.

[22] ITU-T G711. ITU G.711: Pulse code modulation (PCM) of voice frequencies [Internet]. ITU-G Recommendations; 2012 p. 10. Available from: https://www.itu.int/rec/T-REC-G.711

[23] ITU-T Recommendations. ITU H264 standard [Internet]. ITU-T Recommendations; 2012 p. 10. Available from: https://www.itu.int/ITU-T/recommendations/rec.aspx?rec=11466

[24] ITU P.862: Perceptual evaluation of speech quality (PESQ): An objective method for end-to-end speech quality assessment of narrow-band telephone net-works and speech codecs.

[25] ITU G.107: The E-model: a computational model for use in transmission planning,.

[26] ITU. ITU G.722: 7 kHz audio-coding within 64 kbit/s [Internet]. ITU-G Recommendations; 2012 p. 10. Available from: https://www.itu.int/rec/T-REC-G.722/_page.print

[27] Fischer-Hirchert UHP, Hoppstock S, Kußmann P. Intelligent Assistance Systems with Real-Time Sensor Data Analysis-Framework for Digital Care. German Society for Biomedical Engineering, editor. Biomed Eng-Biomed Tech [Internet]. 2020;65((s1)):2. Available from: https://www.edas.info/p27318

[28] CME edu. Acrylic glas properties [Internet]. 2020. Available from: https://www.cs.cmu.edu/afs/cs/academic/class/15294t-s18/resources/Acrylic-data-sheet.pdf

[29] Imani R, Cuellar GH. Introductory Chapter: Optical Fibers. In: Huerta-Cuellar G, Imani R, editors. Optical Fiber Applications [Internet]. Rijeka: IntechOpen; 2020. Available from: https://doi.org/10.5772/intechopen.91397

[30] Fischer UHP, Krips O, Muller E, Jacob a, Müller E, Jacob a. Laser microwelding for fiber-chip coupling modules with tapered standard monomode fiber ends for optical communication systems. Opt Eng

[Internet]. 2002;41(12):3221-9. Available from: http://www.scopus.com/inward/record.url?eid=2-s2.0-0036980315&partnerID=40&md5=2eb8dc59f97d555bdaf5af63609ebc95

[31] Katayama S. Fundamentals and Details of Laser Welding. Berlin: Springer Berlin Heidelberg; 2020. p 198.

[32] Gu M, Sheppard CJR, Gan X. Image formation in a fiber-optical confocal scanning microscope. J Opt Soc Am A [Internet]. 1991 Nov;8(11):1755-61. Available from: http://josaa.osa.org/abstract.cfm?URI=josaa-8-11-1755

[33] Smithwick QYJ, Seibel EJ. Depth enhancement using a scanning fiber optical endoscope. In: Alfano RR, editor. Optical Biopsy IV [Internet]. SPIE; 2002. p. 222-33. Available from: https://doi.org/10.1117/12.465249

[34] Křemenáková D, Militky J, Meryova B, Lédl V. Characterization of Side Emitting Polymeric Optical Fibres. J Fiber Bioeng Informatics. 2012;5:423-31.

[35] Abang A, Webb DJ, Peng G-D. Strain response of POF sensors. In: 22nd International Conference on Optical Fiber Sensors. 2012.

[36] Höll S, Haupt M, Fischer UHP. Design and Development of a injection-molded demultiplexer for optical communication systems in the visible range. Appl Opt [Internet]. 2013;52(18):4103-10. Available from: http://www.ncbi.nlm.nih.gov/pubmed/23842150

[37] G.651 I-T. Characteristics of a 50/125 µm multimode graded index optical fibre cable. 1993.

[38] Haupt M, Fischer UHPHP. WDM over POF - the inexpensive way to break through the limitation of bandwidth of standard POF communication. Proc SPIE Photonics Packag Integr Interconnects VII [Internet]. 2007;6478(6478):64780I-64780I – 10. Available from: http://proceedings.spiedigitallibrary.org/proceeding.aspx?articleid=1298065

[39] Joncic M, Kruglov R, Haupt M, Caspary R, Vinogradov J, Fischer UHP, et al. Four-Channel WDM Transmission Over 50-m SI-POF at 14.77 Gb/s Using DMT Modulation. Photonics Technol Lett IEEE2. 2014;26(13):1328-31.

[40] Fischer UHP, Haupt, Joncic. WDM over POF up to 40 Gbit/s. In: Fraunhofer-Gesellschaft. Dr. Tolga Tekin, editor. 1st Optical Interconnect in Data Centers Symposium [Internet]. Berlin, Germany 2014,: Fraunhofer-Gesellschaft. Dr. Tolga Tekin,; 2014. p. 6. Available from: http://www.phoxtrot.eu/1st-optical-interconnect-in-data-centers-symposium/

[41] Fischer-Hirchert UHP. Beyond the Dispersion Limit of Standard Polymeric Fiber Transmission Systems. In: Prof Abraham Katzir, editor. OASIS 7 (Optical Engineering and Science in Israel) Proceedings [Internet]. Telaviv; 2019. Available from: http://oasis7.org.il/wp-content/uploads/2019/03/Oasis-7-Poster-List-3.pdf

[42] Toshiba Corp. Fiber-Optic Devices TOSLINKTM [Internet]. 2008 p. 16. Available from: http://www.digikey.com/Web Export/Supplier Content/Toshiba_264/PDF/Toshiba_BCE0037_catalog.pdf?redirected=1

[43] Cooperation TM. MOST Technology Report [Internet]. Karlsruhe; 2016. Available from: www.mostcooperation.com

[44] Fischer UHP, [Fischer11] U. H. P. Fischer-Hirchert, M. Haupt, and M. Joncic, Fischer UHP. Optical Transmission Systems Using Polymeric Fibers. In: Predeep P, editor. Optoelectronics- Devices and Applcations [Internet]. Rijeka, Croatia:

intech open; 2011. p. Chapter 22. Available from: http://www.intechopen.com/articles/show/title/optical-transmission-systems-using-polymeric-fibers

[45] Grzemba. MOST. The Automotive Multimedia Network. From MOST25 to MOST150. Poing: Franzis; 2011. 250 p.

[46] Visani D. Fiber-Optic Technologies for Wireline and Wireless In-building Networks [Internet]. alma; 2012. Available from: http://amsdottorato.unibo.it/4535/

[47] Poisel H, Ziemann O. What are POF ? [Internet]. 2015. Available from: https://www.th-nuernberg.de/fileadmin/institute/pof-ac/pof-ac_docs/Was_ist_POF_2017_A5__2017.pdf

[48] Fischer UHP. Dismantling and cutting glass fiber [Internet]. 2010. Available from: https://youtu.be/NZVH8yJcjCM

[49] Fischer UHP, Haupt M. Optische Schlüsselemente für die Polymerfaserübertragung mit Mikrospritzguss. In: Mageburger Maschinenbautage 2009. Magdeburg: Otto von Guericke Universität; 2009. p. 10.

[50] homefibre. POF Gigabit Switches [Internet]. 14.06.2021. 2021. Available from: https://www.home-fibre.ch/shop/en/pof-switches/96-12-4-port-gigabit-pof-switch.html

[51] IEEE. IEEE 802.11n [Internet]. 2009. Available from: https://standards.ieee.org/standard/802_11n-2009.html

# We are IntechOpen, the world's leading publisher of Open Access books Built by scientists, for scientists

6,300
Open access books available

171,000
International authors and editors

190M
Downloads

154
Countries delivered to

Our authors are among the
TOP 1%
most cited scientists

12.2%
Contributors from top 500 universities

BOOK CITATION INDEX
CLARIVATE ANALYTICS
INDEXED

WEB OF SCIENCE™

Selection of our books indexed in the Book Citation Index in Web of Science™ Core Collection (BKCI)

Interested in publishing with us?
Contact book.department@intechopen.com

Numbers displayed above are based on latest data collected.
For more information visit www.intechopen.com

Chapter

# Coded Modulation and Impairment Compensation Techniques in Optical Fiber Communication

*Zhipei Li, Dong Guo and Ran Gao*


## Abstract

This chapter deals with coded modulation and impairment compensation techniques in optical fiber communication. Probabilistic shaping is a new coded modulation technology, which can reduce transmission power by precoding, reduce bit error rate and improve communication rate. We proposed a probabilistic shaping 16QAM modulation scheme based on trellis coded modulation. Experimental results show that this scheme can achieve better optical SNR gain and BER performance. On the other hand, in order to meet the demand of transmission rate of next generation high speed optical communication systems, multi-dimensional modulation and coherent detection are sufficiently applied. The imperfect characteristics of optoelectronic devices and fiber link bring serious impairments to the high baud-rate and high order modulation format signal, causes of performance impairment are analyzed, pre-compensation and receiver side's DSP techniques designed for coherent systems are introduced.


**Keywords:** Coherent Optical Communication, Coded Modulation, Probabilistic Shaping, Digital Signal Processing, Pre-Compensation, Quadrature Amplitude Modulation

## 1. Introduction

With the rapid development of Internet services, higher requirements are put forward for the transmission rate, system capacity and stability of communication. Optical fiber communication has become one of the main communication methods in the world because of its large transmission bandwidth, long-distance transmission and strong anti-interference ability.

The optical fiber communication systems are mainly divided into two types: intensity modulation-direct detection (IM-DD) and coherent optical communication systems. The IM-DD system is mainly used in access networks, passive optical networks (PON) and data centers, and its transmission distance is usually less than 80 km. Specified in the standard, the highest transmission rate with single-wavelength of IM-DD system is 100Gb/s, transmitting 56GBaud 4-level pulse amplitude modulation (PAM4) signal. The coherent optical transmission system, which uses multi-dimensional modulation to improve spectrum efficiency, local oscillator lasers to increase sensitivity, and digital signal processing (DSP) technology for impairment compensation, thereby can greatly improve transmission performance, increase transmission rate and distance, and is usually used in in large-capacity long-distance backbone networks and metropolitan area networks.

Quadrature amplitude modulation (QAM) is commonly used in coherent optical fiber transmission system. In this method, evenly distributed constellation points are arranged in two-dimensional space to form a constellation diagram. The performance loss of the modulation scheme tends to $\pi e/6$ (1.53 dB) from the Shannon limit. To further approach Shannon limit capacity and improve system performance, probabilistic shaping technology can be used [1]. Probabilistic shaping is a new coded modulation technology. It can reduce transmission power by precoding, reduce bit error rate and improve communication rate without changing the original system. And with the change of channel environment, the channel can be matched by changing the size of the shaping, thus improving the flexibility of the system.

The future research direction of high-speed optical fiber communication is digital coherent optical communication technology [2–4]. With the development of high-bandwidth optoelectronic devices, digital-to-analog converter (DAC), analog-to-digital converter (ADC) and application specific integrated circuit (ASIC) chips, beyond 800Gb/s transmission with single wavelength above becomes possible. In order to achieve such high-speed transmission, DSP technology plays an important role in dealing with chromatic dispersion (CD), polarization mode dispersion (PMD), frequency offset and phase noise, by compensating the signal at the transmitter and receiver in the electrical domain. With highly integrated and flexible digital coherent optical detection technology, high-speed, large-capacity and long-distance optical communication can be effectively realized.

The most important technologies in coherent optical communication system are introduced in this chapter, a novel coded modulation technology based on probabilistic shaping and DSP-based Impairment compensation techniques.

## 2. Novel coded modulation technology based on probabilistic shaping

### 2.1 Principle of probabilistic shaping

The main idea of probabilistic shaping is to reduce the probability of occurrence of constellation points in outer ring, increase ones in the inner ring, and change the constellation of uniform distribution into non-uniform distribution. The common distribution matcher is constant composition distribution matcher (CCDM), which makes the occurrence probability of each constellation point conform to Maxwell Boltzmann distribution:

$$P_X(x_i) = \frac{e^{-v|x_i|^2}}{\sum_{j=1}^{m} e^{-v|x_j|^2}} \tag{1}$$

Where, $X = \{x_1, x_2, \ldots\ldots, x_m\}$ is the constellation symbol set, $v$ is the probability distribution factor, and the value range is $0 \sim 1$. The larger value of $v$, the higher the degree of constellation shaping [5].

Taking 16QAM modulation format as an example, the constellation probability distribution diagram is shown in **Figure 1**, and the constellation diagram after recovery at the receiving end is shown in **Figure 2**.

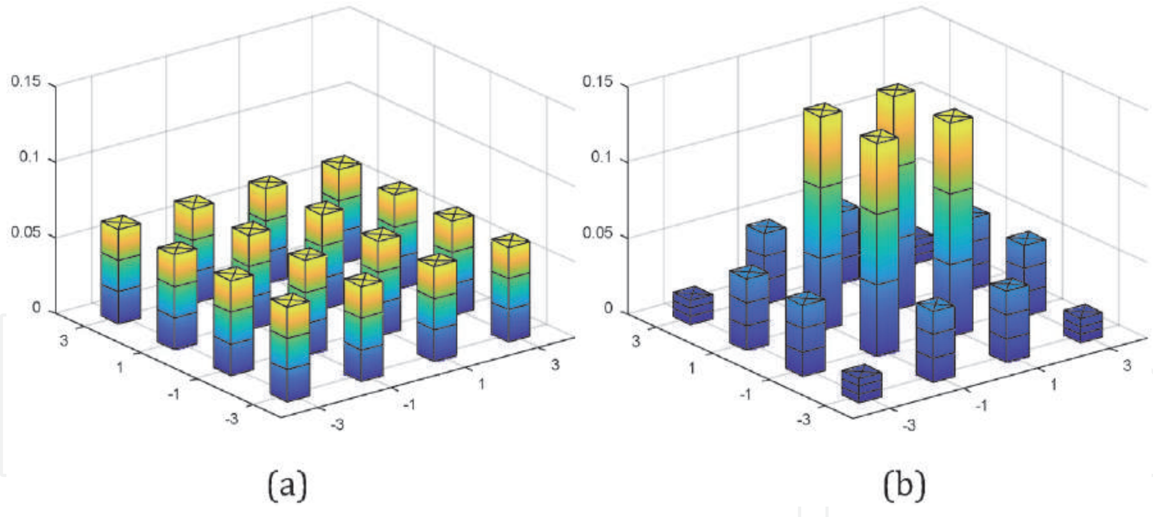


**Figure 1.**
*Probability distribution of 16QAM signal. (a) Uniform 16QAM; (b) PS 16QAM.*

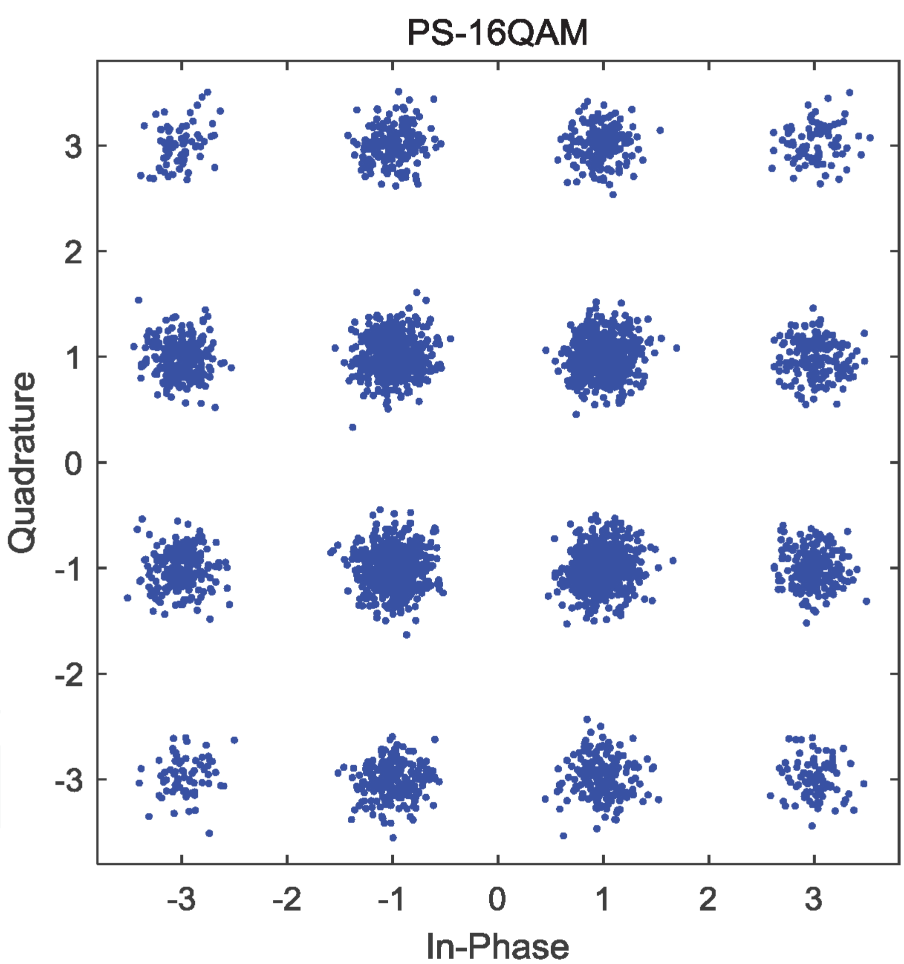


**Figure 2.**
*Constellation for receiver recovery using probabilistic shaping technique.*

## 2.2 Experiment

To evaluate the performance of the proposed scheme, an experiment is carried out by employing the coherent optical communication system setup illustrated in **Figure 3**. The system parameters are shown in **Table 1**. At the transmitter, a 1550 nm lightwave with power of 10 dBm and line-width of 100 kHz is employed as the laser source, followed by a polarization beam splitter to divide the output light

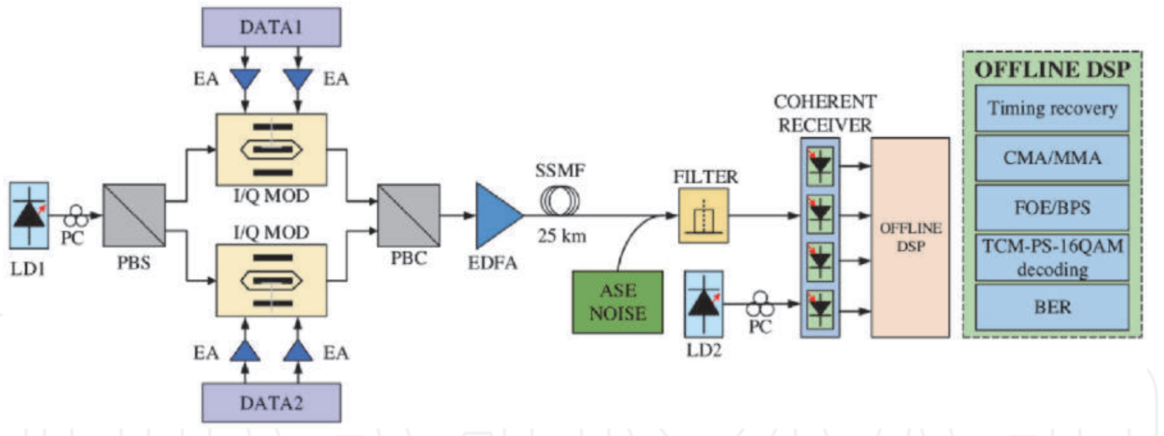


**Figure 3.**
*Experimental setup for PDM single carrier system.*

| Parameter | Specification |
|---|---|
| Center wavelength | 1550 nm |
| Laser linewidth | 100 kHz |
| Input power of fiber | 0 dBm |
| Amplification | EDFA |
| EDFA gain | 20 dB |
| EDFA noise figure | 4 dB |
| Fiber | SSMF |
| Attenuation | 0.2 dB/km |
| Nonlinear coefficient | $1.3(\text{W}\cdot\text{km})^{-1}$ |
| Chromatic dispersion | 17 ps/(nm·km) |
| Span length | 25 km |

**Table 1.**
*System parameters.*

into orthogonal polarized pair. Then two I/Q modulator are applied to modulate two orthogonal light waves, respectively. Trellis-Coded Modulation (TCM)-PS-16QAM signals are generated offline by MATLAB program. And each modulator is driven by two 10Gbaud amplified electrical TCM-PS-16QAM signals with a frame length of 33,336 symbols, and 10 patterns (333,360 symbols) are collected for bit error ratio (BER) calculation. The peak-peak voltage of the two amplified electrical signals are both set as 2.0 V. And a polarized beam combiner is applied to combine two orthogonal modulated lightwaves, which is amplified by an erbium-doped fiber amplifier (EDFA) in the standard single mode fiber (SSMF) for transmission. The gain and the noise figure of the EDFA are 20 dB and 4 dB, respectively. The input power of the fiber is 0 dBm, and the fiber is a SSMF with attenuation of $\alpha$ = 0.2 dB/km, nonlinear coefficient of $\gamma = 1.3\ (\text{W}\cdot\text{km})^{-1}$, and dispersion of $D$ = 17 ps/nm/km. At the receiver, the ASE noise is added to the received optical signal to adjust the received optical signal noise ratio (OSNR) with the resolution of 0.1 nm. The optical signal added with noise is bandpass-filtered and converted into an electrical signal by a coherent receiver. The laser diode (LD) generates a local oscillating light with the power of 5 dBm and linewidth of 100 kHz. In the offline DSP module, timing recovery is implemented by Gardner algorithm and chromatic dispersion is compensated digitally. To process different shaped signals, a pre-convergence constant modulus algorithm with step of 2e-6 and taps of 9 followed by 1% pilot aided multi-modulus algorithm are used for polarization demultiplexing and compensation of polarization mode dispersion without training sequence. In addition, fast Fourier transform based frequency offset estimation (FFT-FOE) algorithm and blind phase search algorithm are applied to realize frequency offset estimation and compensate the laser phase noise, respectively. Finally, TCM-PS-16QAM decoding and statistics of BER are implemented.

To verify our proposed scheme, we compare the performance of 8QAM, TCM-16QAM-4state, TCM-16QAM-8state, TCM-16QAM-16state, and TCM-PS-16QAM-4state respectively. The convolutional encoders and information entropy parameters are displayed in **Table 2**. Here, some modulation formats have different entropy, and lower entropy means a higher baud-rate, which makes their bit-rates consistent.

In the experiment, the TCM-PS-16QAM ($H$ = 2.8 bits/symbol) with OSNR = 15 dB is firstly transmitted. After the optical transmission system, the received signal of the subset S0, S1, S2, S3 and the overall constellation at the receiver is shown in **Figure 4**. The successful transmission of the TCM-PS-16QAM signal means that our proposed novel scheme is reasonable and realizable.

| Scheme | Entropy (bits/symbol) | Baud rate (GBaud) |
|---|---|---|
| 8QAM | 3 | 10 |
| TCM-16QAM-4state | 3 | 10 |
| TCM-16QAM-8state | 3 | 10 |
| TCM-16QAM-16state | 3 | 10 |
| TCM- PS-16QAM-4state | 2.9 | 10.4 |
| | 2.8 | 10.7 |
| | 2.7 | 11.1 |

**Table 2.**
*Modulation format parameters.*

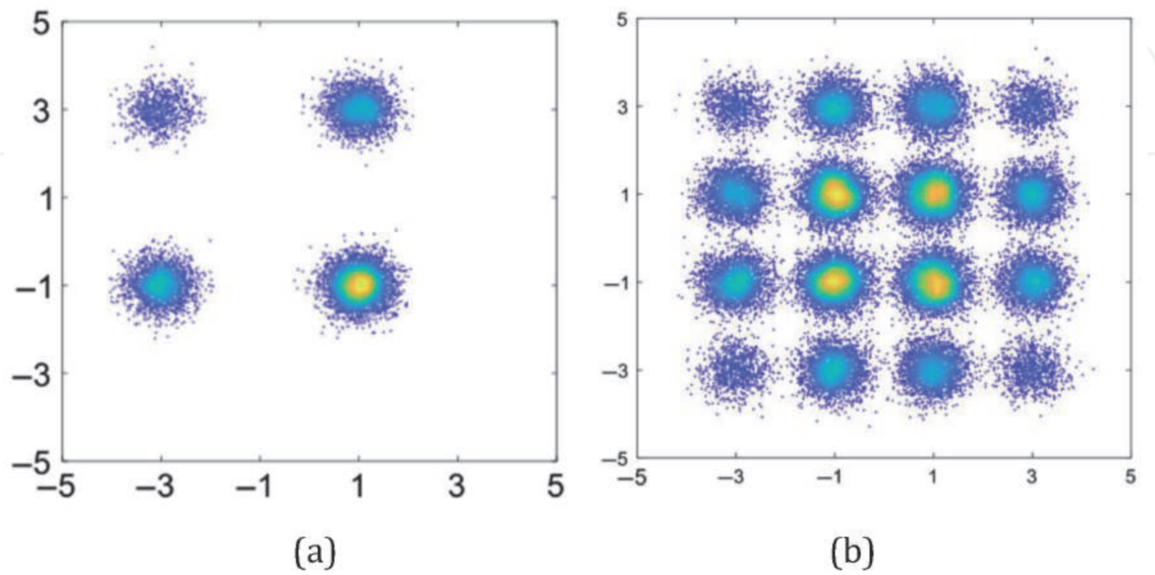


**Figure 4.**
*Probability distribution with the entropy of 2.8 bits/symbol of the proposed (a) subset $S_0$ constellation, (b) TCM-PS-16QAM constellation at the receiver.*

Meantime, it can be seen that the probability distribution of the constellation points achieves the goal of low energy point density and high energy point sparseness.

**Figure 5** depicts the BERs of 8QAM, TCM-16QAM-4state, TCM-16QAM-8state, TCM-16QAM-16state, and TCM-PS-16QAM-4state ($H$ = 2.9 bits/symbol) with the same data rate of 60 Gb/s after 25-km SSMF transmission. It can be seen that when the OSNR is above 5 dB, the performance of TCM-16QAM-nstate (n = 4, 8, 16) is better than 8QAM. And with the increase of OSNR, the BERs of TCM-16QAM-nstate (n = 4, 8, 16) fall faster than 8QAM. At the BER of $1 \times 10^{-3}$, TCM-16QAM-4state obtains the gain of 3.4 dB compared to 8QAM. However, TCM-16QAM-8state slightly outperforms TCM-16QAM-4state and the OSNR gain is just 0.4 dB. Meantime, compared to 8 state, the gain of TCM-16QAM-16state grows only 0.4 dB too. And the decoding complexity double as the number of state double. So, increasing the number of states is not a suitable way to obtain coding gain, especially when the coding gain is close to the limit. The required OSNR for BER of $1 \times 10^{-3}$ is about 7.7 dB for TCM-16QAM-4state, and 6.8 dB for TCM-PS-16QAM-4state ($H$ = 2.9 bits/symbol), The OSNR improvement is increased by 0.9 dB with a little more complexity. Compared to TCM-16QAM-8/16state, TCM-PS-16QAM-4state ($H$ = 2.9 bits/symbol) has lower decoding complexity and better performance. And the gain of TCM-PS-16QAM-4state ($H$ = 2.9 bits/symbol) grows 0.5 dB and 0.1 dB, respectively. This is mainly due to the shaping gain brought by PS. Under the condition that the minimum Euclidean distance in the constellation

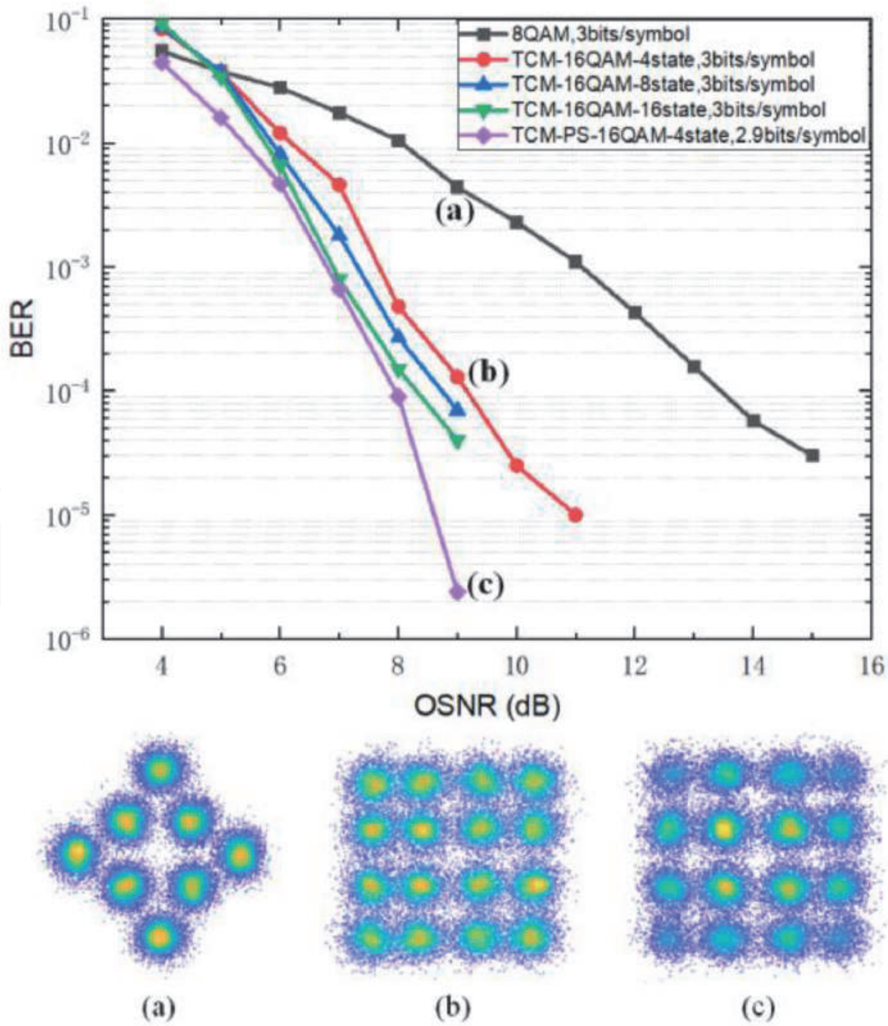


**Figure 5.**
*BER curves and constellations of different modulation formats (H = 2.9 bits/symbol) for 25-km transmission. (a)8QAM, (b)TCM-16QAM-4/8/16state, (c)TCM-PS-16QAM-4state.*

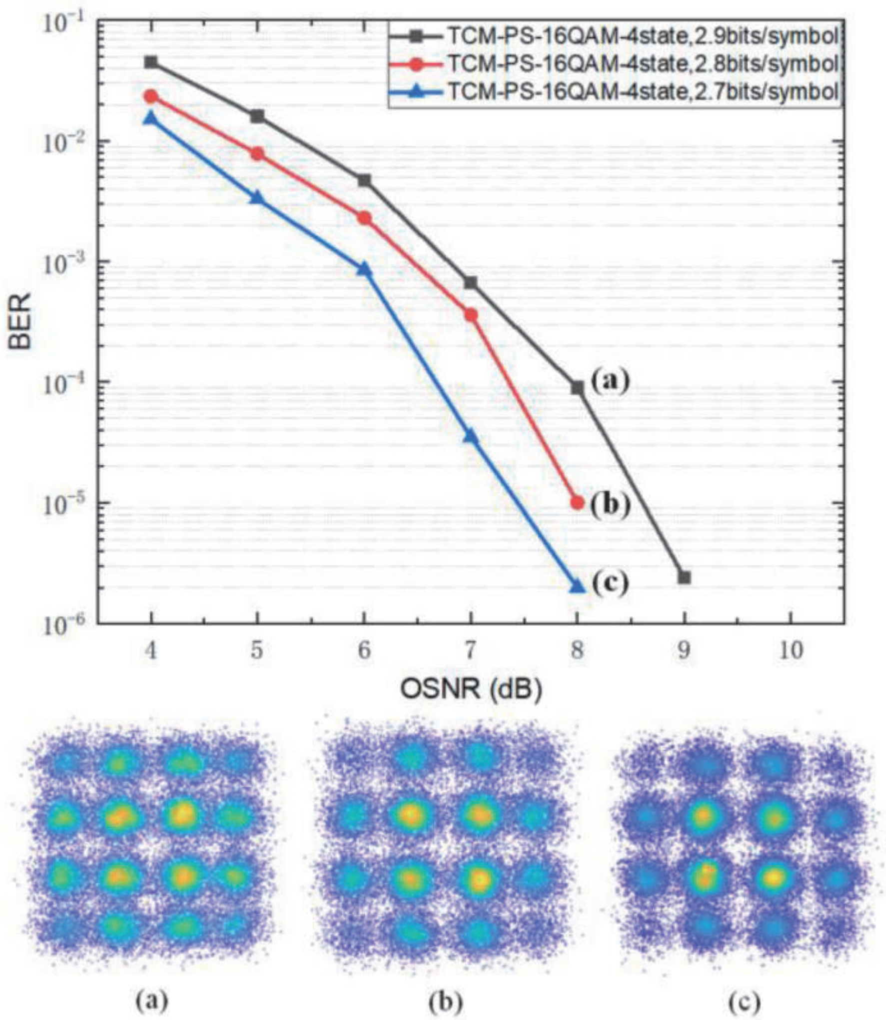


**Figure 6.**
*BER curves and constellations of TCM-PS-16QAM-4state for 25-km transmission. (a) H=2.9 bits/symbol, (b) H = 2.8 bits/symbol, (c) H = 2.7 bits/symbol.*

remains unchanged, the convergence of most constellation points greatly reduces the average power of the constellation, improving the performance of the entire modulation system.

The BER curves of TCM-PS-16QAM-4state with different information entropy after 25-km transmission are also measured, and the measured results are shown in **Figure 6**. In our experiments, according to their different information entropy, the baud rate is set differently, their information entropy is 2.9, 2.8, 2.7 bits/symbol, so the baud rate is 20.7, 21.4, 22.2Gbaud, namely, the bit rate is 60 Gb/s. It can be seen that the required OSNRs are 6.8 dB, 6.5 dB, and 5.9 dB at the BER of $1 \times 10^{-3}$. In other words, TCM-PS-16QAM-4state ($H$ = 2.7 bits/symbol) obtains OSNR gain of 0.6 and 0.9 dB compared with TCM-PS-16QAM-4state ($H$ = 2.8 and 2.9bits/symbol), respectively. This advantage proves that as the information entropy decreases, more shaping gains can be obtained. Obviously, at the same OSNR, the lower the information entropy, the better the BER performance and the more flexible information entropy and gain compared to the traditional TCM-16QAM.

## 3. Impairment compensation techniques in coherent communication

Coherent optical communication systems are implemented in the form of optical modules in commercial communication equipment [6]. As shown in **Figure 7**, The

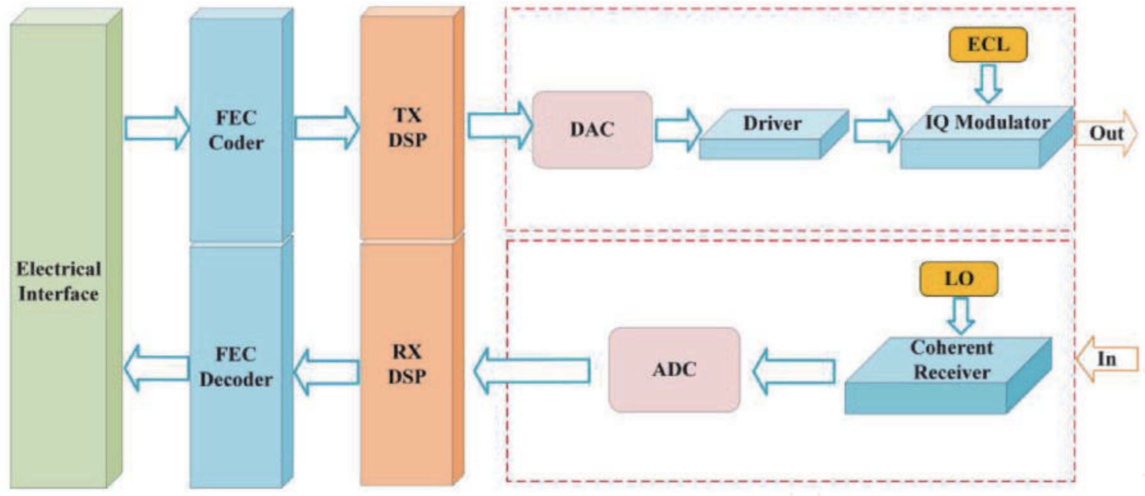


**Figure 7.**
*Coherent optical module structure.*

transmitted information is encoded by forward error correction (FEC) through the electrical interface and then transmitted to transmitter-side (TX) DSP. The TX DSP includes constellation mapping, pulse shaping, pre-equalization, skew compensation, dispersion pre-compensation, etc. The main purpose of implementing DSP-based pre-compensation techniques at the transmitter is to increase the signal-to-noise ratio (SNR) of the transmitted signal while the transmission power is limited, reduce the bandwidth requirement for signal transmission, avoid inter-symbol interference (ISI), and reduce the impairment caused by the optoelectronic devices.

After single mode fiber channel, the coherent optical signal is transmitted into the coherent receiver and ADC to obtain four electrical signals, which consist of dual polarizations X/Y and in-phase/quadrature (IQ) components XI, XQ, YI, and YQ. The receiver-side (RX) DSP contains a series of impairment compensation and equalization algorithms for the optoelectronic devices and fiber link, including IQ signal orthogonalization, normalization, dispersion compensation, clock recovery, polarization demultiplexing, frequency offset estimation, and phase noise recovery. DSP compensation technology at the receiver side is the core of coherent optical communication. It can recover multi-dimensional modulated signals from distorted constellation, to realized large-capacity transmission.

This chapter will introduce the impairment compensation technology based on DSP in two parts, all common compensation techniques are described in detail.

### 3.1 Impairment compensation techniques at transmitter side

Pre-equalization and skew compensation are basic DSP techniques at transmitter side, pre-equalization technique is used to compensate the filtering effect caused by the bandwidth limitation of transmitting devices, and skew compensation is to compensate the delay of XI, XQ, YI and YQ signals while passing through the electrical and optical paths [7]. At the same time, in order to cope with more and more high-speed transmission, such as 400Gb/s, 800Gb/s and 1.2 Tb/s transmission, high-order modulation format and high baud rate signal is generated and transmitted, such as 96Gbaud 32QAM and 80Gbaud 64QAM, which is extremely sensitive to linear and nonlinear impairment of optoelectronic devices, therefore, other pre-compensation algorithms such as look-up table (LUT) and digital predistortion (DPD) are usually added to the next generation coherent optical module's DSP algorithm. In this section, basic principles of the impairment compensation techniques at transmitter side are described for the development of next generation coherent optical transmission systems.

#### *3.1.1 Bandwidth limitation and pre-equalization*

Restricted by material and technical level, the frequency response of the opto-electronic device is not flat in the range of the bandwidth needed to transmit the signal, as shown in **Figure 8**, the transmitted signal will fade at high frequency, which leads to inter symbol interference, the smaller the bandwidth is, the more serious the ISI is and the worse the BER performance.

To suppress the performance degradation of high-speed signal caused by bandwidth limited system, the pre-equalization technology based on DSP can alleviate the bandwidth shortage of the transmitter device, which is an effective bandwidth compensation method. To implement pre-equalization, it is necessary to obtain the frequency response of the transmitter, including DAC, electric driver, modulator and so on. First, we send specific training sequence $X$ without any compensation, then receive the signal $Y$ with a high bandwidth digital sampling oscilloscope, we can estimate the frequency response $H$ of the transmitter by comparing the transmitted and received signals with least square (LS) algorithm

$$H_{LS} = \left(X^H X\right)^{-1} X^H Y \tag{2}$$

Then we multiply the inverse of the estimated frequency response with the transmitted data in the frequency domain

$$X_{TX} = X \cdot H_{LS}^{-1} \tag{3}$$

Thus, the high frequency component of the signal can be raised at the transmitter to resist the low-pass filtering effect of the device. The spectrum of the transmitted signal is flat to reduce the inter symbol crosstalk.

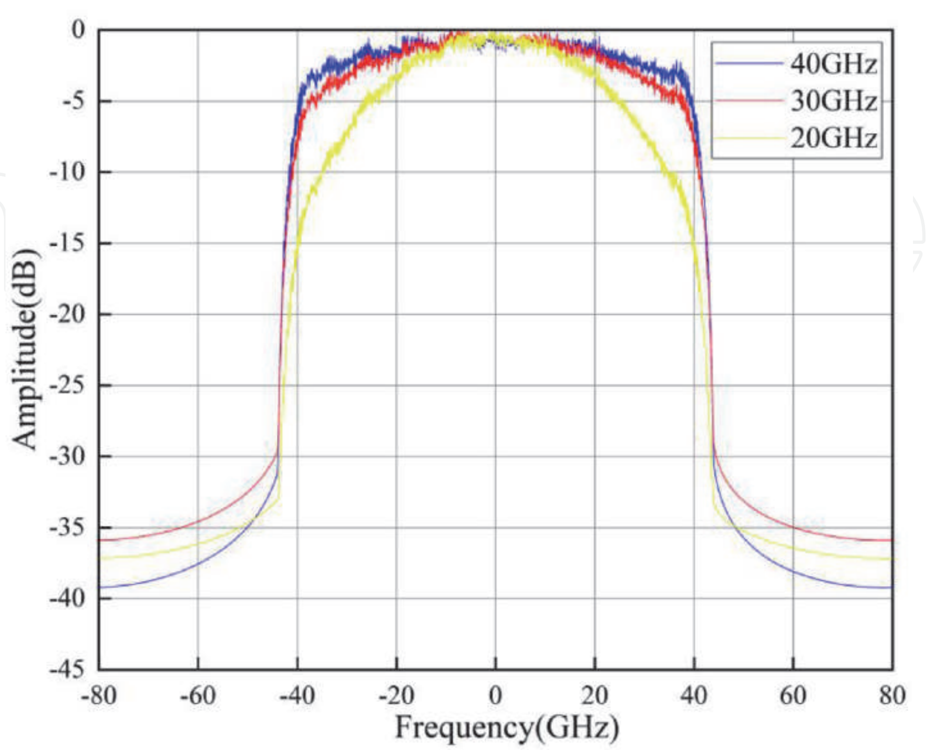


**Figure 8.**
*Spectrum of transmitted signal with different bandwidth limitation.*

### 3.1.2 Look-up table algorithm

LUT is a pre-compensation method, which is used to compensate the memory effect of the amplifier. From the time domain point of view, the memory effect means that the current output symbol of the amplifier is not only dependent on the current input symbol, but also related to the past input symbol value. From the perspective of frequency domain, memory effect can be defined as the phenomenon that the amplitude and phase characteristics of intermodulation distortion term of amplifier change with the variation of envelope frequency of input signal. Considering the influence of $2N + 1$ symbols before and after the symbols at the intermediate time, all possible transmitted sequences are $X(k - N : k + N)$, and the corresponding received sequence is $Y(k - N : k + N)$. All data in lookup table are set to 0 in the initial state, and the sliding window selects $2N + 1$ symbols in the transmission sequence each time, after looking up the index and finding the address of this pattern, the error $E(k)$ is obtained by subtracting the central symbol of the sending sequence and the receiving sequence. As the sliding window moves forward, error values of all transmission modes can be traversed. Suppose the lookup table index is $i$, the number of data stored in index is $M(i)$, and the lookup table is updated as follows

$$LUT(i) = LUT(i) + E(k) \tag{4}$$

$$M(i) = M(i) + 1 \tag{5}$$

$$LUT(i) = \frac{LUT(i)}{M(i)} \tag{6}$$

### 3.1.3 Summary

In terms of modulation and impairment suppression technology in transmitter of optical transmission system, researchers have carried out a lot of research, such as peak to average power ratio (PAPR) reduction technology, DAC resolution enhancement [8], joint pre-equalization in electrical and optical domain, etc. In recent years, artificial intelligence techniques have been recently proposed as a promising tool to address various challenges in optical communication, and machine learning technology based on indirect learning [9] and neural network [10] has also been used for impairment compensation of transmitter devices.

## 3.2 Impairment compensation techniques at receiver side

In the long haul and large capacity optical transmission system, the optical link will introduce chromatic dispersion [11], polarization mode dispersion (PMD) [12], fiber nonlinearity, etc., the laser linewidth and frequency jitter will bring frequency offset and phase noise [13, 14], and the ADC sampling frequency and phase cannot be synchronized with the DAC at the transmitter. All these problems can be solved by using mature DSP technology, so as to avoid the use of a series of complex devices such as phase locked loop. With the development of ASIC chip manufacturing technology, highly integrated and flexible digital signal processing technology can meet the needs of high-speed optical transmission system in the future.

As shown in the **Figure 9**, the basic DSP algorithm flow of a typical coherent optical communication receiver, including IQ imbalance compensation, CD compensation, timing recovery, polarization demultiplexing, frequency offset estimation, and carrier phase recovery. According to the algorithm design, different

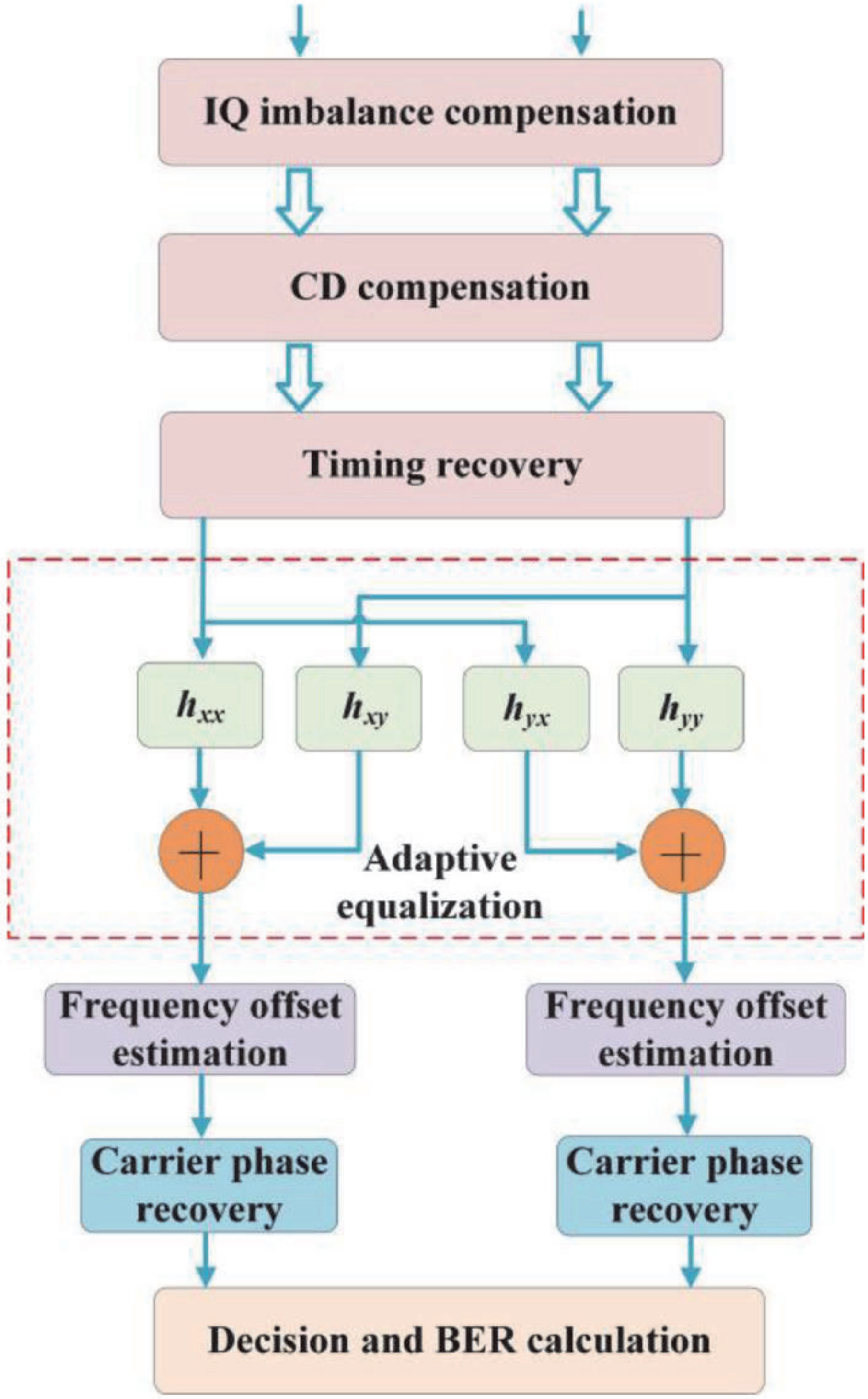


**Figure 9.**
*DSP flow of coherent optical transmission system.*

algorithms may have nested or parallel processing, these algorithms are closely linked and indispensable, which is the basis of coherent optical communication with high baud rate and high order modulation format.

### *3.2.1 I/Q imbalance compensation*

Ideally, the I and Q components in the received signal are completely orthogonal, but in the actual system, for the extinction ratio of the two arms of the IQ modulator is not completely consistent, the division ratio of the 3 dB coupler in the receiver is asymmetric, and the response of the balance detector is inconsistent, the amplitude and phase of the two IQ components will be imbalanced. So, it is necessary to implement IQ imbalance compensation and normalization in the first step of digital signal processing. In general, Gram-Schmidt orthogonalization procedure (GSOP) algorithm is used to map one set of non-orthogonal vectors as reference variables and the other set as orthogonal variables. Suppose that $I_{in}(k)$ and $Q_{in}(k)$ are non-orthogonal vectors, and $I_{out}(k)$ and $Q_{out}(k)$ are vectors processed by GSOP, as

$$I_{out}(k) = \frac{I_{in}(k)}{\sqrt{P_I}} \tag{7}$$

$$Q'(k) = Q_{in}(k) - \frac{\rho I_{in}(k)}{P_I} \tag{8}$$

$$Q_{out}(k) = \frac{Q'(k)}{\sqrt{P_Q}} \tag{9}$$

where $\rho = E\{I_{in}(k) \cdot Q_{in}(k)\}, P_I = E\{{I_{in}}^2(k)\}, P_Q = E\left\{{Q'}^2(k)\right\}$, and $E\{\cdot\}$ represents expectation.

*3.2.2 Chromatic dispersion compensation*

Chromatic dispersion is a static impairment for optical signal in fiber transmission. The main factor of CD is that the characteristics of optical fiber material lead to different propagation group velocity of different frequency components of optical signal, which is similar to the multipath effect in wireless communication, resulting in time-domain pulse broadening. For the early optical fiber communication system, chromatic dispersion is mainly compensated by negative dispersion coefficient media such as dispersion compensation fiber, fiber Bragg grating and other dispersion compensation modules. With the development of DSP technology, digital signal processing technology can completely replace the function of optical dispersion compensation module, it is easy to realize dispersion compensation based on DSP.

Generally, dispersion coefficient $D$ is used to quantify the pulse broadening caused by fiber dispersion, the unit is $ps/nm/km$. The partial differential equation of the influence of fiber dispersion on signal envelope is derived, and the frequency domain transmission equation can be obtained by Fourier transform

$$G(z,w) = exp\left(-j\frac{D\lambda^2}{4\pi c}\omega^2\right) \tag{10}$$

where $\lambda$ is the wavelength of light wave, $c$ represents light speed, and $\omega$ is arbitrary frequency component. The frequency-domain transfer function of the dispersion compensation filter is obtained by inversing the dispersion coefficient of the transfer function as

$$G(z,w) = exp\left(j\frac{D\lambda^2}{4\pi c}\omega^2\right) \tag{11}$$

In the long-distance optical communication system, the signal sub block must be large enough to compensate for the dispersion effect in the transmission. Therefore, an overlapped frequency domain equalization structure is proposed to improve the transmission and DSP efficiency by forming overlaps between sub blocks as shown in **Figure 10**.

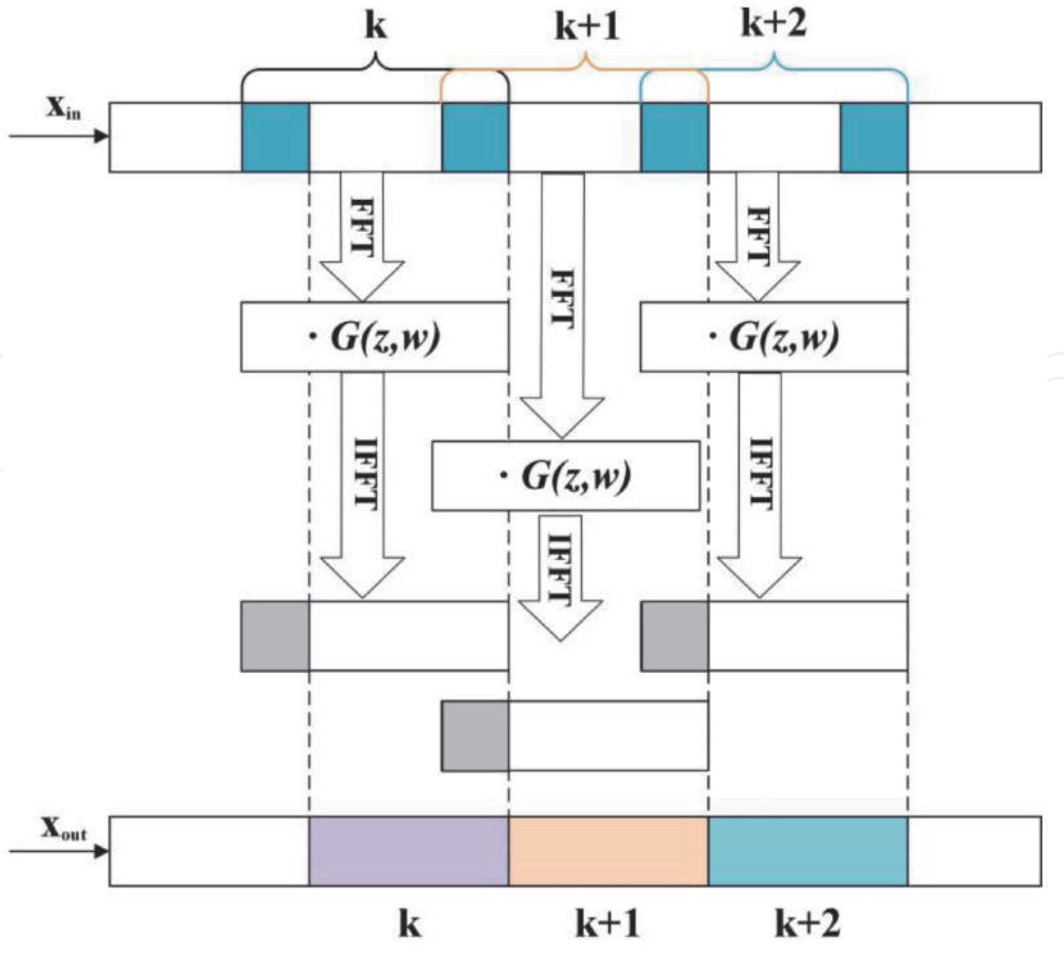


**Figure 10.**
*Frequency domain dispersion equalization with overlap method.*

### *3.2.3 Clock recovery*

After photodetection, the electrical signal is sampled and digitized by the ADC. However, in the actual system, because the local sampling clock is not synchronized with the transmitter signal clock, the sampling point of the ADC is not the best sampling point of the signal in most cases. On the other hand, due to the instability of the local clock source itself, it may also cause the sampling error of the system. This sampling error includes both the sampling phase error and the sampling frequency error. The clock error of the sampling signal, on the one hand, is due to the imperfection of the sampling point, causing interference between sampling symbols; on the other hand, the jitter of the sampling clock will also cause fluctuations in signal performance. Therefore, in order to achieve optimal digital signal recovery, a clock recovery module is needed in the actual system to eliminate the impact of clock sampling errors. Considering that the dispersion will cause the disappearance of the clock component, usually, the clock recovery module is placed after the dispersion compensation or works with the dispersion compensation module to form a unified balanced feedback module.

The feedback time-domain clock recovery algorithm is proposed by Gardner [15]. This algorithm uses a feedback clock synchronization structure to estimate the phase of the retiming digital clock source feedback by calculating the timing error. The estimation of the timing error can track the frequency jitter of the signal, and the application of this algorithm can achieve dynamic clock recovery. On the other hand, the Gardner clock recovery algorithm only needs two samples per symbol and the algorithm complexity is low. It is widely used in the digital signal processing module of the coherent optical communication system.

### *3.2.4 Adaptive equalization and polarization demultiplexing*

As CD compensation technology has been well promoted in optical fiber communication systems, PMD becomes the primary impairment which limits the information capacity and transmission distance for over 40Gbit/s systems [16–18]. Besides, PMD is a stochastic impairment that converts with time, temperature, wavelength and fiber conditions which makes PMD hard to estimate and compensate. In recent years, the research on how to overcome the performance deterioration of optical communication system caused by PMD effect has been a hot topic, most of which focuses on PMD compensation [19, 20].

The adaptive equalizer is generally used to polarization demultiplex and PMD compensation of channels. A two-by-two multiple-input multiple-output (MIMO) structured finite impulse response (FIR) filters as shown in **Figure 11** is used to estimate the inverse Jones matrix of the dynamic channel [17].

The input sequence of the filter is symbol-spaced with index $n$, while the $N$ tap FIR filters, $h_{xx}$, $h_{xy}$, $h_{yx}$ and $h_{yy}$ are the column vector of length $N$. Tap weights are updated every two samples as the input sequence is two-fold sampled. Therefore, $x_i$ and $y_i$ represent a sliding block of $N$ samples such that

$$x_i(n) = [x_i(n), x_i(n-1) \dots x_i(n-N)] \tag{12}$$

$$y_i(n) = [y_i(n), y_i(n-1) \dots y_i(n-N)] \tag{13}$$

We consider that $u_i(\text{n}) = [x_i(n), y_i(n)]$, $h_x(\text{n}) = [h_{xx}(n), h_{xy}(n)]$, $h_y(\text{n}) = [h_{yx}(n), h_{yy}(n)]$. And the filters outputs form as

$$x_o(n) = h_x^H(n) u_i(n) \tag{14}$$

$$y_o(n) = h_y^H(n) u_i(n) \tag{15}$$

where superscript$(.)^H$ means the conjugate transpose.

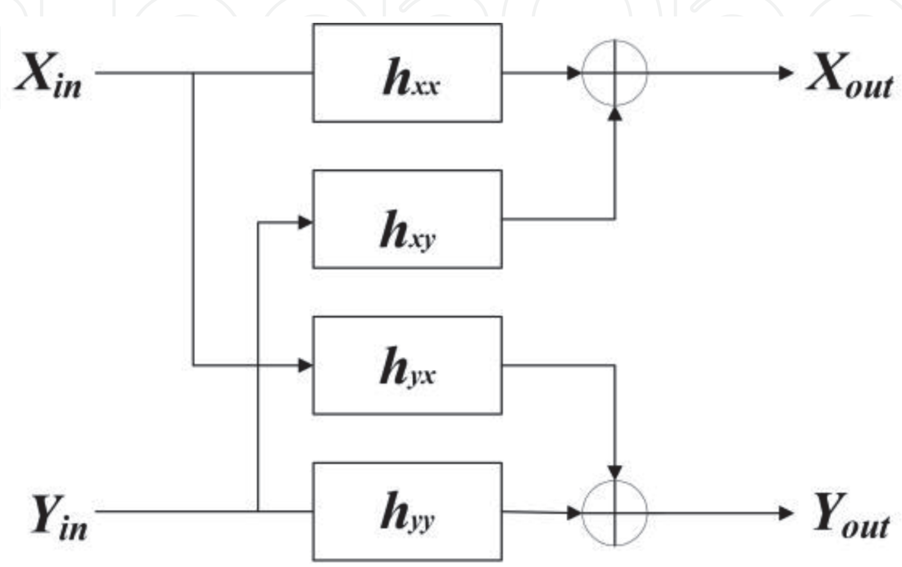


**Figure 11.**
*Framework of 2 × 2 MIMO structured FIR filters.*

For fast adaptive equalizer, we generally use stochastic gradient descent (SGD) optimizer to update the tap weights. Meanwhile, we need to choose a cost function to describe the error degree of the output samples so that the equalizer can get the response and update tap weights. For constant modulus algorithm (CMA), its cost functions are given as

$$\varepsilon_x(n) = R_2 - |x_o(n)|^2 \tag{16}$$

$$\varepsilon_y(n) = R_2 - |y_o(n)|^2 \tag{17}$$

where $R_2$ is the real-valued constant and given by $R_2 = E|X_{sym.}|^4/E|X_{sym.}|^2$. The update equations of FIR filters are given as

$$h_x(n+1) = h_x(n) + \mu\varepsilon_x(n)x_o^*(n)u_i(n) \tag{18}$$

$$h_y(n+1) = h_y(n) + \mu\varepsilon_y(n)y_o^*(n)u_i(n) \tag{19}$$

where $\mu$ is the step size parameter and the superscript$(.)^*$ means the complex conjugate operation.

The cost functions of CMA describe error degree between the amplitude of output symbols and the proposed convergence radius [17, 18]. By updating the tap weights of FIR filters with cost functions, the error degree can be minimized in a certain extent and the output symbols can converge on a circle with the proposed radius that equals to $\sqrt{R_2}$. The value of the constant $R_2$ and step size can significantly affect the convergence degree of CMA. Appropriate $R_2$ helps CMA to converge in less steps. Shorter step size can help CMA to get better convergence, but the computation of the algorithm is also increased. CMA needs enough steps to update and optimize its FIR filters. The output performance of CMA will be insufficient if the proposed convergence length is not long enough.

All tap weights are initialized to zero except the central tap of $h_{xx}$ and $h_{yy}$, which are initialized to unity. The filter taps of $h_{xx}$, $h_{xy}$, $h_{yx}$ and $h_{yy}$ estimate the components for data sequences. At the transmitter, data sequences for X and Y polarization are independent and only contain their own information. Thus, the central tap of $h_{xx}$ and $h_{yy}$ are set to unity. After fiber transmission, the received signal is contaminated by channel impairments and noise. With the contamination of noise and the channel impairments caused by linear effects such as CD, PMD etc. or fiber nonlinear effects, the received data sequences for X and Y polarization are no longer independent. One or more symbols in the received sequences can interfere other symbols, while the symbols for one polarization can interfere other symbols for another polarization. The interference between polarizations can be estimated by filter taps of $h_{xy}$ and $h_{yx}$. Though updating filter tap weights, the $2 \times 2$ MIMO structured FIR filters can gradually identify the components of each data sequence, and the dynamic impairments of channel can be compensated. This process can also achieve polarization demultiplexing.

It is worth noting that the CMA can be implemented in a full-blind mode, but it set no constrain with its outputs. Therefore, it is possible for the equalizer to converge on the same output, corresponding to the Jones matrix becoming singular. In practice, we need to check if $h_x$ and $h_y$ become singular after the algorithm running for certain steps, and if so, a mathematic process is necessary to make $h_x$ and $h_y$ nonsingular and the whole algorithm should be restarted.

CMA is especially suited to the modulation format with constant amplitude such as quadrature phase-shift keying (QPSK) and M-ary phase-shift keying (MPSK). For the formats with inconstant amplitudes such as quadrature amplitude modulation, the CMA error cannot converge to zero as extra noise is introduced during equalizing. To improve the SNR performance for the formats with inconstant amplitudes, several multi-modulus algorithms such as radius-directed algorithm (RDA) and cascaded multi-modulus algorithm (CMMA) are established [21, 22].

As CMA set at real-valued constant $R_2$, CMMA set several constants which depends on the ideal constellations. According to the distance between the input symbol and the constellation origin, the algorithm estimates which circle the symbol belongs to. Then CMMA calculates the error using the estimated radius. The rest of CMMA algorithm steps are same as CMA.

Compared with CMA, the CMMA significantly improves the SNR performance for high order QAM. But it reduces the robustness of the filter converging process. This is because multi-modulus algorithm depends on correct decision on symbol radius. For high order QAM format, the distance between different circles is less than the minimum symbol interval. Therefore, the algorithm may make massive mistake over the circle decision if the signal is severely contaminated by channel impairments and noise.

### *3.2.5 Frequency offset estimation*

In the coherent optical communication system, the transmitting laser and the local oscillator laser work independently, so the central wavelength cannot be exactly the same, so there is a certain frequency deviation $\Delta f$. It will introduce a continuous phase variation along with time to the received signal, resulting in constellation rotation, so it is necessary to estimate and compensate the frequency offset by DSP. Through FFT operation, the spectrum of received symbol's fourth power value is obtained and analyzed, it can be found that there is a peak component at the frequency of $4\Delta f$, therefore, $\Delta f$ can be obtained by searching for the maximum spectral component of the fourth-power value of received symbol. Usually, due to the lack of spectral resolution and other reasons, there will be residual frequency offset after estimation, which can be looked at as additional phase noise and recovered by carrier phase recovery.

### *3.2.6 Carrier phase recovery*

Carrier phase recovery (CPR) is an essential DSP unit in coherent systems and has been extensively investigated for QPSK and QAM signals. Like frequency offset estimation algorithms, carrier recovery algorithms can be classified as either blind or data-aided estimation techniques. And the algorithms can be implemented in feedforward manner or in feedback structure [23, 24]. Compared to the constellation for QPSK, the constellation points for QAM vary in both phase and amplitude. Moreover, the modulated signal phase is with multiple values. Viterbi-Viterbi phase estimation (VVPE) algorithm using a fourth-power operation which is suitable for QPSK is hard to completely remove the signal phase and estimate the carrier phase. At present, the algorithms for QAM CPR mainly include Blind phase searching (BPS), improved BPS (BPS/maximum likelihood), decision aided maximum likelihood (DA-ML), etc. [25–27]

BPS is recognized as a favorable solution due to its high performance and suitability for parallel processing and can be used in feedforward manner.

**Figure 12** shows the block diagram of the BPS algorithm in pure feedforward manner. The input signal $x_i$ is sampled at the symbol rate. The received signal $x_i$ is rotated by $B$ test carrier angles $\varphi_b$ with

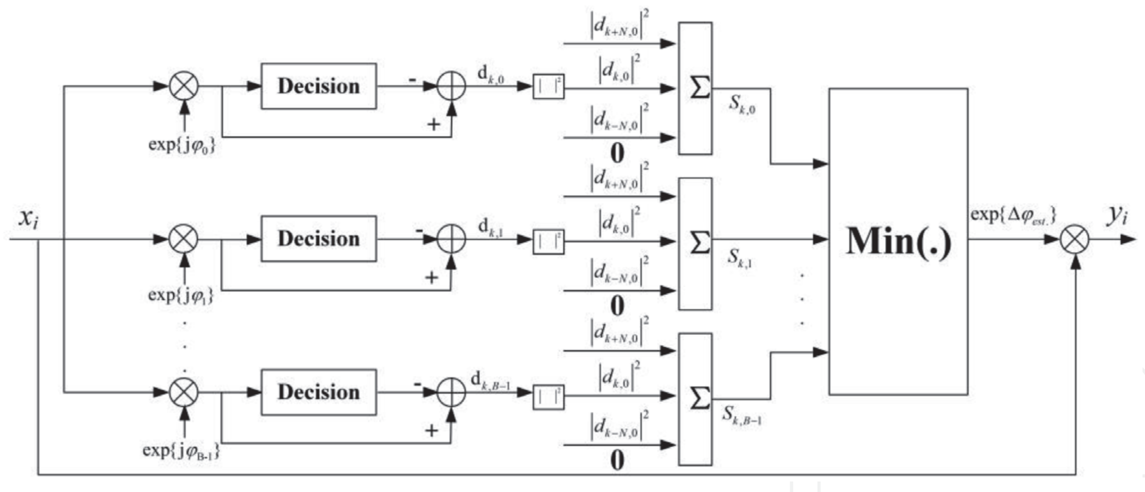


**Figure 12.**
*BPS diagram in feedforward manner.*

$$\varphi_b = \frac{b}{B} \bullet \frac{\pi}{2}, b \in \{0, 1, \ldots, B-1\} \tag{20}$$

then all rotated symbols are fed into a decision circuit, which output the ideal constellation points with the minimum Euclidean distance to the input symbols. The squared distance $|d_{k,b}|^2$ to the closest constellation point is calculated in the complex plane

$$|d_{k,b}|^2 = \left|x_k \exp\{j\varphi_b\} - \lfloor x_k \exp\{j\varphi_b\}_D \rfloor\right|^2 \tag{21}$$

in order to remove the other initial noise distortions from the receiver, the distance of 2N + 1 consecutive test symbols rotated by the same carrier phase angle $\varphi_b$ are summed up

$$s_{k,b} = \sum_{n=-N}^{N} |d_{k-n,b}|^2 \tag{22}$$

the optimum value of the filter half width N depends on the laser linewidth times symbol rate product. N = 6, … ,10 is generally a good choice.

After filtering the optimum phase angle $\Delta\varphi_{est.}$ by searching the minimum sum of distance values, then the output symbols $y_i$, which is the input symbols $x_i$ rotated by $\Delta\varphi_{est.}$, is outputted for the following DSP in coherent systems.

Due to the 4-fold ambiguity of the recovered phase in the square M-QAM, the blind algorithms may cause incorrect phase estimation by a multiple of π/2 causing cycle slip. This problem can be solved by using framing information or by applying differential coding [23–25].

Though BPS shows a good tolerance to laser phase noise and can be flexibly applied to higher order QAM, with an increasing modulation order a larger number of test phases are required and the computation complexity increases. Therefore, an improved BPS algorithm with a two-stage diagram has been established [24]. The first stage of improved BPS just requires rough estimation and the required number of test phase $\varphi_b$ can be reduced. A maximum likelihood phase estimator is introduced in the second phase to improve the accuracy. This two-stage BPS/ML algorithm effectively improves the performance with the computation complexity and availability of BPS algorithm remained.

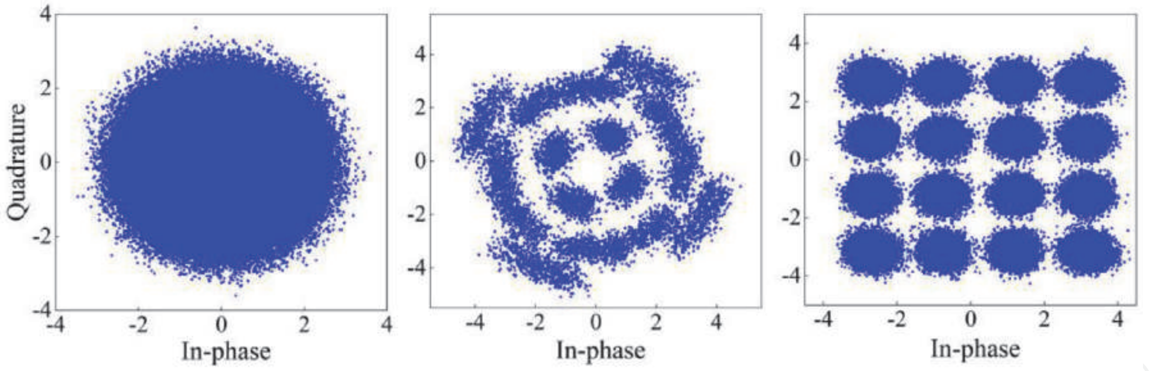


**Figure 13.**
*Constellations after CD compensation, polarization demultiplexing, and carrier phase recovery.*

*3.2.7 Summary*

This section introduces a series of impairment compensation algorithms for coherent optical communication system. Here, the constellation diagrams of 60GBaud 16QAM signal in DSP process is given in the **Figure 13**. Through the algorithms in this section, we can realize the signal orthogonalization and normalization, compensate the fiber dispersion, eliminate the clock sampling error, depolarize the multiplexing and equalize channel response at the same time, and finally recover the carrier phase to get the constellation of the original transmission signal. A series of impairment compensation algorithms based on DSP at the receiver end lay the foundation for high-speed, large-capacity and long-haul optical transmission.

## 4. Conclusion

In this chapter, first we propose a probabilistic shaping 16QAM modulation scheme based on trellis coded modulation. Through non-uniform probability mapping of TCM-16QAM subset, an effective and good overall probability distribution of 16QAM constellation is obtained. The scheme is successfully demonstrated in a 25 km single-mode fiber transmission system, and better OSNR gain and BER performance are obtained. Then impairment compensation techniques in coherent optical communication are introduced from two aspects, transmitter side and receiver side, pre-emphasis and look-up table technology have been widely used in the impairment compensation of the transmitting devices, while the DSP process at the receiver side is more complicated, including GSOP, clock recovery, dispersion compensation, dynamic equalization, and carrier phase recovery. Using DSP technology can effectively mitigate the impairment of optoelectronic devices and optical fiber links, and it is an effective method to realize ultra-high speed, large-capacity and long-haul transmission.

## Acknowledgements

This work is supported by National Natural Science Foundation of China No.62022016, No.61835002, No.61727817, National Key R&D Program of China from Ministry of Science and Technology, China No.2019YFA0706300, Open Fund of IPOC (BUPT) No.IPOC2020A007, No.IPOC2020A006, and China Postdoctoral Science Foundation No.2020 M680384, No.2020 M680385.

IntechOpen

IntechOpen

## Author details

Zhipei Li, Dong Guo and Ran Gao*
School of Information and Electronics, Beijing Institute of Technology, Beijing, China

*Address all correspondence to: 6120190142@bit.edu.cn

IntechOpen

© 2021 The Author(s). Licensee IntechOpen. This chapter is distributed under the terms of the Creative Commons Attribution License (http://creativecommons.org/licenses/by/3.0), which permits unrestricted use, distribution, and reproduction in any medium, provided the original work is properly cited. CC BY

## References

[1] Yankov M P, Zibar D, Larsen K J, Christensen L, Forchhammer S. Constellation Shaping for Fiber-Optic Channels with QAM and High Spectral Efficiency. IEEE Photonics Technology Letters, 2014; 26(23):2407-2410. DOI: 10.1109/LPT.2014.2358274

[2] Gui T, Wang X, Tang M, Yu Y, Li L. Real-Time Demonstration of 600-Gb/s DP-64QAM Self-Homodyne Coherent Bi-Direction Transmission with Un-Cooled DFB Laser. Optical Fiber Communication Conference. 2020

[3] Napoli A, Sun H, Maher R, Torbatian M, & Zhang J, 800G DSP ASIC Design Using Probabilistic Shaping and Digital Sub-Carrier Multiplexing. Journal of Lightwave Technology, 2020; 38(17): 4744-4756. DOI: 10.1109/JLT.2020.2996188

[4] Zhou X, Urata R, Liu H. Beyond 1Tb/s Datacenter Interconnect Technology: Challenges and Solutions. Optical Fiber Communication Conference. 2019.

[5] Raphaeli D, Gurevitz A, Constellation shaping for pragmatic turbo-coded modulation with high spectral efficiency. IEEE Transactions on Communications, 2004; 52, 341–345. DOI: 10.1109/tcomm.2004.823564

[6] Zhang Z, Li C, Chen J, Ding T, Wang Y, Xiang H, Xiao Z, Li L, Si M, Cui X. Coherent transceiver operating at 61-Gbaud/s. Optics Express, 2015; 23 (15):18988-95. DOI: 10.1364/OE.23.018988

[7] Napoli A, Berenguer P W, Rahman T, Khanna G, Mezghanni M M, Gardian L, Riccardi E, Piat A C, Calabrò S, Dris S. Digital pre-compensation techniques enabling high-capacity bandwidth variable transponders. Optics Communications, 2017; S0030401817308465. DOI: 10.1016/j.optcom.2017.09.062

[8] Sadot D, Yoffe Y, H Faig, Wohlgemuth E. Digital Pre-Compensation Techniques Enabling Cost-Effective High-Order Modulation Formats Transmission. Journal of Lightwave Technology, 2018; 37(2): 441-450. DOI: 10.1109/JLT.2018.2888941

[9] Paryanti G, Faig H, Rokach S L, Dan S. A Direct Learning Approach for Neural Network Based Pre-Distortion for Coherent Nonlinear Optical Transmitter. Journal of Lightwave Technology, 2020; 38(15): 3883-3896. DOI: 10.1109/JLT.2020.2983229

[10] Freire P J, Neskorniuk V, Napoli A, Spinnler B, Turitsyn S. Complex-Valued Neural Network Design for Mitigation of Signal Distortions in Optical Links. Journal of Lightwave Technology, 2021; 39(6):1696-1705. DOI: 10.1109/JLT.2020.3042414

[11] Prince M. Performance Limitations of an Optical TDM Transmission Link Caused by Fiber Chromatic Dispersion. 2020 FORTEI-International Conference on Electrical Engineering (FORTEI-ICEE); 2020. DOI:10.1109/FORTEI-ICEE50915.2020.9249807

[12] Ip E, Kahn J M. Digital Equalization of Chromatic Dispersion and Polarization Mode Dispersion. Journal of Lightwave Technology, 2007; 25(8): 2033-2043. DOI: 10.1109/JLT.2007.900889

[13] Huerta-Cuellar G, Pisarchik A N, Barmenkov Y O. Experimental characterization of hopping dynamics in a multistable fiber laser. Physical Review E, 2008; 78(3):035202. DOI: 10.1103/PhysRevE.78.035202

[14] Fatemi F K, Lou J W, Carruthers T F. Frequency comb linewidth of an actively mode-locked fiber laser. Optics Letters, 2004; 29(9):944-946. DOI: 10.1364/OL.29.000944

[15] Gardner F M. A BPSK/QPSK timing-error detector for sampled receivers. IEEE Transactions on Communications, 1986; 34(5):423-429. DOI: 10.1109/TCOM.1986.1096561

[16] Kikuchi K, Fundamentals of Coherent Optical Fiber Communications. Journal of Lightwave Technology, 2016; 34(1):157-179. DOI: 10.1109/JLT.2015.2463719.

[17] Faruk M S, Savory S J. Digital Signal Processing for Coherent Transceivers Employing Multilevel Formats. Journal of Lightwave Technology, 2017, 35(5): 1125-1141. DOI:10.1109/JLT.2017.2662319

[18] Lagha M K, Gerzaguet R, Bramerie L, Gay M, Scalart P, Blind Joint Polarization Demultiplexing and IQ Imbalance Compensation for *M* -QAM Coherent Optical Communications. Journal of Lightwave Technology. 2020, 38, 4213-4220. DOI: 10.1109/JLT.2020.2986601

[19] El-Fiky E, Chagnon M, Sowailem M, Samani A, Morsy-Osman M, Plant D V. 168-Gb/s Single Carrier PAM4 Transmission for Intra-Data Center Optical Interconnects. IEEE Photonics Technology Letters, 2017; 29(3):314-317 DOI: 10.1109/LPT.2016.2647232.

[20] Yu Z, Zhao Y, Hu S, Wan Z, Xu K. PDL and CD insensitive low complexity equalizer for short reach coherent systems. Optics Express, 2021; 29(5), 6657-6667. DOI: 10.1364/OE.418456

[21] Zhang T, Xiang Q, Zhang S, Liu L, & Zuo T. Cost-effective digital coherent short-reach transmission system with D8QAM and low-complexity DSP. Optics Express, 2021; 29, 11892-11902. DOI: 10.1364/OE.422456

[22] Zhang Q, Li X, Zhang N, Hu L, Xi L, A Low Complexity Frequency Domain Adaptive Equalizer for Coherent Optical Receivers. Asia Communications and Photonics Conference/International Conference on Information Photonics and Optical Communications 2020 (ACP/IPOC), 24-27 October 2020; Beijing, China. M4A.287.

[23] Pfau T, Hoffmann S, R. Noe. Hardware-Efficient Coherent Digital Receiver Concept with Feedforward Carrier Recovery for MM -QAM Constellations. Journal of Lightwave Technology, 2009; 27(8): 989-999, DOI: 10.1109/JLT.2008.2010511

[24] X. Zhou. An Improved Feed-Forward Carrier Recovery Algorithm for Coherent Receivers With M-QAM Modulation Format. IEEE Photonics Technology Letters, 2010; 22(14): 1051-1053. DOI: 10.1109/LPT.2010.2049644.

[25] Zhao J, Chen L K. Carrier Phase Recovery Based on KL Divergence in Probabilistically Shaped Coherent Systems. Journal of Lightwave Technology. 2021; 39, 2684-2695. DOI: 10.1109/JLT.2021.3054949

[26] Borjeson E, Fougstedt C, Larsson-Edefors P. VLSI Implementations of Carrier Phase Recovery Algorithms for M-QAM Fiber-Optic Systems. Journal of Lightwave Technology. 2020: 38, 3616-3623. DOI: 10.1109/JLT.2020.2976166

[27] Lu J, Fu S, Hu Z, D Lei, Tang M, D Liu. Carrier Phase Recovery for Set-Partitioning QAM Formats. Journal of Lightwave Technology, 2018; 36(18): 4129-4137. DOI: 10.1109/JLT.2018.2859238

We are IntechOpen,
the world's leading publisher of
Open Access books
Built by scientists, for scientists

6,300
Open access books available

171,000
International authors and editors

190M
Downloads

154
Countries delivered to

Our authors are among the
TOP 1%
most cited scientists

12.2%
Contributors from top 500 universities

WEB OF SCIENCE™
Selection of our books indexed in the Book Citation Index
in Web of Science™ Core Collection (BKCI)

Interested in publishing with us?
Contact book.department@intechopen.com

Numbers displayed above are based on latest data collected.
For more information visit www.intechopen.com

Chapter

# Optical Fiber Tweezers for the Assembly of Living Photonic Probes

*Xing Li and Hongbao Xin*

IntechOpen


## Abstract

Optical fiber tweezers, as a versatile tool for optical trapping and manipulation, have attracted much attention in cell trapping, manipulation, and detection. Particularly, assembly of living cells using optical fiber tweezes has become a significant attention. Advanced achievements have been made on the assembly of fully biocompatible photonic probes with biological cells, enabling optical detection in biological environment in a highly compatible manner. Therefore, in this chapter, we discuss the use of optical fiber tweezers for assembly of living photonic probes. Living photonic probes can be assembled by the trapping and assembly of multiple cells using optical fiber tweezers. These photonic probes exhibit high biocompatibility and show great promise for the bio-applications in bio-microenvironments.


**Keywords:** Optical fiber tweezers, living photonic probes, optical trapping, optical manipulation, cell assembly

## 1. Introduction

The development of optical fiber tweezers (OFTs) makes it a versatile candidate for optical trapping and manipulation of targets ranging from different dielectric particles to biological cells and biomolecules [1–3]. This is because OFTs possess exceptional advantages in manipulation flexibility, due to the simple structure with only optical fibers. This simple structure also avoids the use of a high numerical-aperture objective which is necessary for the light focusing in conventional optical tweezers system [4, 5]. It is much easier to handle and manipulate the microscopic objects after trapped with OFTs [6, 7]. And it is much more suitable for practical use such as in trapping, levitating and rotating of microscopic particles in different environments [8–10]. The OFTs tip can be inserted into thick samples and turbid media, which greatly increases the sample applicability. In addition, OFTs exhibit a low-cost manipulation technique and can also be integrated into small devices, such as optofluidic channels [11]. OFTs enable the trapping and manipulation of different single targets. For the further biological detection in bio-environments, it is highly desired to form biocompatible photonic probes that can minimize the physical damage to the biological samples. Unfortunately, most photonic probes are made from inorganic and artificial materials, which are incompatible and invasive when interfacing with biological systems. It is still a big challenge to find out a biomaterial to assemble biophotonic probes that are noninvasive and highly biocompatible to biological systems. Fortunately, it is found that living cells, which are abundant in the natural world, show the capability for light manipulation and propagation with high biocompatibility, and can thus be used for the assembly of living photonic probes. In this chapter, recent advances of OFTs in trapping and manipulating of cells, particularly in assembly of living photonic probes based on biological cells, were discussed. These formed living photonic probes provide a promising approach for bio-detection in biological environments with highly biocompatibility [12, 13].

## 2. Working principle of OFTs

OFTs, generally based on a tapered fiber probe, can be fabricated by drawing a commercial single-mode optical fiber through a flame-heating technique. The shape of OFTs tip can be controlled by controlling the heating temperature and the drawing speed. The operation principle of typical OFTs has been detailedly analyzed and described [14]. As schematically shown in **Figure 1a**, an OFT is immersed in water. $D_A$ means the axial distance of a dispersed particle to the OFTs tip, while $D_T$ means the transverse distance. With a laser beam launched into the OFTs, particle will be trapped and manipulated by the generated optical force. There two components of the optical force, *i.e.*, gradient force ($F_g$) and scattering force ($F_s$). $F_g$ is directed to the region with stronger light intensity and

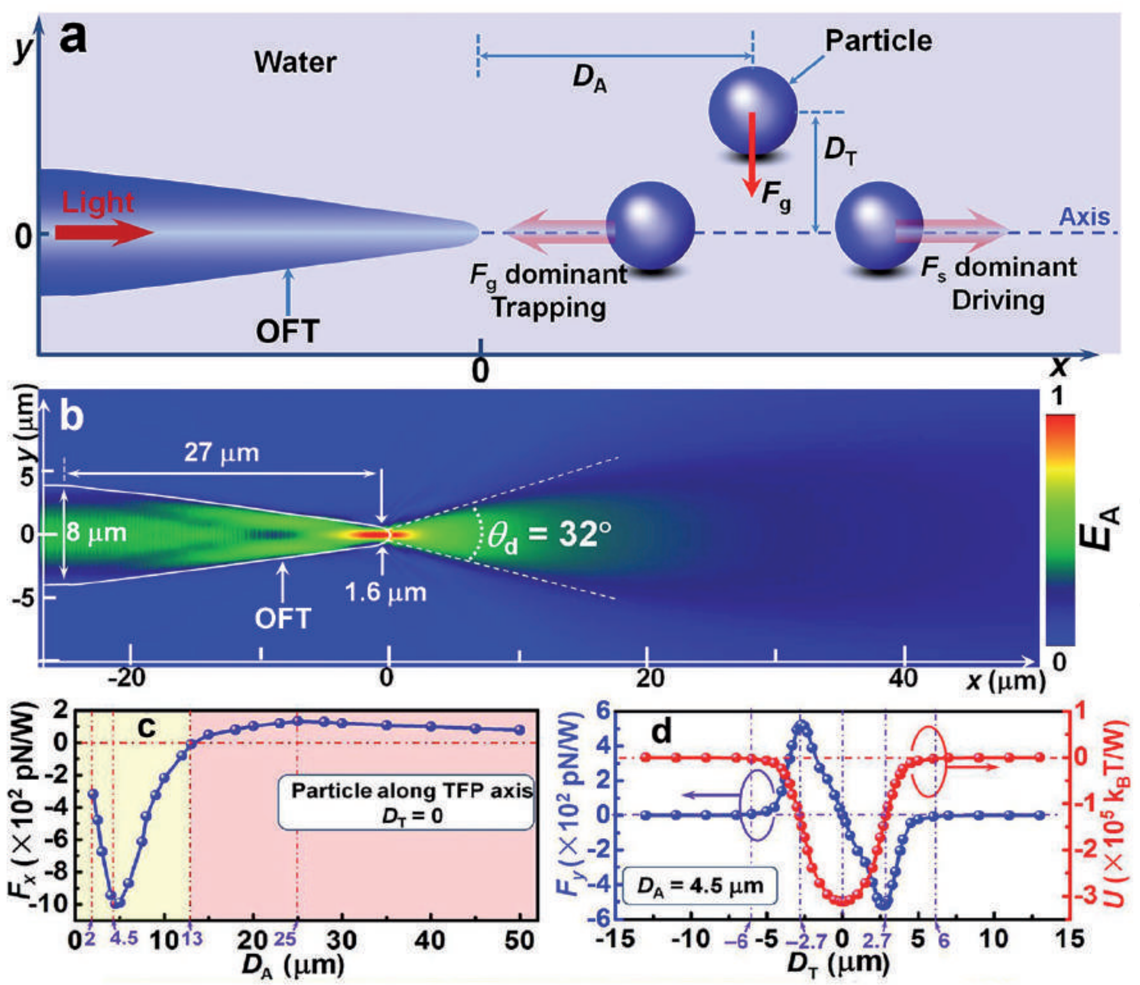


**Figure 1.**
*Principle of a single optical fiber tweezers for trapping of particles [14]. (a) Schematic of particle manipulation by an OFT with light launched. (b) Simulated electric field amplitude ($E_A$) distribution by FDTD method. (c) Calculated optical force exerted on particles along the x direction. (d) Calculated optical force and trapping potential along the y direction.*

is responsible to trap the particle, while $F_s$ is directed along the light propagation and can push particles away from the OFTs tip. When a particle is near the axial axis of the OFTs, it will be trapped to the axis by $F_g$. For particle near the OFTs tip, the dominated $F_g$ can trap the particle to the fiber tip. As the distance to the tip increases, $F_s$ will become larger than $F_g$, and the dominated $F_s$ will push the particle away from the fiber tip. The electric field amplitude ($E_A$) distribution around the OFTs was shown in **Figure 1b**, with a laser beam at a wavelength of 980 nm launched into the fiber probe. It can be seen that the light outputted from the OFTs is firstly focused at the tip and subsequently diverged out in water with a divergence angle of 32°. **Figure 1c** shows the calculated optical force exerted on a 3-μm silica particle along the $x$ direction. It can be seen that, near the fiber tip, the force is negative, indicating a trapping force for particles. Therefore, particles near the fiber tip can be trapped by the OFTs. As the distance increases, the force is positive, indicating a driving force for particles. Therefore, particles can be pushed away by the OFTs. **Figure 1d** shows the calculated force and trapping potential in the y direction. It can be seen that the trapping potential on the axis is the smallest, and therefore particles beside the axis can be trapped at the axis. These optical forces enable the trapping capability of OFTs. By simply moving the fiber probe, the trapped particles can be manipulated in a highly flexible manner.

## 3. Manipulation of single cell and multiple cells by OFTs

OFTs can serve as a powerful tool for the trapping and manipulation of cells. Using *Escherichia coli* as an example, both single and multiple motile bacteria have been trapped and manipulated in a non-contact manner [15]. **Figure 2a** shows the experimental schematic for non-contact trapping of *E. coli* using OFTs. In this scenario, a laser beam at a wavelength of 980 nm was launched into the OFTs. A *E. coli* bacterium that was randomly swimming in the suspension was then trapped by the OFTs. The trapping was a non-contact trapping, and the bacterium was in the trapping position with several microns to the tip of the OFTs. During the trapping, the highly active bacterium was struggling around the trapping region. **Figure 2b–d** shows the detailed process for the trapping and struggling dynamics. The bacterium was trapped by the OFTs in a non-contact manner. However, due to the motility, the trapped bacterium was struggling after trapping. This phenomenon provides a new method for the studying of bacteria dynamics using OFTs.

In addition to the trapping and manipulation of single cells, OFTs can also be used for the trapping and assembly of multiple cells. For example, **Figure 3a** shows a schematic for the trapping and assembly of multiple *E. coli* cells in a microfluidic channel using OFTs [16]. Light output from the OFTs can trap the *E. coli* bacteria delivered by microfluidics. After a single bacterium was trapped, light can further propagate along the cell, and can be used for the trapping of other bacteria. Therefore, multiple bacteria can be trapped and assembled into cell chains with different lengths. To show the multiple trapping capability, **Figure 3b** shows the simulated light propagation along multiple cells. It can be seen that, light can propagate along the trapped cells, and the exerted optical force can be used for further trapping of other bacteria (**Figure 3c**). To experimentally demonstrate stable trapping and connecting of multiple *E. coli* cells with highly organized orientation, i.e., realization and retaining of *E. coli* cell–cell contact, the 980-nm wavelength laser with an optical power was launched into the fiber probe. **Figure 3d** shows the trapped multiple cells and formed cell chains with different numbers of cells at different input optical powers. By moving the fiber probe, the assembled cell chains can further be flexibly manipulated.

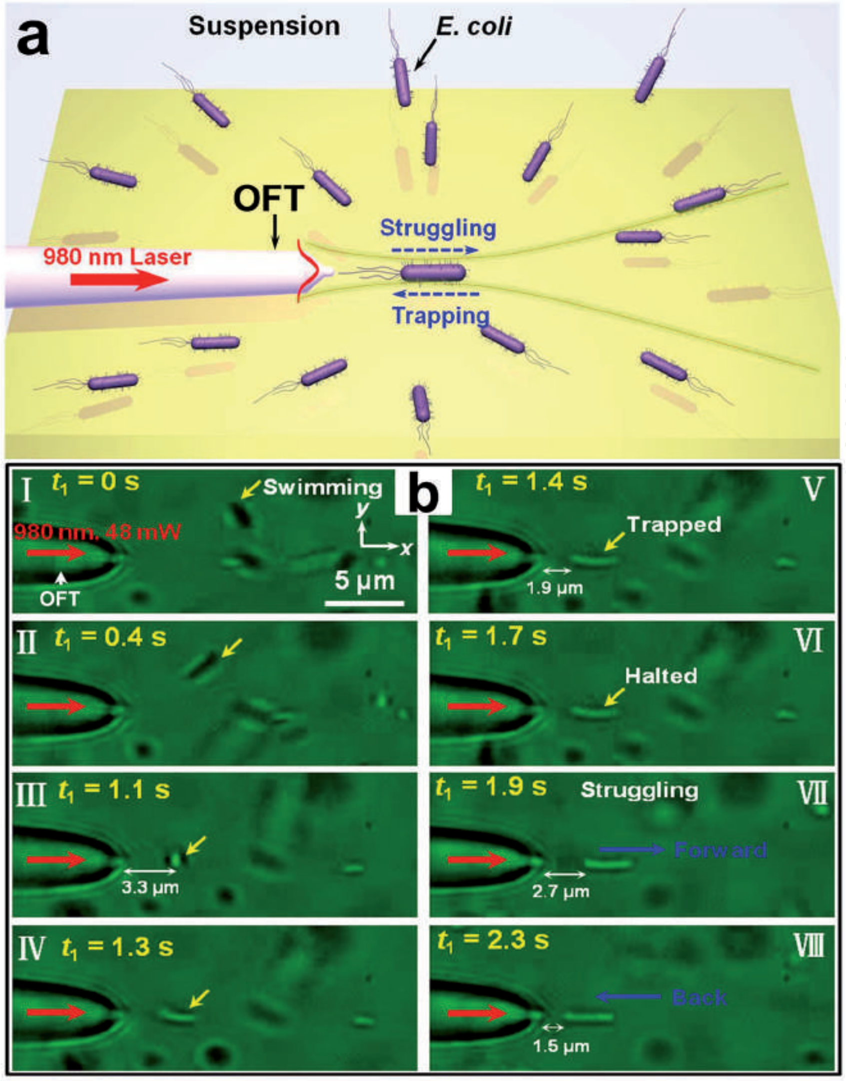


**Figure 2.**
*Optical trapping of a single bacterium using OFTs [15]. (a) Schematic illustration of the non-contact optical trapping of a single bacterium and the struggling dynamics. (b) Optical microscope images of the trapping and struggling process of a single bacterium.*

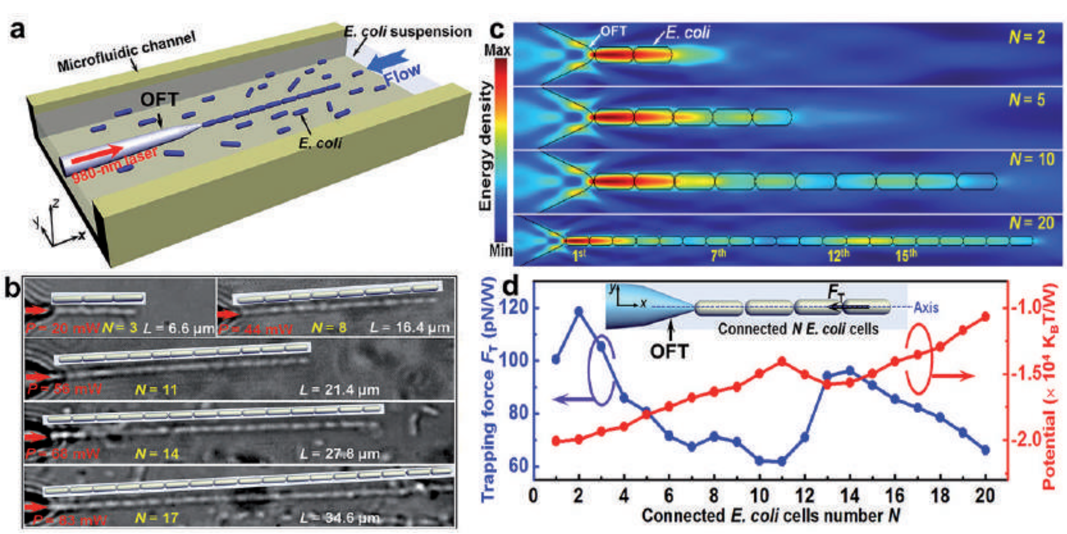


**Figure 3.**
*Optical trapping of multiple cells using OFTs [16]. (a) Schematic of multiple E. coli trapping using OFTs. A laser at 980 nm wavelength was launched into the fiber probe which was placed in a microfluidic channel with a flowing suspension of E. coli cells. Multiple E. coli cells were trapped and connected orderly at the tip of the fiber probe. (b) Simulated light propagation along multiple bacteria. (c) Simulated light distribution along the assembled cell chains. (d) Calculated optical trapping force exerted on the last cell of each cell chain and the trapping potential.*

## 4. Assembly of cell-based biophotonic waveguides by OFTs

Based on the multiple cell trapping capability of OFTs, direct formation of biophotonic waveguides with *E. coli* were reported [17]. By launching a laser of 980 nm wavelength into the OFTs, multiple *E. coli* were trapped and connected together with highly ordered organizations, forming biophotonic waveguides with different lengths (**Figure 4a**). By coupling a visible laser beam into the formed biophotonic waveguides, light propagation along these biophotonic waveguides can be directed observed as indicated by the red-light spots at the end of the waveguides (**Figure 4b**). The light propagation loss along the formed waveguides can be measured using an optical power meter by coupling another tapered optical fiber at the end of the formed biophotonic waveguide. As shown in **Figure 4c** and **d**, the measured propagation loss was measured to be 0.23 dB/μm.

In addition to the linear biophotonic waveguides, using OFTs, branched photonic probes can also been assembled. For example, **Figure 5** shows the assembled branched photonic probes with *E. coli* bacteria [18]. By designing a specially segmented tapered optical fiber, light output from the fiber can be divided into three individual beams, and *E. coli* bacteria can be trapped by the individual beams, further forming into branched biophotonic probes with different lengths (**Figure 5**). These branched photonic probes show strong stability, and can be used for further applications. By moving the OFTs, the formed biophotonic probes can be flexibly manipulated to different designated positions for further applications. These results show that the OFTs offer a seamless interface between optical and biological worlds for biophotonic probes formation with natural

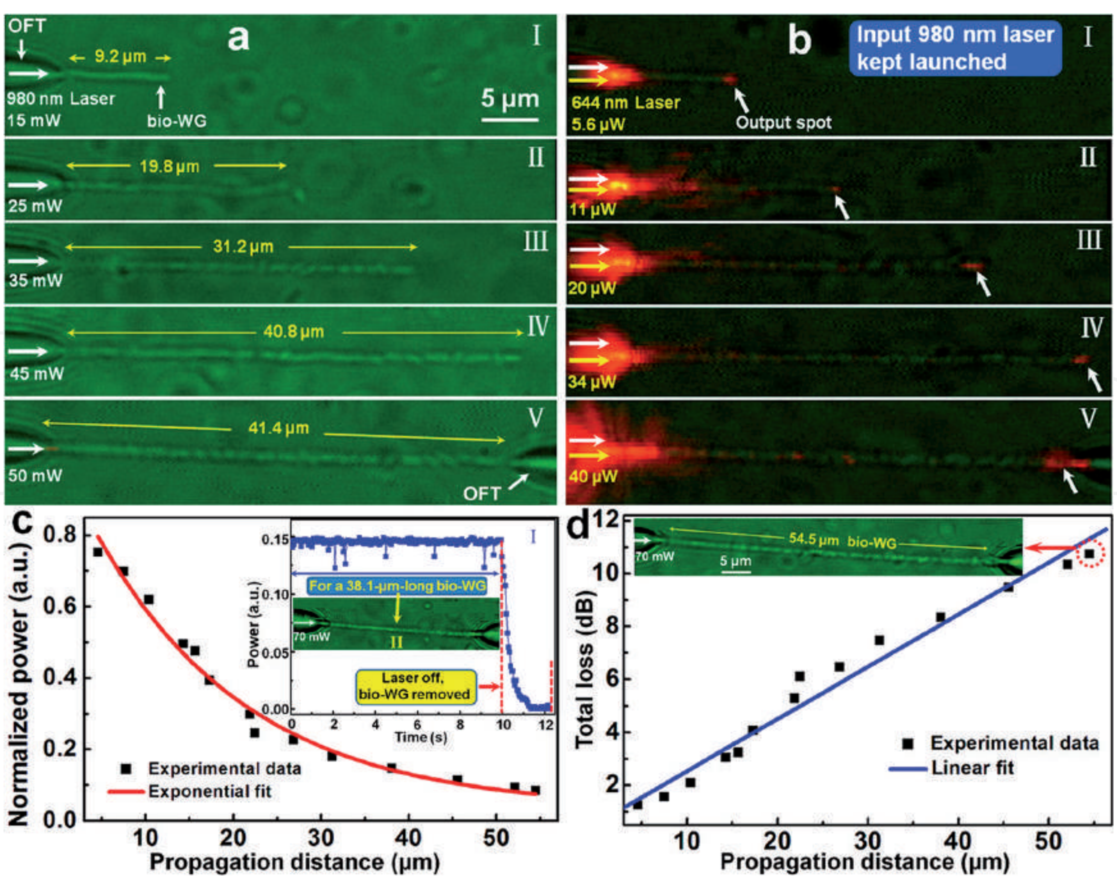


**Figure 4.**
*Biophotonic waveguides formation [17]. (a) Optical microscope images of formed bio-waveguides (bio-WGs) with different lengths. (b) Light propagation observation along the formed biophotonic waveguides. (c) Normalized optical power measured at the end of each waveguides. (d) Measured optical loss of the waveguides.*

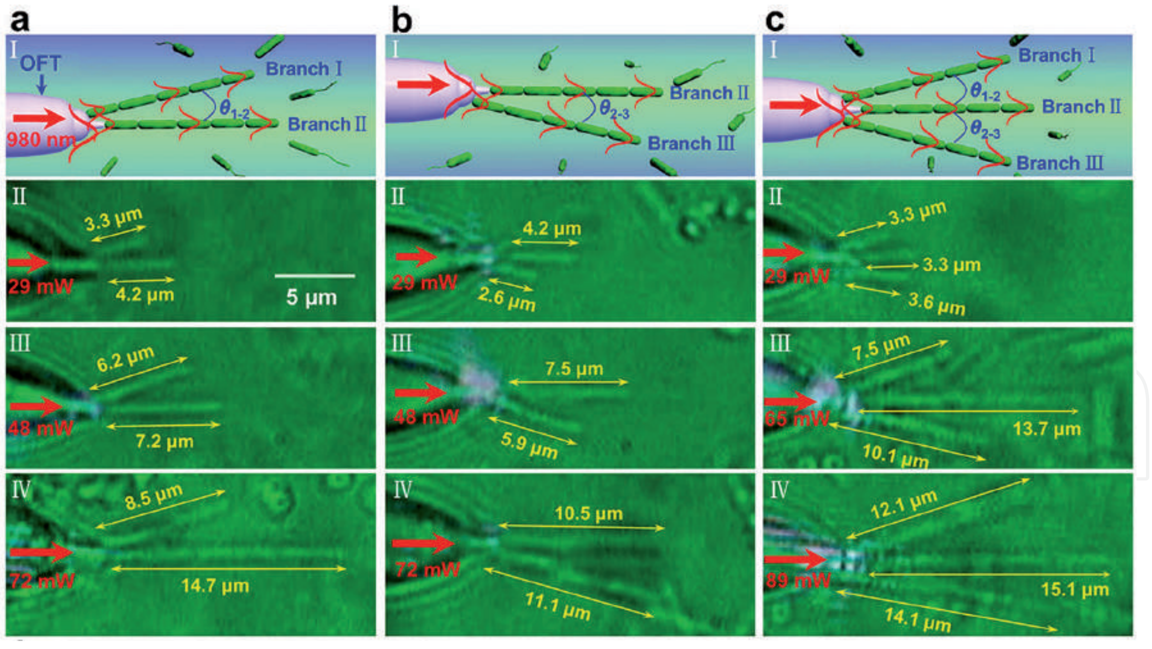


**Figure 5.**
*Optical assembly of branched biophotonic structures [18]. (a, b) Assembly of two-branch structures. (c) Assembly of three-branch structures.*

materials, and provides a new opportunity for direct sensing and detection of biological signal and information in biocompatible microenvironments.

## 5. Assembly of cell-based periodical structures by OFTs

In addition to the assembly of biophotonic waveguides with one type of cells, assembly of periodical structures of different types of cells was also demonstrated using OFTs [19]. Using *E. coli* cells and *Chlorella* cells as examples, different cells are flexibly patterned into one-dimensional (1D) periodic cell structures with controllable configurations and lengths (**Figure 6**), by periodically connecting one type of cells with another by optical force. Further demonstration shows that the structures show good performance for light propagation and can be moved flexibly. Real-time light signals can be detected from these photonic structures. These features make these photonic structures excellent candidates for the detection of signals transducing among different patterned cells. This assembly and patterning technique can also be applicable for other cells, such as mammalian cells and human cells.

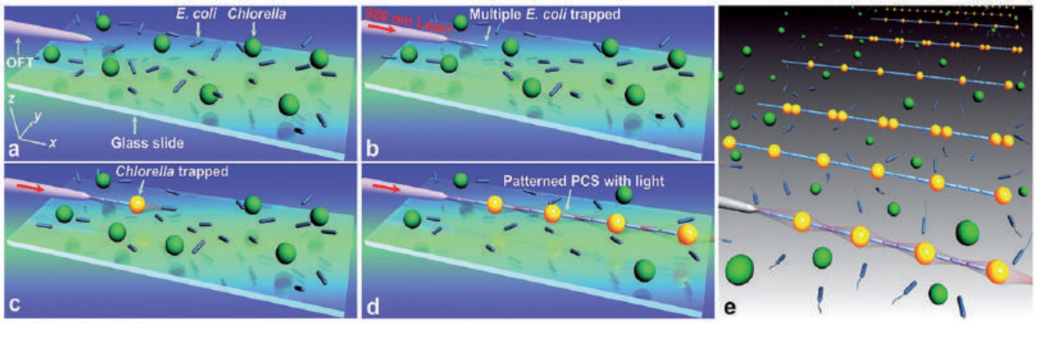


**Figure 6.**
*Experimental schemes for cell assembly into periodical structures [19]. (a) an OTF is placed in cell suspensions. (b) Laser launched, multiple E. coli cells trapped. (c) a Chlorella cell is trapped and connected to the former trapped E. coli cells. (d) a periodical structure is formed, and light propagates along the periodical structure. (e) Schematic shows the assembled periodical biophotonic structures.*

## 6. Assembly of cell-based structures in vivo by OFTs

The assembly capability can also be used for in vivo applications. For example, a non-contact intracellular binding and controllable manipulation of chloroplasts *in vivo* was demonstrated using OFTs [12]. By launching a laser beam at 980 nm wavelength into the tapered fiber, which was placed above the surface of a living plant (*Hydrilla verticillata*) leaf with a gap of about 3 μm to the leaf surface, chloroplasts with different numbers were stably bound and arranged into one-dimensional chains and two-dimensional arrays inside the leaf by optical force without damage to the chloroplasts, by the cooperation of scattering force $F_s$ and gradient force $F_g$ (**Figure 7**). The formed chloroplast chains were controllably transported inside the living cells. This non-invasive and non-contact method of organelle binding and manipulation could provide a way for biological and biochemical research *in vivo*, especially for investigating signal transduction and communication between intracellular organelles via organized organelle-organelle contact.

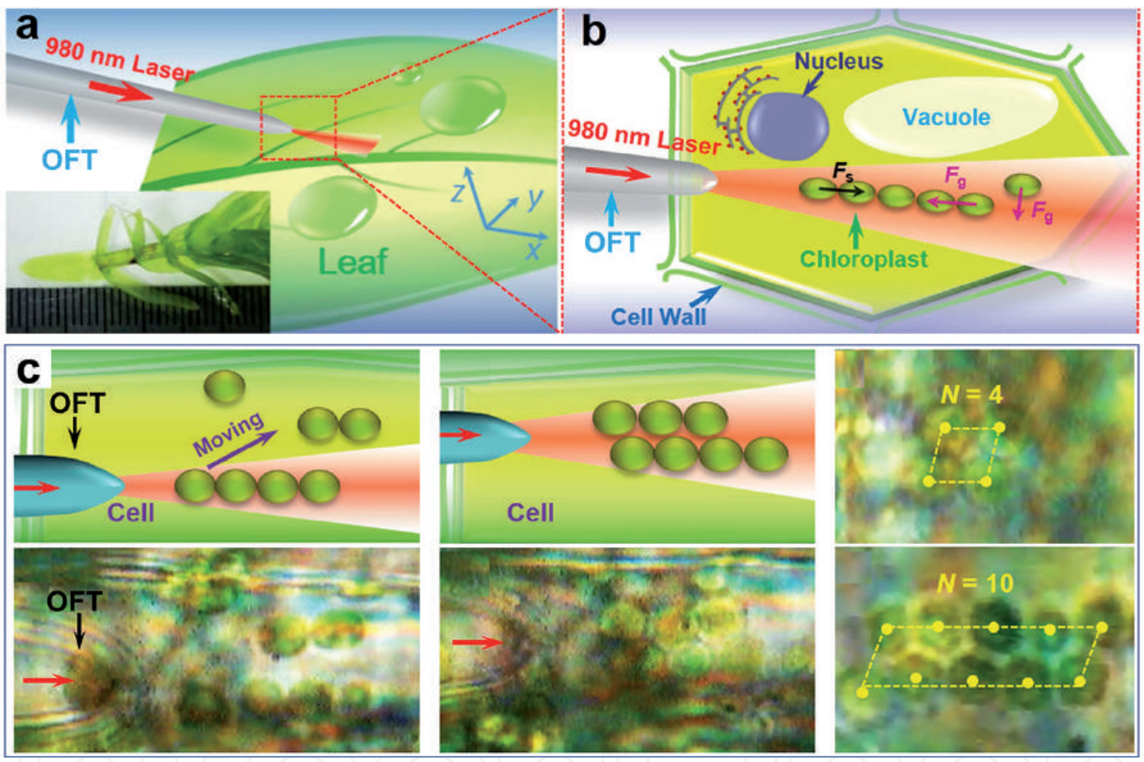


**Figure 7.**
*Assembly of biophotonic probes in vivo [12]. (a) Schematic illustration of biophotonic probe assembly inside a leaf using OFTs. (b) Schematic illustration of biophotonic probe assembly based on a chain of chloroplasts. The chloroplasts inside a leaf are trapped and assembled by the cooperation of $F_g$ and $F_s$. (c) Schematics and microscope images of the manipulation and assembly of organelle-based biophotonic probes in vivo.*

## 7. Assembly of living photonic probe by OFTs for bio-probing and detection

Recently, using OFTs, a fully biocompatible living photonic probe for subwavelength probing of localized fluorescence from leukemia single-cells in human blood has been created [13]. The high-aspect-ratio living photonic probe based on a yeast cell (1.4 μm in radius) and Lactobacillus acidophilus (*L. acidophilus*) cells (2 μm in length and 200 nm in radius) is formed at the tip of a tapered optical fiber by optical trapping (**Figure 8a**). In the assembly, the authors have precisely moved the fiber to approach a yeast cell. Benefited from the spherical shape of the yeast, the trapping laser beam was focused into a tiny region and exerted a strong optical force on a *L. acidophilus* cell that traps it behind the yeast. With this alignment, the trapping laser beam propagates through the *L. acidophilus* cell and exert an optical force on other *L. acidophilus* cells, which were orderly bound together by optical binding effect and finally formed the living photonic probe. **Figure 8b** shows a formed probe assembled with a yeast and five *L. acidophilus* cells. To view the light propagation, after assembly of the probe, the trapping laser remained on, and a visible illumination light was launched into the probe. **Figure 8c–e** show the illumination light propagating along the tapered fiber. At the output port of the probe, a tiny light spot was observed with full width at half maximum (FWHM) of 345, 282, and 248 nm for the illumination wavelengths of 644, 532, and 473 nm, respectively.

As a benefit of the highly focused effect of the living cells, the living photonic probe can also deliver subwavelength excitation light to biological samples, and detect optical signals with a subwavelength spatial resolution. Moreover, within human blood, selective probing of the localized fluorescent signals on single leukemia cell surface can be realized via the precise manipulation of the living photonic probe. Due to the high biocompatibility and resolution, these photonic probes hold great promises for biosensing and imaging in bio-microenvironment. Furthermore, the living photonic probe can be integrated in the available near-field scanning optical microscopy, functioning as a biocompatible and non-invasive scanning probe for near-field imaging of living cells. **Figure 9**, as an example, shows the use of the living photonic probe in probing localized fluorescence of leukemia cells in human blood [13]. **Figure 9a–d** shows the spot excitation capability by manipulating the living photonic probe to approach the cell membrane. As shown in **Figure 9a**,

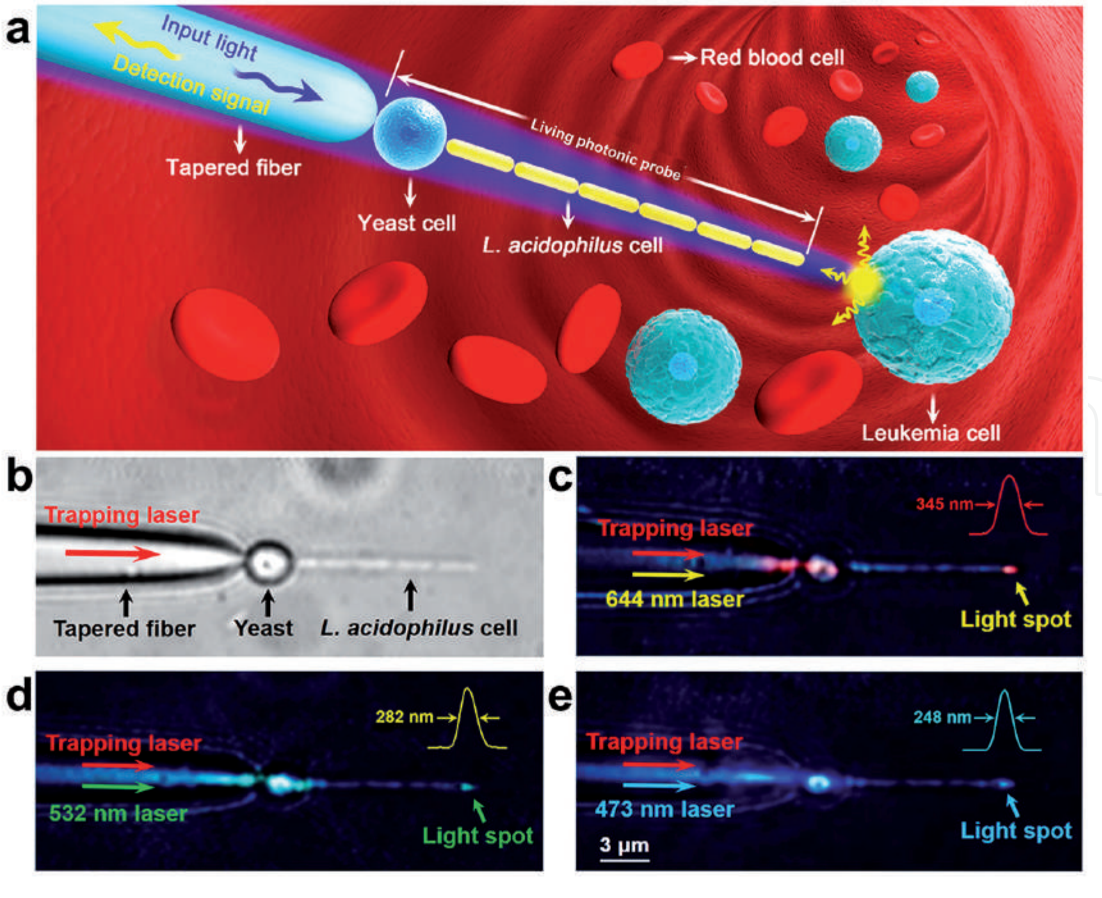


**Figure 8.**
*Assembly of living biophonic probes for bio-probing [13]. (a) Schematic illustration for assembly of living photonic probe by OFTs. (b) Image of a formed living photonic probe. (c)-(e) images showing light propagation along the formed living photonic probes. Light spots can be observed at the end of each photonic probes.*

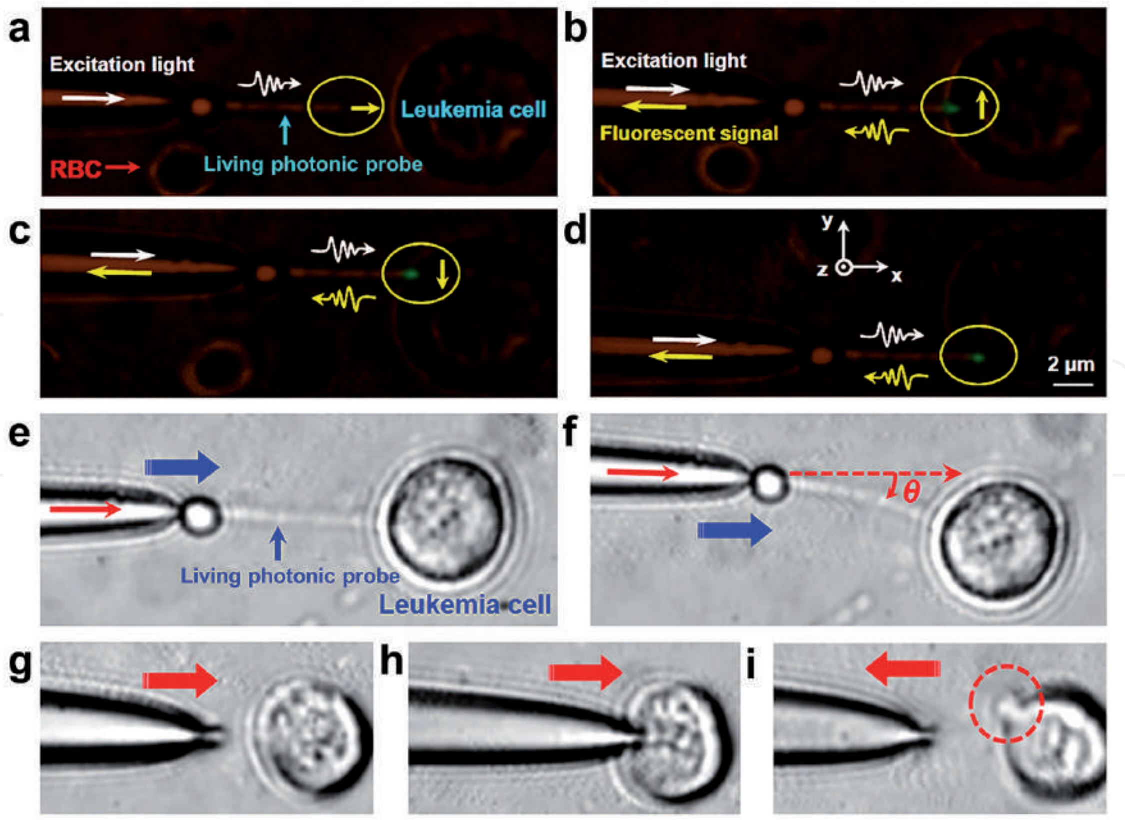


**Figure 9.**
*Living photonic probe for single-cell probing and detection [13]. (a-d) Excitation and detection of local fluorescence from a leukemia cell in human blood by manipulating the living photonic probe to scan a cell. (e,f) Flexibility testing of the probe by pushing the probe against the leukemia cell membrane. (g-i) Touching and punching of the cell directly using a tapered optical fiber tip, to compare the flexibility of the living photonic probe.*

there was no fluorescent signals when the distance between the living photonic probe and the surface of a leukemia cell was 3 μm. But the fluorescent signal was detected with a distinct fluorescent spot observed at the cell membrane when the probe was in contact with the cell (**Figure 9b**). The fluorescent signals at other locations were also detected by scanning the cell surface via precisely moving the probe (**Figure 9c** and **d**). Flexibility and deformability of the living photonic probe have also been demonstrated by interacting with biospecimens. As shown in **Figure 9e** and **f**, the living photonic probe was forced against a leukemia cell, then the living photonic probe was bent to an angle θ of 15° without puncture to the cell membrane. A certain degree of the deformability of the probe has no obvious influence on the scanning capabilities. For comparison, the authors pushed a fiber probe with a sub-micrometer tip, which is commonly used in scanning probe microscopes, against the leukemia cell (**Figure 9g**). As a result of the relatively large dimension and rigid structure, the fiber probe could easily insert into the cell (**Figure 9h**), and rupture the cell membrane (**Figure 9i**).

## 8. Conclusions

In this chapter, we reviewed the trapping and assembly of biological cells using OFTs, and finally extended the trapping capability for the assembly of living photonic probes such as cell-based biophotonic waveguides, cell-based periodical structures, cell-based structures in vivo, and living photonic probe for bio-probing and detection. These living photonic probes exhibit extremely high biocompatibility for further biological applications in bio-environment. As a benefit of the light focusing ability of the cells, the biocompatible living photonic probes allow the trapping, manipulation, sensing, and diagnostics in vivo. Furthermore, the living photonic probes assembled using OFTs offer an biophotonic bridge between optical and biological worlds with natural materials. With the advantages of its biocompatibility, the living photonic probes are envisioned to provides a new opportunity for direct sensing and detection of biological signal and information in biocompatible microenvironments.

## Acknowledgements

This work was supported by the National Natural Science Foundation of China (No. 61975065, 11904132), Guangdong Basic and Applied Basic Research Foundation (2019B151502035), and Science and Technology Program of Guangzhou (202102010088).

## Conflict of interest

The authors declare no competing financial interests.

IntechOpen

## Author details

Xing Li and Hongbao Xin*
Institute of Nanophotonics, Jinan Universtiy, Guangzhou, China

*Address all correspondence to: hongbaoxin@jnu.edu.cn

IntechOpen

© 2021 The Author(s). Licensee IntechOpen. This chapter is distributed under the terms of the Creative Commons Attribution License (http://creativecommons.org/licenses/by/3.0), which permits unrestricted use, distribution, and reproduction in any medium, provided the original work is properly cited.

## References

[1] Ashkin A, Dziedzic JM, Bjorkholm J. Observation of a single-beam gradient force optical trap for dielectric particles. Opt. Lett. 1986;11:288-290. DOI: 10.1364/OL.11.000288

[2] Ashkin A, Dziedzic JM. Optical trapping and manipulation of viruses and bacteria. Science. 1987;235:1517-1520. DOI: 10.1126/science.3547653

[3] Zhao X, Zhao N, Shi Y, Xin H. Optical fiber tweezers: a versatile tool for optical trapping and manipulation. Micromachines. 2020;11:114. DOI: 10.3390/mi11020114

[4] Fuh MRS, Burgess LW,Hirschfeld T. Single fiber optic fluorescence pH probe.Analyst. 1987;112:1159-1163. DOI: 10.1039/an9871201159

[5] Hu Z, Wang J, Liang J. Manipulation and arrangement of biological and dielectric particles by a lensed fiber probe. Opt. Express. 2004;12:4123-4128. DOI: 10.1364/OPEX.12.004123

[6] Lyons ER, Sonek GJ. Confinement and bistability in a tapered hemispherically lensed optical fiber trap. Appl. Phys. Lett. 1995;66:1584-1586. DOI: 10.1063/1.113859

[7] Taguchi K, Ueno H, Hiramatsu T. Optical rapping of dielectric particle and biological cell using optical fiber. Electron. Lett. 1997;33:413-414. DOI: 10.1049/el:19970247

[8] Taguchi K, Ueno H, Ikeda M. Rotational manipulation of a yeast cell using optical fibers. Electron. Lett. 1997;33:1249-1250. DOI: 10.1049/el:19970827

[9] Taguchi K, Atsuta K, Nakata T. Levitation of a microscopic object using plural optical fibers. Opt. Commun. 2000;176:43-47. DOI: 10.1016/S0030-4018(00)00499-5

[10] Frick M, Haller T, Dietl P. Combined optical tweezers and optical stretcher in microscopy. SPIE. 2001;4434:227-232. DOI: 10.1117/12.446684

[11] Ribeiro RSR, Soppera O, Oliva AG. New trends on optical fiber tweezers. J. Lightwave Technol. 2015;33:3394-3405.

[12] Li Y, Xin H, Liu X. Non-contact intracellular binding of chloroplasts in vivo. Sci. Rep. 2015;5:10925. DOI: 10.1038/srep10925

[13] Li Y, Xin H, Zhang Y. Living nanospear for near-field optical probing. ACS Nano. 2018;12:10703. DOI: 10.1021/acsnano.8b05235

[14] Xin H, Xu R, Li B. Optical trapping, driving, and arrangement of particles using a tapered fiber probe, Sci. Rep. 2012;2:818. DOI: 10.1038/srep00818

[15] Xin H, Liu Q, Li B. Non-contact fiber-optical trapping of motile bacteria: dynamics observation and energy estimation. Sci. Rep. 2014;4:6576. DOI: 10.1038/srep06576

[16] Xin H, Zhang Y, Lei H. Optofluidic realization and retaining of cell-cell contact using an abrupt tapered optical fiber. Sci. Rep. 2013;3:1993. DOI: 10.1038/srep01993

[17] Xin H, Li Y, Liu X. Escherichia coli-based biophotonic waveguides. Nano Lett. 2013;13:3408. DOI: 10.1021/nl401870d

[18] Xin H, Li Y, Li B. Bacteria-based branched structures for bionanophotonics. Laser Photonics Rev. 2015;9:554. DOI: 10.1002/lpor.201500097

[19] Xin H, Li Y, Li B. Controllable patterning of different cells via optical assembly of 1D periodic cell structures. Adv. Funct. Mater. 2015;25:2816. DOI: 10.1002/adfm.201500287